EXPERIMENTAL STUDY ON THE FRICTION AND HEAT TRANSFER IN A FIWIHEX

M.B.A.Vlot

Delft University of Technology
Department of Applied Physics

Delft, June 2003

Kramers Laboratorium voor Fysische Technologie
Prins Bernhardlaan 6
2628 BW Delft

Professor: prof. dr. ir. C.R. Kleijn

Abstract

In this report, measurements are described that were done on the wire cloths of a Fine Wire Heat Exchanger. This heat exchanger consists of a centrifugal fan and a circular set of wire-cloths that are surrounding the fan. The fan blows air along the wire cloths, that consists of copper wire woven on capillaries through which (warm or cold) water flows.
The ratio between heat transfer and friction of this Fiwihex fan is so high, that it becomes possible to heat a room with a temperature difference of only $5°C$ between the water and the desired room temperature. Therefore, a Fiwihex can be used well in combination with other heat producing systems than a boiler, for example a solar panel, and heat storage in ground water.
To gain more insight in the heat transfer and the friction of air that flows along such a wire cloth, measurements were done, in which the heat transfer coefficient, expressed as $StPr^{2/3}$, and the friction factor were measured. For these measurements two types of wire cloths were used, the distance between the capillaries was 8 or 12mm. The heat transfer and the friction of the 8mm wire cloths was measured at different mutual distances.
A mass balance was used to measure the friction on a single object, but the influence of the wall seemed to be too large and to uncertain to use this kind of set-up. In further measurements the cloths were placed in a stack in a tube, the pressure was measured with a pressure difference meter, the heat transfer was measured by temperature sensors.
The heat transfer per cloth seemed to be between 2 and 4 times higher than that of a flat plate with the same size. The heat transfer per cloth increased, with increasing mutual distance (from 0.007 to 0.011 m).
The friction factor of the wire cloths was lower than what would be expected according to the theory.
The ratio of heat transfer and friction, expressed as $\frac{StPr^{2/3}}{f}$, is found to be between 1.1 and 1.8. Usual heat exchangers do not reach more than 0.5.

Samenvatting

In dit verslag zijn de metingen beschreven die gedaan zijn aan de geweven matjes van een Fiwihex, een dunne draad warmtewisselaar. Deze warmtewisselaar bestaat uit een centrifugaal ventilator, waar omheen een aantal geweven matjes geplaatst zijn. De ventilator blaast lucht langs de geweven matjes, die bestaan uit koperdraad, geweven op capillairen waardoor (warm of koud) water stroomt. De verhouding tussen warmteoverdracht en wrijving van deze Fiwihex fan is zo hoog, dat het mogelijk wordt om een kamer te verwarmen met een temperatuursverschil van slechts $5°C$ tussen water en de gewenste kamertemperatuur. Daarom kan een Fiwihex goed toegepast worden in combinatie met andere warmteproducerende systemen dan een verwarmingsketel, bijvoorbeeld een zonneboiler, en warmteopslag in grondwater.
Om meer inzicht te verkrijgen in de warmteoverdracht en de wrijving van de lucht die langs zo'n matje stroomt, zijn metingen gedaan waarin de warmteoverdrachtscoëfficiënt, uitgedrukt als $StPr^{2/3}$, en de frictie factor bepaald zijn. Voor deze metingen zijn twee types matjes gebruikt, waarbij de afstand tussen de capillairen 8 of 12mm was. De warmteoverdracht en de wrijving van de 8mm matjes is gemeten op verschillende onderlinge afstanden.
Er is gebruik gemaakt van een massabalans om de wrijving op een enkel voorwerp te meten De invloed van de wand bleek echter te groot en te onzeker te zijn om deze opstelling te kunnen gebruiken. In latere metingen zijn de matjes gestapeld in een rechthoekige buis geplaatst. De druk werd gemeten met een drukverschilmeter, de warmteoverdracht werd gemeten door temperatuursensoren.
De warmteoverdracht per matje bleek tussen de 2 en 4 keer hoger te zijn dan voor een vlakke plaat met dezelfde afmetingen. De warmteoverdracht per matje nam toe met toenemende onderlinge afstand (van 0.004 tot 0.011 m).
De frictie factor van de matjes was lager dan verwacht zou worden volgens de theorie.
De verhouding tussen de warmteoverdracht en de wrijving, uitgedrukt in $\frac{StPr^{2/3}}{f}$ bleek tussen 1.1 en 1.8 te liggen. Bestaande warmtewisselaars halen niet meer dan 0.5.

List of symbols

Roman Symbols

Symbol	Description	S.I. units
a	Thermal diffusivity	m^2/s
A	Area	m^2
$A_\perp$	Projected area in the direction of the flow	m^2
b	Width of the cloth	m
B	Blowing parameter	$-$
B_f	Blowing parameter for friction	$-$
B_h	Blowing parameter for heat transfer	$-$
c	Specific heat	J/kgK
C_D	Drag coefficient	$-$
d	Diameter	m
D_h	Hydraulic diameter as defined in [Kays and London, 1984]	m
e_{fr}	Dissipated energy per unit mass	m^2/s^2
f	Friction factor	$-$
F_D	Drag force	N
F_∞	Drag force on an object in an infinite fluid	N
g	Gravitational constant, g = 9.81 m/s^2	m/s^2
h	Heat transfer coefficient	W/m^2K
K_w	Friction coefficient	$-$
l	Prandtl mixing length	m
L	Length (in direction of the flow)	m
L_p	Distance between ends of the pressure meter	m
n	Number of measurements	$-$
n_{cap}	Number of capillaries in a cloth	$-$
n_{rev}	Number of revolutions per minute	min^{-1}
Nu	Nusselt number	$-$
p	Pressure	Pa
Pr	Prandtl number	$-$
P	Power	W
P_w	Power of the water heater	W
q	Heat transfer	W/K
q''	Heat flux	W/m^2
Q	Heat	W
Re	Reynolds number	$-$
Re_D	Reynolds number with D_h as characteristic lengthscale	$-$

Re_L	Reynolds number with L as characteristic lengthscale	$-$
s	Distance between the wire cloths	m
St	Stanton number	$-$
T	Temperature	K
$T_{a,in}$	Temperature of the air before the wire cloth	K
$T_{a,end}$	Temperature of the air after the wire rack	K
$T_{a,mid}$	Temperature of the air before the wire rack	K
$T_{a,out}$	Temperature of the air after the wire cloth	K
T_L	Temperature at the edge of the laminar layer	K
T_p	Temperature of the water after the solar panel	K
T_w	Wall temperature	K
$T_{w,in}$	Temperature of the incoming water	K
$T_{w,out}$	Temperature of the outflowing water	K
T_∞	Temperature of the fluid in the core	K
u	Velocity in x-direction (in the direction of the flow)	m/s
$\overline{u}$	Mean velocity in x-direction	m/s
u_L	Velocity in x-direction at the edge of the boundary layer	m/s
U^+	Dimensionless velocity in x-direction	$-$
v	Velocity	m/s
v'	Instantaneous velocity component in y-direction	m/s
x	Distance in the direction of flow	m
y^+	Dimensionless y-coordinate	$-$
z	Height	m

Greek Symbols

Symbol	**Description**	**S.I. units**
δ	Thickness of the boundary layer	m
ΔP	Pressure difference	Pa
ΔP_{tot}	Total pressure difference over the cloth	Pa
ΔT_{ln}	Logarithmic temperature difference	K
ϵ	Wall roughness height	$-$
ϵ_H	Eddy conductivity	m^2/s
ϵ_M	Eddy viscosity	m^2/s
η	Dynamic viscosity	kg/ms
η^*	Dimensionless similarity variable	$-$
λ	Blockage ratio	$-$
λ	Heat conductivity	W/mK
ν	Kinematic viscosity	m^2
ρ	Density	kg/m^3
τ	Shear stress	N/m^2
ϕ_m	Mass flow	kg/s
$\phi_{m,a}$	Mass flow of the air	kg/s
$\phi_{m,w}$	Mass flow of the water	kg/s
Ψ	Stream function	m^2/s

Subscripts

Subscripts	Description
a	Air
app	Apparent
bar	Bar
c	Copper
cap	Capillary
$cloth$	Wire cloth
cyl	Cylinder
f	Free flow area
fin	Fin (half of the length of the wires between the capillaries)
h	Heat transfer
l	Laminar
obj	Object
$overall$	Overall
pp	Pingpong-ball
r	Wire rack
t	Turbulent
$tube$	Tube
x	Local value at distance x in the direction of flow
w	Wall
w	Water
$wire$	Wires
$wire \rightarrow a$	From wires to air
0	Unhindered
∞	Core
$\bar{}$	Mean

Contents

Chapter 1

Introduction

The experiments that are described in this report are done on a Fiwihex, which is a fine wire heat exchanger. The invention of a fine wire heat exchanger was made at Akzo Nobel for the cooling of mainframe computers. As a spin-off of these activities at Akzo Nobel, the company Fiwihex, after extensive research, has applied for a patent on this special compact arrangement for the heating and cooling of rooms. The heat exchanger that they have designed is called Fiwihex, after FIne WIre Heat Exchanger.
In section 1.1 the challenge of environmental problems for engineers is discussed. Then, in section 1.3.1 a short introduction will be given on the properties of the Fiwihex, but first something will be said on heat production systems and heat emission systems in sections 1.2.1 and 1.2.2. After the introduction on the Fiwihex, some of its advantages and disadvantages are mentioned in section 1.3.2. Two examples of applications of the Fiwihex are given in section 1.3.3 and 1.3.4, in section 1.3.5 other applications are mentioned. Finally, the contents of this thesis is described in section 1.4.

1.1 The environmental challenge

'Each year another 6 million hectares of productive dry land turns into worthless desert. More than 11 million hectares of forests are destroyed yearly. In Europe, acid precipitation kills forests and lakes and damages the artistic and architectural heritage of nations. The burning of fossil fuels puts into the atmosphere carbon dioxide, which is causing global warming..', this words were written by the world commission on environment and development in their report "Our common future" in 1987 [Brundtland et al., 1987].
The industrial world first became interested in the concept of sustainable development in the 1960s. In these years a number of publications drew attentions to global development issues, like "The Silent Spring" [Carson, 1962] or "Limits to growth" [Club of Rome, 1972]. The optimism on technology in the fifties, that technology would solve problems and reconstruct the world after the war, began to change in the sixties. The way in which technologists dealt with nature was held responsible for environmental exploitation and destruction. The alternatives that were presented were often to far away to be taken seriously by technologists. Technological solutions that seem to work were annihilated by the 'rebound' effect: the increased use of the technology that is caused by its improved characteristics. This is also called the 'saving bulb'-effect: people tend to light more lamps since the economical light bulb has been invented, so that its saving in energy is nullified.
However, this gloomy point of view has changed. In 1987 the Brundtland commission defined

sustainable development as development which meets the needs of the present without compromising the ability of future generations to meet their own needs. In this sustainable development, technologist are needed to develop new sustainable technologies, but the consumers should see the benefits of it and should use it correctly. After all, if a technologist designs a saving bulb, it is not useful if no one uses it or if everyone lights more lamps.
This section, in which a short introduction on environmental problems and challenges is given, is based on [Mulder, 2000] and [Boeker and Grondelle, 1995].

1.1.1 Environmental problems

When we talk about environmental problems, we should notice that these are of human origin. It has however become increasingly difficult to establish whether man or nature has caused a certain catastrophe, or whether human actions made the 'natural' catastrophe worse.
There are several reasons to categorize a phenomenon as an 'environmental problem':

- our health is endangered by it
- nature is (irreversibly) affected
- 'nature' can not be used the way we want it
- the possibility for people from developing countries to use 'nature' in the same way as we do is restricted
- the possibility for future generations to use 'nature' in the same way as we do is restricted

Some examples of environmental problems are:

- global warming, caused by exhaust gases (CO_2-emissions and other greenhouse gases)
- loss and degradation of fresh water supply
- loss of arable soil
- deforestation
- loss of biodiversity

Because environmental problems can differ enormously in space and time, several questions can arise. For example: When industrialised countries caused the greenhouse effect, should they compensate inhabitants of countries like Bangladesh that will be flooded more often? Or: If the amount of resources is limited, who has the right to use them? Do we have to leave crude oil for future generations, or can we use it until there is nothing left? In this thesis these kind of questions are not further discussed, but they are mentioned here to give an idea of the considerations that play a role in sustainable development.
To solve environmental problems, some general principles however can be used for future development:

- The recovering capability of the nature is limited, so that we should burden it less than we do now

- It is expected that the population of the world will almost double in the next years to 9 - 9.5 billion people in 2050. Birth control measures will only lead to a stable population after at least 30 but more probably 50 years.
- When the consumption in the North grows with 1.5 % and in the South with 5-6 % per year to reach about half of the wealth in the North, this will lead to a growth factor of 4-8 in average consumption levels by 2050.

A very simplified equation to calculate the environmental burden was introduced by [Commoner, 1972]. He determined the environmental impact as the product of the population, the affluence (consumption of services and products per capita) and technology (the environmental burden per product or service unit. Of course many objections can be brought forward to this reasoning, but it can be used to give an idea of the environmental efficiency that is needed to decrease the environmental impact of our activities. When the environmental impact has to decrease by a factor two, the environmental efficiency by which goods and services are produced should have been decreased by roughly a factor 20 in 2050.

1.1.2 The problem of the energy consumption

Two large environmental problems are the rise in temperature of the earth, due to the greenhouse effect, and the exhaustion of the world's resources. These problems are related to each other. The gases that are released in the combustion of the fossil energy, contribute to the greenhouse effect. Therefore there are two important reasons to limit the energy use from fossil fuels: the limited supplies and the emissions of CO_2 and other pollutants.
The energy consumption per head of the populations is still increasing. In figure 1.1 the energy consumption per capita is given for the world as a whole, for the United States and for India. In this figure also the world population since 1800 is plotted [Boeker and Grondelle, 1995].
Another way of looking at the energy use, is by dividing it by the gross national product. In figure 1.2 it can be seen that for example in a country like Switzerland, in which the banking and service sector is important, has a low energy consumption compared to its gross national product [Boeker and Grondelle, 1995]. In Japan considerable investments have been done in energy conservation, stimulated by a high energy price. The yearly consumption of fossil fuels and the resources that are proven to be commercially recoverable are given in table 1.1 together with the emission [Boeker and Grondelle, 1995].

	Consumption (1995) /(10^{18} J/year)	Resources (10^{18} J)	CO_2 emission (g/10^6 J)	Other emissions
Oil	120	5900	74	High
Natural gas	85	5500	56	Low
Coal	103	22000	104	High

Table 1.1: World consumption of fossil fuels, proven commercially recoverable resources and emissions (for the year 1995).

In 1999 the total world energy demand of fossil fuels had increased to $319 \cdot 10^{18}$ J [Arkel et al., 2001]. In Europe, the amount of oil resources in 2000 was enough for 8 years, if the demand for oil remains the same as in 1999 and the supplies for gas for 19 years. For the whole world, the gas reserves in 2000 were enough for 64 years and the oil reserves in 1995 for almost 50 years. However, when the resources become scarce and therefore expensive, the amount of commercially recoverable resources will increase, because more resources can then be exploited and it is worthwhile for exploration companies to look further.

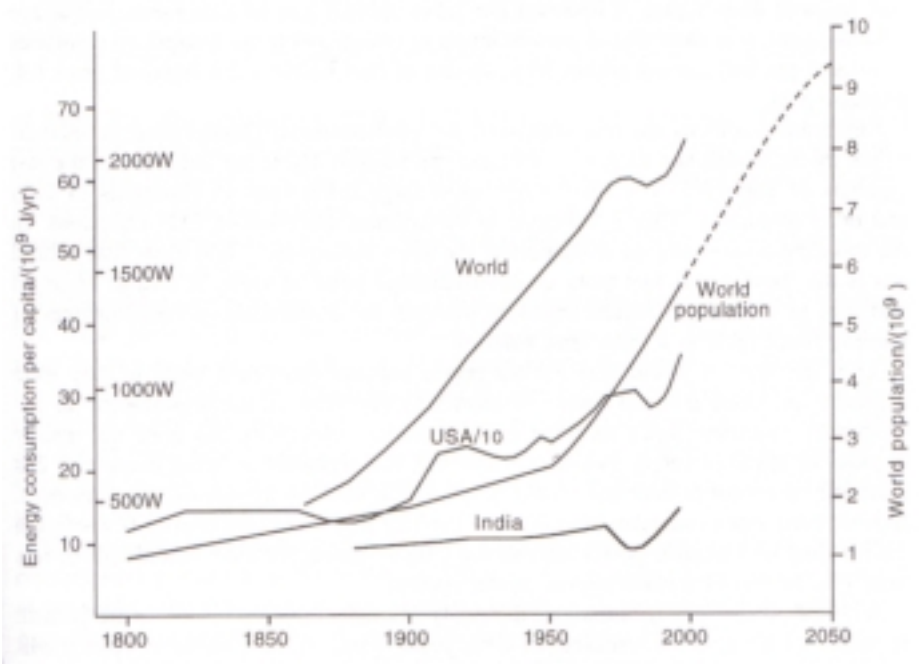

Figure 1.1: Energy use per capita for the world, USA and India and the world population since 1800. The energy use per capita of the USA is divided by 10 to fit into this graph.

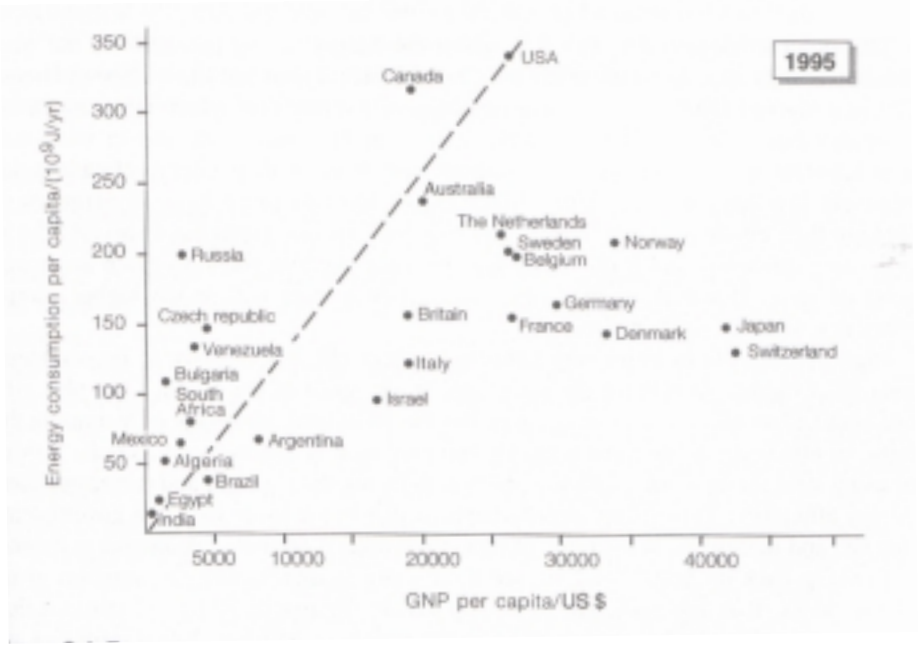

Figure 1.2: Energy consumption and gross national product per capita for a variety of countries in 1995

The actual problems with the energy supply, for example for the problem of CO_2-emission, exhaustion of fossil fuels and excessive use of energy, different solutions exist:

- Energy from sustainable sources can be used: sun, wind, waves or biomass.
- The use of energy can be decreased by: isolation of buildings, recycling, other product designs.
- Raising the consciousness of the consumer

The best way to come to a sustainable energy supply is by combining these different types of solutions. In the case of the Fiwihex fan, it is a combination of the first two types: the heat exchanger itself is a new product design, but it makes the use of solar energy more efficient.

1.1.3 Energy use in the Netherlands

In the Netherlands, the energy consumption was 2612 PJ in 2001, of which about 18% is used in households. The total CO_2-emission was 123 Mton.
In table 1.2 the distribution of this energy consumption and emission over the different sectors can be seen. [ECN, 2003] The energy consumption of households consists mainly of gas (79%)

sector	Energy use (PJ)	Energy use (perc. of total)	CO_2-emission (Mton)
Households	469	18%	21
Industry	1110	42%	46
Agri- and Horticulture	210	8%	10
Building industry	34	1%	1
Service industry	322	12%	11
Transport	467	18%	33

Table 1.2: Energy use and CO_2-emission in different sectors in the Netherlands

and elektricity (18%). Gas is used for heating (77%), hot water (20%) and cooking (3%). Of the elektricity use, 15 % is used for hot water [CBS, 2003b]. In 2001 there were 6.9 million households in the Netherlands. The energy use for heating is 32.9 GJ per household per year, for warm water 10.0 GJ/year is used.
With heat pumps 20 Million m^3 gas was saved, this is 0.10 GJ per household per year. Other sources of sustainable energy, like wind energy produced $3.0 \cdot 10^{15}$ J, which is averaged per household 0.43 GJ/year. Finally, photovoltaic systems produce about $2.8 \cdot 10^{13}$ J/year, which is averaged per household 0.040 GJ/year.

1.2 Heat production, emission and storage systems

In this section an overview is given of heat producing systems in section 1.2.1 and of commonly used heat emission systems in section 1.2.2. In section 1.3 is explained how the Fiwihex works.

1.2.1 Heat production systems

The warm water that is needed for the heating of houses, can be produced by a (condensing) boiler. In a 'normal' boiler the flue gas that results from the combustion of gas is used to heat water. In a condensing boiler the flue gas is cooled by a heat-exchanging surface until it condenses, so that higher efficiencies are reached.
Another heat production system is a heat pump. The great majority of them works on the principle of the vapour compression cycle in which the main components are the compressor, the expansion valves and two heat exchangers, called the evaporator and the condenser. Usually electricity is used to compress the vapour from the evaporator, this vapour condenses in the condenser and gives off useful heat. The coefficient of performance (COP) of a heat pump is the supplied heat divided by the consumed power. This coefficient increases when the temperature difference between evaporator and condenser is lowered.
In an electrical power plant a lot of heat is produced. This heat can be used for heating buildings. This is called Combined Heat Power or Co-generation and is mostly used in combination with collective heating. In the transport from the power plant to the houses, heat is lost. To minimise this heat loss the transportation temperature should be as low as possible.
Sustainable energy resources that can be used for the production of heat are for example solar systems. Solar energy is the least polluting and most inexhaustible of all known energy sources. The main difficulty with solar heating is that there is a mismatch between solar radiation and heating demand, so that seasonal storage is needed.

1.2.2 Heat emission systems

Perhaps the best known heat emission system is a 'normal' radiator, but there are many types of radiators and other heat emission systems. In this section a few of them will be mentioned, this overview is taken from [Tjallema, 2001].
In most of the Dutch houses a normal radiator is installed, which is usually designed for a water temperature of $90°C$ with a return temperature of about $70°C$. The area of the radiator can also be enlarged by using plate-fins, this is called a Low Temperature radiator and is designed for $60°C$ inlet and $45°C$ return temperature.
The basic type of a convector consists of a finned tubular element mounted near the bottom of a sheet metal casing, such that a chimney effect is created. A low temperature convector is designed for water of $60°C$.
Floor, wall or ceiling heating consist of polyethylene tubes that are embedded in the floor, wall or ceiling. The installation of this system is therefore quite expensive compared to radiator or convector systems. It has a slow dynamic response. The designed temperature of the inlet flow is between 43 and $29°C$.

1.3 The Fiwihex and its use

1.3.1 Introduction to the Fiwihex

When warm water flows through a tube, the wall of the tube is heated and successively the air around it as well. This heat transport is more effective if the heat exchanging surface (the warm surface that is in contact with the air) is larger or when the air around the tubes is flowing. The smaller the tubes are, the more of their heat is transferred to the air. In the Fiwihex fan these

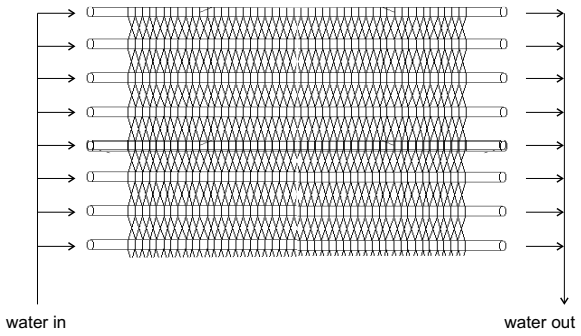

Figure 1.3: Sketch of the lay-out of one wire cloth.

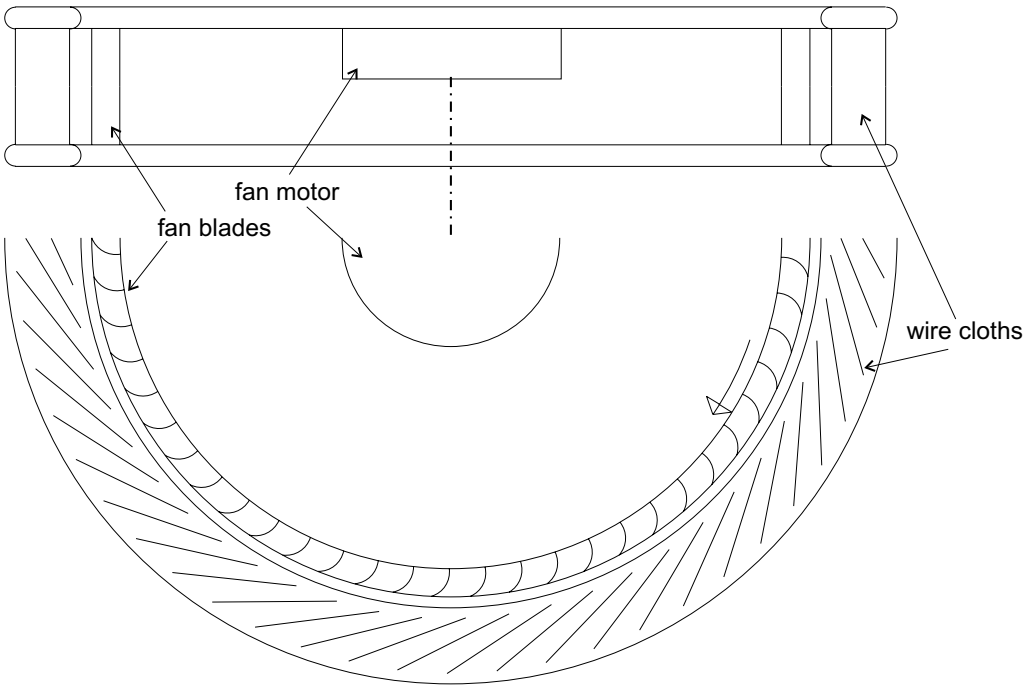

Figure 1.4: Sketch of the lay-out of the Fiwihex, side and top view.

aspects are optimized.
The Fiwihex fan consists of a slow turning fan that blows the air along cloths in which the actual heat transfer takes place, see figure 1.4. These cloths are made of small capillaries through which warm water flows and around which copper wire is woven to extend the heat exchanging area, see figure 1.3. The fan that is used is a forward curved, so-called sirocco or squirrel cage fan. A squirrel-cage fan has a large width to diameter ratio and it has a large number (ca. 60) of short chord blades. This fan keeps the noise as low as possible and is driven by a small electrical engine. It should be attached to the ceiling. Just like a common radiator a Fiwihex alone is not capable of heating or cooling a house. It is just the heat exchanging part of the heating system and it has to be fed with warm water in order to heat air.
A standard Fiwihex fan has a diameter of 635 mm and can reach 195 revolutions per minute. The heat transfer, q, of this fan (in W/K) can be approximated by this rule of thumb:

$$q = 8 \cdot D_{fan}^2 n_{rev}^{0.8} \tag{1.1}$$

in which D_{fan} is the diameter of the fan (in m) and n_{rev} is the number of revolutions per minute. For the standard Fiwihex the heat transfer is around 220 W/K. This Fiwihex can for example heat

a room of $80m^3$ (4 x 8 x 2.5 m) from 10 to 20 degrees with water of $25°C$ in about 8 minutes, when heat loss to the surroundings is left out of consideration. The heat transfer can be regulated by the number of revolutions per minute of the fan, so that the temperature of a room can be regulated very fast and exactly. The power that is needed by the fan motor, P_{fan} (in W), can be approximated by:

$$P_{fan} = 3.10^{-5} \cdot D_{fan}^4 n_{rev}^3 \tag{1.2}$$

For the standard fan at full speed this is approximately 36 W. This leads to a COP of approximately 31, when the temperature difference between water and air is 5K.

1.3.2 Advantages and disadvantages of the Fiwihex

When a heat exchanging system like a radiator is replaced by a Fiwihex, the energy that is needed in a room for heating still remains the same and is independent of the heat exchanging system. The important advantage of the Fiwihex is not that it needs less energy to heat a room, but that it needs energy of lower value. This makes it possible to use heat that would else have been worthless. Advantages of the Fiwihex fan due to its low supply temperatures are:

Higher efficiency of condensing boilers. The return water from the heating system is used to cool the flue gases. In combination with a Fiwihex, the return temperature is low enough to cool the gas below the condensate temperature. The efficiency of the condensing boiler becomes about 10 % higher of this.

Less heat loss in distribution networks This is due to the smaller temperature difference between the pipes and the surrounding air.

More efficient use of solar energy The efficiency of a solar boiler is higher if the desired water temperature is lower. Besides, the solar panel can be engineered more simple (and cheaper) and can provide enough warm water for heating at the start and the end of the heating season.

Use of heat pumps The coefficient of performance of a heat pump increases when the temperature difference is smaller

Cooling with water of $10 - 15°C$ The mean temperature of ground water is $12°C$, so that this can be used to cool buildings.

If the Fiwihex is used in combination with a solar boiler, another advantage exists. Water of lower temperature can also more easily be stored in groundwater. Because of the lower temperature, the layers that are used can lie closer to the surface, because their thermal pollution is smaller. In summer warm water can be made that is used to heat the ground water, while cold ground water is used to cool the building. In winter the warm groundwater can be used to heat the building, while cold water pumped into the ground, so that the groundwater level remains the same.

The disadvantages of the Fiwihex do not lie in the technical area, but are more economical and social. They will be shortly mentioned here.

Price Installing the Fiwihex in combination with other heat production systems, might be more expensive than common systems, the time in which this is regained depends on the configuration of the set-up.

Noise The fan turns around and makes some noise. At full speed, this is about 59 dB at one meter (comparable to an elektrical toothbrush), at 75% of its maximal power, its noise is 50 dB(A) at one meter (comparable to a fridge or in a forest) and at 50% of its maximal power, the noise is 37 dB (comparable to the noise in a library or soft whispering).

Novelty People tend to use products they know and that they trust. They have to get used to and trust the Fiwihex fan.

Esthetics A fan at the ceiling looks different from a radiator beneath the window. The esthetics of the Fiwihex could be improved by making a nice casing.

Draft The air circulation due to a radiator is slower than that from the Fiwihex. However, the air that comes out from the Fiwihex is directed along the ceiling, so that the air velocity closer to the floor will be not so high.

1.3.3 The Fiwihex in houses

When the Fiwihex is used to heat a house, its power should be high enough to reach the desired temperature even if it is very cold outside, the minimum outside temperature is taken to be $-7°C$. It is usual to demand that the living room and the bath room should reach at least $20°C$, the kitchen at least $18°C$ and the sleeping rooms, the hall and the attic at least $16°C$.
The maximum power that is needed is calculated for three types of reference houses: a terraced or row house, a semidetached house and an apartment building of 24 apartments. These reference houses and their data are given by [Novem, 2002]. The building plots of these reference houses can be seen in figure 1.5. The heat losses from these reference data were not specified for each of the different rooms, so that in the calculation the ground floor is assumed to be $20°C$, the second floor and attic are assumed to be $16°C$. For the apartments half of the building is assumed to be at $20°C$, the other half at $16°C$. The temperature of the ground under the house is assumed to be $12°C$.
With these assumptions and the heat transfer coefficients for the different parts of the reference houses from [Novem, 2002], the maximum needed power of the Fiwihex fan is calculated, see table 1.3. In the last column the number of standard Fiwihex fans are given that are needed.

kind of house	max. power (W)	number of Fiwihex fans
row house (middle)	2303	2.1
row house (corner)	2819	2.6
semidetached house	3564	3.2
apartment (aver. per house)	2301	2.1

Table 1.3: Maximum needed power or number of standard Fiwihex fans for four types of houses

Of course it is not possible to reach a pleasant temperature in all the rooms if one places three Fiwihex fans in the living room of a row house, in this way not all rooms will be heated enough. The temperature of each room should be regulated separately. This can be done by placing a Fiwihex fan in each room, so that each room has its own fast heating system. The disadvantage of this is that it is quite expensive because the heat transfer system is over-dimensioned. For the living room a standard Fiwihex fan of 1100 W is probably about the right size, but if the needed heating power is calculated for a room of $3x4m^2$, of which one of the shorter sides is the facade, and it has a window of 1.5x1.5 m, its maximal needed heating power is only 204 W, which is less than 1/5 of the maximum power of a standard Fiwihex fan. It will usually be warmer than $-7°C$ outside, so that even less power is needed.

(a) building plot of row house

(b) building plot of semidetached house

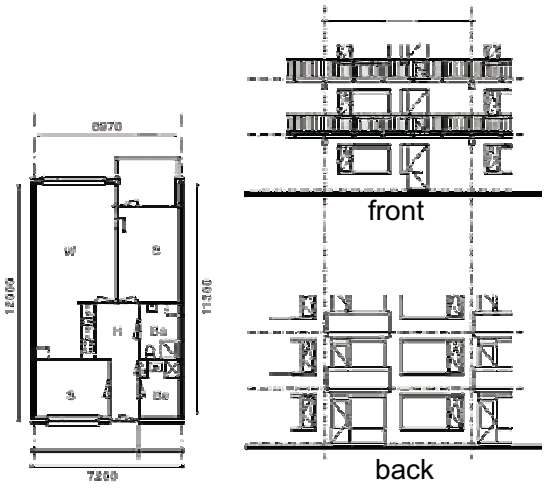

(c) building plot of apartment house

Figure 1.5: Building plots of the three types of reference houses

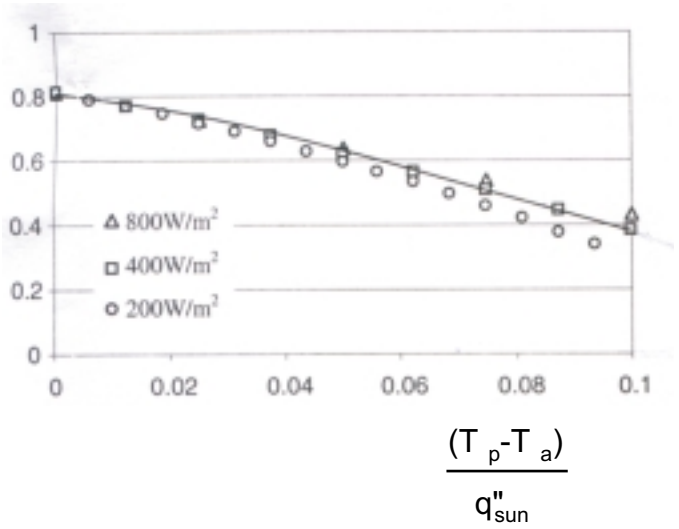

Figure 1.6: Collector efficiency as function of $\frac{T_p - T_a}{q"_{sol}}$

The power that is needed, is not constant over the day. Therefore if the needed heating power is not so high, this does not mean that the Fiwihex has to turn very slowly all day long. It will have to heat the house in the morning and has to start up again when it becomes too cold. The advantage of a Fiwihex is that its heat transfer can be regulated, so that a room can be heated as fast as possible, and when it is warm enough, the Fiwihex turns off and the heat transfer immediately is almost zero.
A solution to this over-dimensioning would be to produce Fiwihex fans in all kinds of sizes, so that for each room a suitable fan can be found. The disadvantage of this is that it is more expensive to produce different kind of Fiwihex fans. Another possibility would be to heat the air for different smaller rooms at a central place, and then transport it to the separate rooms by a ventilation system. The disadvantage of this is that it takes extra energy to transport the air to another room.
The average energy that is needed per year to heat the reference houses according to [Novem, 2002] is given in table 1.4

kind of house	transmission loss (GJ)	ventilation loss (GJ)	sun gain (GJ)	internal heat production (GJ)	total needed heat (GJ)
row house (middle)	18.7	8.9	-5.0	-11.8	10.8
row house (corner)	23.5	8.9	-5.7	-11.8	14.9
semidetached house	30.0	10.7	-6.5	-14.4	19.8
apartment (aver. per house)	14.2	6.0	-4.7	-7.9	7.7

Table 1.4: Survey of the needed heating energy per year for four types of houses

Sources of heat The Fiwihex can be used in combination with a solar boiler and a heat storage system in the ground. The efficiency of this boiler depends on the water temperature: the lower the desired temperature of the water, the higher the efficiency. In figure 1.6 the efficiency of a collector, with a black absorber plate and no convection suppression, is drawn against $\frac{T_p - T_a}{q"_{sol}}$ in which T_p is the temperature of the water when it leaves the collector, T_a is the ambient temperature of the air and $q"_{sol}$ the power of the solar radiation in W/m^2. In a usual heat boiler system, the desired water temperature is about $80°C$, so that the efficiency is low. The efficiency also depends on the

solar insulation, which depends strongly on the season and on the direction of the solar collector. The percentage of the total solar radiation that reaches the surface of the sun collector, depending on its angle with the horizontal plane and the orientation, is given in table 1.5 [Ecofys, 2003]. In

orientation	$\alpha = 0°$	$\alpha = 30°$	$\alpha = 45°$	$\alpha = 60°$	$\alpha = 90°$
South	87 %	98 %	97 %	94 %	74 %
South-East/ South-West	87 %	95 %	94 %	85 %	70 %
East / West	87 %	84 %	78 %	73 %	56 %
North	87 %	65 %	52 %	42 %	33 %

Table 1.5: Percentage of total solar radiation that reaches the surface of the solar collector depending on its angle, α, with the horizontal plane and the orientation in the Netherlands

the calculation of the gain of the solar collector, it is assumed that it heats water up to $30°C$ from April until September. The efficiency of the solar collector is estimated using figure 1.6 and table 1.5. In table 1.6 the heat gain of the sun collector per month is given, assuming that the water is heated up to $30°C$, that the angle of the solar panel with the horizontal is 30° and that it is directed South. With this estimation, the total heat gain is 1.5 GJ/m^2 per year. In table 1.7 an

month	solar radiation (GJ/m^2/month)	mean day temperature ($°C$)	energy gain (GJ/m^2/month)
April	0.39	12.9	0.12
May	0.53	17.6	0.31
June	0.52	19.8	0.32
July	0.53	22.1	0.36
August	0.47	22.3	0.31
September	0.31	18.7	0.12

Table 1.6: Heat gain of a sun collector, with an angle of 30° with the horizontal plane and directed South

estimation is given for the total heat gain that can be stored for the different types of reference houses if the whole roof is covered with solar panels. The area of the roof is about $55m^2$ for the reference row house and about $67m^2$ for the semidetached house, but these are usually gable roofs, so that both sides are not placed in the same direction. Under the assumption that half of the houses in the Netherlands are built in North-South-direction and half of the houses in East-West direction, the mean percentage of the solar radiation that reaches the surface of the solar collector is at least about 70%. The area of the apartment building is about $465m^2$, which is $19m^2$ per apartment. For the percentage of the solar radiation that reaches the surface of the solar collector at an apartment building 95 % is taken (30° and South-East or South-West).
The heat should be stored in summer and can be used in winter, the efficiency of the storage depends on the kind of storage. In table 1.7 the superfluous energy is given in percentages of the total heat gain to indicate the maximum heat loss that is allowed in storage and transport. In the last column also the solar panel area is given that is needed to cover the yearly energy demand, without heat losses in storage and transport.
Because of the low temperatures that are used, the heat can be stored in a layer near to the surface, so that it is less expensive to drill holes in the ground to pump groundwater into and from. In summer the cold groundwater is pumped from the ground to cool the house and the warm water is pumped into the ground. In winter this is done the other way around.

Examples of other sources of heat
The low temperature of the water makes it also possible to use other sustainable heat sources than a solar panel. Residual heat from industrial plants or power plants can be used to heat

kind of house	total needed heat (GJ/year)	total heat gain (before storage) (GJ/year)	superfluous energy (perc. of total gain)	minimum area (without heat losses) (m^2)
row house (middle)	10.8	63.5	83%	9.3
row house (corner)	14.9	63.5	77%	12.9
semidetached house	19.8	77.4	74%	17.1
apartment (aver. per house)	7.7	28.3	73%	5.3

Table 1.7: Energy demand and gain for four types of houses

houses. In the Rijnmond area, for example, a cooperation of government and companies, called ROM Rijnmond, is looking for opportunities to use residual heat from industrial plants in some residential areas of Rotterdam.
In the former coal mines in Heerlen, large rooms that are left behind in the rocks are slowly filled with water. These reservoirs lie between 420 and 825 m deep. Every 100 m deeper in the mines, the water temperature increases with $3°C$, because it is heated by the earth. The mean temperature of the water lies between $20°C$ and $35°C$, depending on the depth of the shaft. In this way these former mines could again be a source of heat [Pisters, 2003].
In the Netherlands every year 40 km^2 of asphalt is constructed for new or the renovation of old roads. This asphalt can be used as an asphalt collector, when water is flowing below the surface of the road. In summer this water is used to cool the road, so that the asphalt will not get too hot, so that wheel tracks are formed. In winter, the warm water that was stored in summer is used to heat the road, so that no brine has to be used. In summer more heat can be stored than is necessary in winter, so that the superfluous heat can be used to heat some buildings.

1.3.4 Fiwihex in greenhouses

In the Netherlands between 1994 and 1998, horticulture in greenhouses needed an average of 135 PJ per year for heating, which is 1.5 GJ/m^2 per year [CBS, 2003a]. In most of the current projects to save energy, heat is generated in water carrying solar panels, stored in the ground and in winter the warm groundwater is heated with a heat pump and used to heat the greenhouse. Common heat exchangers need a temperature difference of about $25°C$ between air and water, to heat the air sufficiently. If they are used with a smaller temperature difference, the air has to pass the heat exchangers multiple times, which would cost too much mechanical energy. Therefore the air of the greenhouse can not be used to heat the groundwater in summer and it is not possible to heat the greenhouse with groundwater without using a heat pump.
As a Fiwihex needs a much smaller temperature difference, it might be possible to use the Fiwihex to heat the groundwater in summer and the air in the greenhouse in winter. In the design of a greenhouse, the following aspects should be taken into account:

- The greenhouse has to be heated in winter
- The greenhouse has to be cooled in summer (either by cooling the air or by ventilation)
- To regulate the moisture in the greenhouse, cooling must be also available in winter, to condensate water locally.
- If the greenhouse is closed, more CO_2 has to be supplied. The advantage of closing the greenhouse, is that the danger of contagion, from outside to inside the greenhouse or the other way around, is decreased.

For the heat transfer from the air in the greenhouse to the groundwater, Fiwihex heat exchangers could be installed underneath the plants, so that they do not take too much light away from the plants. The movement of the air that comes out of the Fiwihex is also of importance to get the heat down from under the ceiling.
For heat storage in the ground, usually deep aquifers are used, because the temperatures of the water vary between 5 and $90°C$ which is so different from the usual ground temperatures that the surroundings could be damaged. In a heating system with Fiwihex fans, the groundwater temperatures lie between 10 and $25°C$, which is in the range of naturally occurring ground temperatures. At these temperatures also PVC tubes can be used and decalcification is not necessary. However, the groundwater is almost always anaerobe and contains Fe^{II} that precipitates at the tube wall after contact with air, so that the water should not be in contact with air. If the ground consists of impenetrable clay, deeper layers have to be used. For each separate ground water installation one has to apply for a new permit, because the subsoil can differ so much for different locations.
The roof of the greenhouse can consist of glass. The average heat transfer coefficient of such a roof is $6.92 W/m^2K$ and its solar transmission is 92 %. To get a larger heat production in the greenhouse, channel plates can be used of which the heat transfer coefficient is smaller ($3.46 W/m^2K$), but the transmission is also lower (86 %). The mean energy from the sun is 3.5 GJ/m^2 per year. If the greenhouse is large enough, only the heat loss through the roof can be taken into account. If the greenhouse is closed, and no cooling or heating occurs, the air in the greenhouse will reach a mean temperature of $15°C$ (with a glass roof) or $28°C$ (with channel plate) above the outside temperature.
These temperatures are too high, so the sun provides more than enough energy to heat the greenhouse. The energy that remains after subtracting the heat that is needed for heating and the heat loss during storage and transportation, can be used for other purposes, for example heating of surrounding buildings or, in future, photo-voltaic foil can be spread out to generate electricity on sunny days.
For a more accurate calculation of the energy that can be stored in the ground, more information is needed on the soil, the desired temperatures in the greenhouse and the size of the greenhouse [Andel, 2002].

1.3.5 Other applications of the Fiwihex

In the previous two sections, the application of the Fiwihex in houses and greenhouses is described. Of course there are many other places where a Fiwihex fan could be used.
In office buildings there is often so much electrical equipment, that the demand for heat is small, but on the other hand more cooling is necessary. If the Fiwihex is used to heat and cool the building, in summer heat from solar panels can be stored in the ground water. In winter this warm groundwater can be used to heat the building and, if necessary, further cooled with open air so that a large amount of cold groundwater is again available for cooling in summer.
In industry the demand for heat is so dependent on the kind of industry, that it is not possible to make general statements on the use Fiwihex fans in industry.

1.4 Contents of this thesis

In this thesis experiments are described that are done on the Fiwihex.
The importance of using less fossil energy is sketched in section 1.1.1 and 1.1.2. Therefore research should be done on possibilities to save energy, such as a Fiwihex fan. One of the advantages of a Fiwihex is that it is not very expensive and that it can improve the actual heat system in houses,

because it can be used for cooling as well. Earlier measurements indicated an unexpectedly high ratio between the heat transfer and friction of a Fiwihex. If it would be clear why the ratio between the heat transfer and friction is so high, then it could be possible to design the best configuration of the wire cloths, without making a large number of prototypes.
Therefore, the main questions in this thesis were:

- What is the ratio between heat transfer and friction factor, $\frac{StPr^{2/3}}{f}$, of the Fiwihex?
- How high is this ratio compared to flat plates?
- Why is $\frac{StPr^{2/3}}{f}$ so high?

The experiments were done on the individual wire cloths, so that almost uniform flow could flow around them. In this way it was also easier to measure the temperature difference over the cloth and to change the mutual distance. The heat transfer and friction of these wire cloths is measured for different mutual distances and two types of cloth. For these measurements a stack of cloths was used, these cloths can be seen as flat plates, but also as the walls of a rectangular channel.
In chapter 2 the theory of heat transfer and friction is described for flat plates and channels. In chapter 3 preliminary, but unsuccessful, measurements in which a mass balance was used to measure the friction, are described. The set-up and results of the friction measurements with a pressure tube and the heat transfer measurements are described in chapter 4 to 6. Finally, conclusions and recommendations are given in chapter 7.

Chapter 2

Theory on heat transfer and friction

There has been a lot of research on the heat transfer and friction of surfaces. Before the experiments are described in this chapter the theory is given of friction and heat transfer along different surfaces, so that the results of the experiments can be compared to what already is known for other surfaces. In the experiments the single wire cloths of the Fiwihex will be used, but also placed above each other in a stack, so that they form a pile of rectangular channels. Therefore in this chapter attention will be paid to the heat transfer and friction of flow past a flat plate and flow in a tube. The heat transfer and friction can be expressed in dimensionless numbers, to simplify the comparison between different configurations. In section 2.1 the Reynolds number and hydraulic diameter are explained. The dimensionless number in which the heat transfer is expressed is the Stanton number, this is given in section 2.2. The dimensionless drag coefficient and friction factor that are used for the friction are explained in section 2.3.
After explaining the dimensionless numbers that are used, a short introduction to the theory of laminar and turbulent flow is given in section 2.4. The theoretically expected values for flow past a flat plate are given in section 2.5 and for flow in a tube in section 2.6. These theoretical values are for developed flow, the theoretically expected heat transfer and pressure drop in the entrance region of a tube are given in section 2.7. The influence of blowing, suction, injection, mass transfer etc. at the surface is discussed in section 2.8. The last section in this chapter, section 2.9, deals with the theoretically expected analogies between heat and mass transfer.

2.1 The Reynolds number and hydraulic diameter

A dimensionless number for the velocity of the fluid is the Reynolds number which indicates how turbulent a flow is. The Reynolds number is given by:

$$Re = \frac{\rho v D}{\eta} \tag{2.1}$$

D is the characteristic length scale and is dependent on the flow configuration. In a circular tube the characteristic length scale is the diameter, but for flow along a flat plate it is the distance to the leading edge.
In the case of flow in a channel that is not circular, the hydraulic diameter usually is used. The definition for the hydraulic diameter that will be used here comes from [Kays and London, 1984]

and is defined as 4 times the minimum free flow area, A_f times the length of the channel, divided by the total heat transfer area, A_h:

$$D_h = 4\frac{A_f L}{A_h} \tag{2.2}$$

2.2 The Stanton number

The heat, Q, that is transferred from one place to the other can be expressed by Newton's law of cooling, equation (2.3):

$$Q = hA_h \cdot \Delta T \tag{2.3}$$

In this equation the temperature difference ΔT is the driving force behind this heat transfer. A_h denotes the area through which the heat transfer takes place and h is the heat transfer coefficient expressed in $\frac{W}{m^2 K}$. In the results for the heat transfer of heat exchangers often the Stanton number is used, abbreviated as St. This Stanton number can be calculated by:

$$St = \frac{h}{\rho c v} \tag{2.4}$$

in which ρ is the density, c is the specific heat and v is the velocity of the fluid. The Stanton number can therefore be seen as the heat that is transferred, divided by the heat capacity of the fluid, i.e. the amount of heat that is convected per second, per unit of cross-sectional area and per Kelvin temperature difference. It relates to the (more familiar) Nusselt, Prandtl and Reynolds number as:

$$St = \frac{Nu}{Re \cdot Pr} \tag{2.5}$$

The Stanton number indicates the effect that the heat transfer has on the fluid. For example when the velocity of the fluid is large compared to the heat transfer, the increase in temperature of the fluid is smaller and the Stanton number is also smaller.

2.3 Drag coefficient and friction factor

An object that is moving through a fluid or around which a fluid is moving, experiences a force that is exerted by the fluid. This force is dependent on the relative velocity of the object and the fluid, the viscosity and density of the fluid and the shape and dimensions of the object. The total drag force of the fluid on the object can be split into two terms: form drag and friction drag.
The first is due to normal forces exerted by the fluid on the object. The fluid that approaches the object is slowed down and a stagnation pressure is formed before the object. Behind the object, in the wake, energy is dissipated by eddies. The pressure difference over the object causes a force in the direction of the flow.
The friction drag is due to tangential forces exerted by the fluid along the surface. At the surface the velocity of the fluid is zero, so that a boundary layer is formed at the surface. The shear stress, τ_w that is exerted by the fluid on the wall can be calculated as:

$$\tau_w = \eta[\frac{dv}{dr}]_{wall} \tag{2.6}$$

in which η is the dynamic viscosity of the fluid.
The dimensionless friction factor, f, is given by:

$$f = \frac{-\tau_w}{\frac{1}{2}\rho < v >^2} \tag{2.7}$$

From the shear stress, the shear drag force can be obtained. Shear and drag force together are usually modeled through a drag coefficient, C_D as:

$$F_D = C_D \cdot A_\perp \cdot \frac{1}{2}\rho v^2 \tag{2.8}$$

in which $A_\perp$ is the projected area in the direction of the flow, C_D is the drag coefficient and v the velocity of the fluid.
The friction factor of a tube can be used to calculate the pressure drop over it. Therefore the mechanical energy balance is used, which reads for fluids with constant density between point 1 and 2 along a streamline in a tube:

$$0 = \phi_m[\frac{1}{2}v_1^2 + \frac{p_1}{\rho} + gz_1 - \frac{1}{2}v_2^2 - \frac{p_2}{\rho} - gz_2] + \phi_w - \phi_m e_{fr} \tag{2.9}$$

In this equation is ϕ_m the mass flow of the fluid, v its velocity, p the pressure, ρ the density, g the gravitational constant, z the height and ϕ_w the work that is done on the fluid. The amount of energy that is dissipated per unity of mass is given by e_{fr}. To calculate e_{fr} the friction factor of the tube is needed, but also the friction coefficients K_w of all the 'obstacles' such as fittings, sudden changes in diameter or valves. In equational form:

$$e_{fr} = \sum_i (4f\frac{L}{D_h}\frac{1}{2}\langle v\rangle^2)_i + \sum_j (K_w\frac{1}{2}\langle v\rangle^2)_j \tag{2.10}$$

The hydraulic diameter, D_h is defined in the next section in equation (2.2).

2.4 Laminar and turbulent flow

For the friction and the heat transfer in a flow, it is of great importance whether the flow is laminar or turbulent. Turbulent flow is characterised by chaotic movements of parts of the fluid in different directions. In a turbulent flow the velocity can be split into two terms: a time-averaged velocity and an instantaneous fluctuation velocity that is added to it. These fluctuation velocities may be positive or negative; their time average is zero. The amplitude of velocity fluctuation can be expressed in terms of the mean of their squares. A turbulent flow adjacent to a solid surface differs little whether it is a pipe or a flat plate. In a turbulent flow two regions can be observed:

(1) A predominantly viscous region immediately adjacent to the wall where viscous shear and molecular conduction play a role. This is called the viscous sublayer.

(2) A fully turbulent region, where velocity is nowhere independent of time, where eddy viscosity is observed and where momentum and heat are transported at rates much greater than can be accounted for by viscous shear and molecular conduction.

Using equation (2.6), with the kinematic viscosity $\nu = \frac{\eta}{\rho}$ and for a non-circular arrangement the shear stress, τ, is

$$\tau = \rho\nu\frac{\partial u}{\partial y} \tag{2.11}$$

in which ν is the kinematic viscosity. For turbulent flow the shear stress can be split up into a laminar component, τ_l and a turbulent component, τ_t:

$$\tau = \tau_l + \tau_t = \rho(\nu + \epsilon_M)\frac{\partial u}{\partial y} \tag{2.12}$$

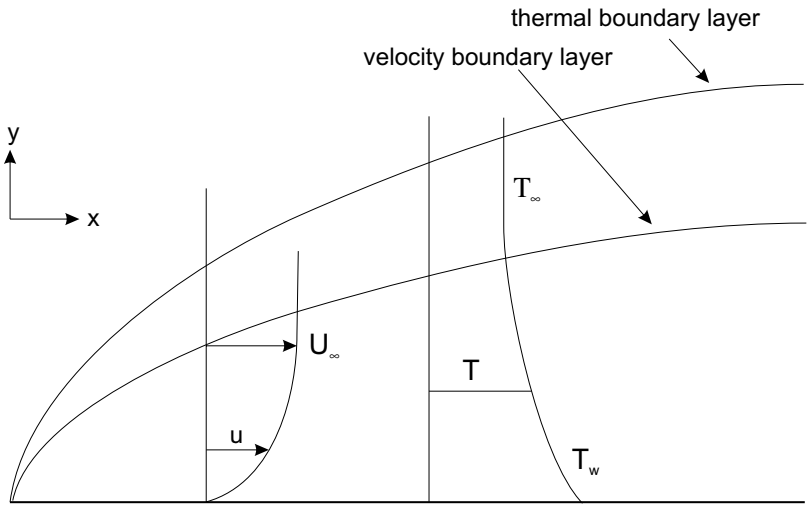

Figure 2.1: Sketch of boundary layer flow past a flat plate, showing the typical velocity and temperature profiles.

in which ϵ_M is the eddy viscosity; it varies with geometry and Reynolds number. The directions of y and u are the same as in figure 2.1. Near the wall $\nu \gg \epsilon_M$, but in the turbulent region it is the other way around: $\epsilon_M \gg \nu$.
The molecular heat flux, q'', can be described by Fourier's law:

$$q'' = -\lambda \frac{\partial T}{\partial y} \tag{2.13}$$

Similarly as for the shear stress, the following expression can be given for the total (laminar and turbulent) heat flux:

$$q'' = -\rho c(a + \epsilon_H) \frac{\partial T}{\partial y} \tag{2.14}$$

where $a = \frac{\lambda}{\rho c}$ and ϵ_H is the eddy thermal diffusivity owing to the net effect of turbulent velocity and temperature fluctuations.

2.5 Flow past a flat plate

In this section the theoretical results for the heat transfer and friction of flow past a flat plate are given. In this kind of flow a boundary layer exists close to the plate, outside this boundary layer the flow is almost unhindered by the plate. In figure 2.1 the boundary layers are sketched. In this figure also the directions of x, y, u and v are drawn.

2.5.1 Laminar flow past a flat plate

In figure 2.1 the boundary layer flow past a flat plate is sketched. For laminar flow past a flat plate, the boundary layer equations for momentum and energy reduce to:

$$u \frac{\partial u}{\partial x} + v \frac{\partial u}{\partial y} = \nu \frac{\partial^2 u}{\partial y^2} \tag{2.15}$$

for momentum, and for energy:

$$u\frac{\partial T}{\partial x} + v\frac{\partial T}{\partial y} = a\frac{\partial^2 T}{\partial y^2} \tag{2.16}$$

in which $\nu = \frac{\eta}{\rho}$, $a = \frac{\lambda}{\rho c}$ and assuming constant ρ, η and λ and negligible dissipation. Blasius [White, 1988] reasoned that the velocity profiles along the plate would be similar in shape. Lord Rayleigh [White, 1988] had already established that the thickness of the boundary layer, δ, grew approximately as $x^{1/2}$. He introduced the stream function Ψ, which satisfies the following equations:

$$u \equiv \frac{\partial \Psi}{\partial y} = U_\infty \cdot g'(\eta^*) \tag{2.17}$$

$$v \equiv -\frac{\partial \Psi}{\partial x} = \frac{1}{2}(\frac{U_\infty \nu}{x})^{1/2}(\eta^* g' - g) \tag{2.18}$$

In which $\eta^* = y(\frac{U_\infty}{\nu x})^{1/2}$ is the dimensionless similarity variable and g is a function of η^*. From the combination of these equations The Blasius equation can be derived [White, 1988]:

$$g''' + \frac{1}{2}gg'' = 0 \tag{2.19}$$

There is no analytic solution for this equation, but it can be calculated by using a numerical technique. This is described in more detail in [White, 1988] or [Kays and Crawford, 1980]. The shear stress appears to increase as velocity to the 3/2 power. For the local friction factor the following expression is found:

$$f_x = \frac{0.664}{Re_x^{1/2}} \tag{2.20}$$

in which $Re_x = \frac{U_\infty x}{\nu}$. Under the assumption that the temperature ratio is a function of η^* only, $\frac{T-T_w}{T_\infty - T_w} = \Theta(\eta^*)$, and by substitution in equation (2.16) and solving the differential equation that is derived, we obtain in the end:

$$Nu_x = Re_x^{1/2} \cdot \Theta'(0) \tag{2.21}$$

If $Pr > 0.5$ equation (2.21) can be approximated with an error less than 2% by equation (2.22):

$$Nu_x \approxeq 0.332 Pr^{1/3} Re_x^{1/2} \tag{2.22}$$

Re_L is the Reynolds number with the length of the plate as characteristic length scale. The Nusselt-number and the friction factor above are both local numbers, the average drag and heat transfer are given by:

$$\overline{f} = \frac{1}{L}\int_0^L f dx = \frac{1.328}{Re_L^{1/2}} \tag{2.23}$$

$$\overline{St} \approxeq \frac{0.664}{Pr^{2/3} Re_L^{1/2}} \tag{2.24}$$

This derivation is valid only for laminar flow past a flat plate. The transition to turbulent takes place approximately at Re_x=500,000, but this varies according to:

- the particular velocity and length scale used
- the geometry of the flow
- additional effects, such as wall roughness, freestream noise, pressure gradient

2.5.2 Turbulent flow past a flat plate

In a region close enough to the wall, the mean velocity is only a function of y. When the pressure gradient $\frac{dP}{dx} = 0$ and only averaged velocity components in flow direction exist, the following expression can be derived for the viscous sublayer:

$$\overline{u} = \frac{\tau_w}{\eta} y \tag{2.25}$$

and for the fully turbulent region the viscous effects in equation (2.12) were negligible:

$$\frac{\tau_w}{\eta} = \epsilon_M \frac{d\overline{u}}{dy} \tag{2.26}$$

With the mixing length theory of Prandtl this becomes according to [Kays and Crawford, 1980]:

$$u^+ = 2.44 ln(y^+) + 5.0 \tag{2.27}$$

with $u^+ = \frac{\overline{u}}{\sqrt{\tau_0/\rho}}$ and $y^+ = \frac{y U_\infty \sqrt{f/2}}{\nu}$. A power-law can sometimes be more convenient than a logarithmic form, therefore equation (2.28) can be used instead of equation (2.27) for $y^+ < 1500$ [Kays and Crawford, 1980].

$$u^+ = 8.75 (y^+)^{1/7} \tag{2.28}$$

With the assumption that equation(2.28) is valid over the entire boundary layer this leads to [Kays and Crawford, 1980]:

$$f = 0.0718 Re_L^{-0.2} \tag{2.29}$$

which is valid for Reynolds numbers up to several million. To obtain a solution for the heat-transfer coefficient, we make two simplifying assumptions:

- both the thermal and momentum boundary layers have the same thickness
- the two laws of the wall are reasonable approximations for the entire boundary layer

In a turbulent boundary layer, the momentum layer provides the main transport mechanism (eddy diffusivity), therefore it is not possible that the thermal layer has a thickness that is significantly different. According to [White, 1988] this leads to a Nusselt number that is:

$$Nu = 0.037 Re_L^{0.8} Pr^{1/3} \tag{2.30}$$

Expressed in the Stanton number this is:

$$St = \frac{0.037}{Re_L^{0.2} Pr^{2/3}} \tag{2.31}$$

An alternative, more accurate and more general formula is equation (2.32) [White, 1988]:

$$St = \frac{0.0359 Re_L^{-0.2}}{0.189 Re_L^{-0.1} (13.2 Pr - 10.16) + 0.9} \tag{2.32}$$

2.6 Flow inside tubes

The airflow in a tube is different for flow along a flat plate. In this section the friction and heat transfer are given for laminar and turbulent flow in tubes.

2.6.1 Laminar flow inside tubes

The friction factor for laminar flow in a circular tube is:

$$f = \frac{16}{Re_D} \tag{2.33}$$

In this equation the diameter of the tube is used as characteristic length scale for Re_D. For a tube with an elongated rectangular cross section, with a ratio between the width and the height of about 20 the friction factor is:

$$f = \frac{22.5}{Re_D} \tag{2.34}$$

As characteristic length for the Reynolds number the hydraulic diameter is used [Kays and Crawford, 1980], see also equation (2.2). The calculation of the heat transfer for laminar flow in a tube with constant surface temperature leads to $Nu = 3.66$, but this is valid for a circular tube. For a rectangular tube with the same ratio of 20 between the width and height, Nu is much higher: $Nu \approxeq 7.7$ according to [Kays and Crawford, 1980].

2.6.2 Turbulent flow inside tubes

The difference between turbulent flow inside a tube and along plates is that in a tube the boundary layers can only grow until they meet at the tube centerline. Thereafter no further growth is possible. The friction factor in turbulent flow is less dependent on Re. For pipes with a smooth wall Blasius found experimentally this equation which is valid for $4000 < Re < 10^5$ [Beek and Muttzall, 1975]:

$$f = 0.079 Re_D^{-0.25} \tag{2.35}$$

Equation (2.35) is also valid for tubes with non-circular cross-section if the hydraulic diameter is used. But a more accurate formula, which also takes the roughness of the wall into account is [White, 1988]:

$$f = \frac{1}{4 \cdot (-1.8 log_{10}\{(\frac{\epsilon}{3.7 D_h})^{1.11} + \frac{6.9}{Re_D}\})^2} \tag{2.36}$$

In this equation ϵ is the average wall roughness height. The Nusselt number for turbulent flow in a tube is [White, 1988]:

$$\bar{Nu} = 0.027 Re_D^{0.8} Pr^{1/3} \tag{2.37}$$

This is, expressed in the Stanton number:

$$\bar{St} = \frac{0.027}{Re_D^{0.2} Pr^{2/3}} \tag{2.38}$$

2.7 Entrance and exit effects

The friction factors and Nusselt numbers that were given in the preceding sections are based on developed flow. If the flow however enters a tube entrance different effects occur. In this section the influences of these effects are given.

2.7.1 Sudden contraction

When the cross-section of the tube is suddenly reduced, this causes a pressure drop due to the friction of this contraction and because of the increase in velocity. To calculate this pressure drop

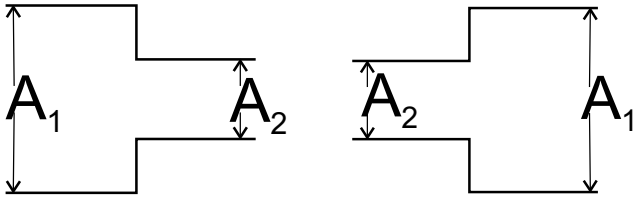

(a) Sudden contraction (b) Sudden expansion

Figure 2.2: Sketch of sudden contraction and expansion

equation (2.9) and (2.10) can be used. For the friction coefficient equation (2.39) can be used, see also figure 2.2 [Janssen and Warmoeskerken, 1987].

$$K_w = 0.45(1 - \frac{A_2}{A_1}) \tag{2.39}$$

This friction coefficient should be used in combination with downstream flow conditions.
The contraction also causes an acceleration, because the mass flow should remain constant. The new mean velocity becomes:

$$v_2 = \frac{A_1}{A_2} v_1 \tag{2.40}$$

The pressure drop, ΔP_{entr}, that is caused by both effects can be calculated using equation(2.9):

$$\Delta P_{entr} = -(P_1 - P_2) = -\frac{1}{2}\rho v_2^2 (1.45 - 0.45\frac{A_2}{A_1} - (\frac{A_2}{A_1})^2) \tag{2.41}$$

2.7.2 Developing flow

When a fluid enters a duct, it has a velocity profile that is determined by upstream conditions. After a distance, the velocity at the center has increased, while the velocity near the walls has decreased. The flow is fully developed when the fluid velocities no longer change with axial distance. The part of the duct before this point is called the entrance region. The axial pressure gradient is higher in the entrance region than in the developed flow because of two effects [Fleming and Sparrow, 1969]:

1. The increase in momentum of the fluid as the velocity distribution becomes less uniform
2. The higher wall shear, caused by higher transverse velocity gradients.

When the entrance length is a significant part of the total length of the duct, the pressure drop and the heat transfer will be remarkably larger than for fully developed flow.
The hydrodynamical entry length for laminar flow in a tube is $0.035 \cdot D \cdot Re$ according to [Bird et al., 2002], and $0.05 \cdot D \cdot Re$ according to [Kays and Crawford, 1980]. When Pr is low, the temperature profile develops more rapidly than the velocity profile, the thermal entry length is approximately given by: $0.05 \cdot D \cdot RePr$. The hydrodynamical entry length for turbulent flow is typically less than 10-15 tube diameters, and depends heavily on the geometric character of the entrance. [Kays and Crawford, 1980]
The friction factor depending on the distance in the tube is given in figure 2.3, in which x is the distance from the entry of the tube. In this figure three friction factors are plotted: the local, mean and the total apparent friction factor. The local friction factor is based on the local shear

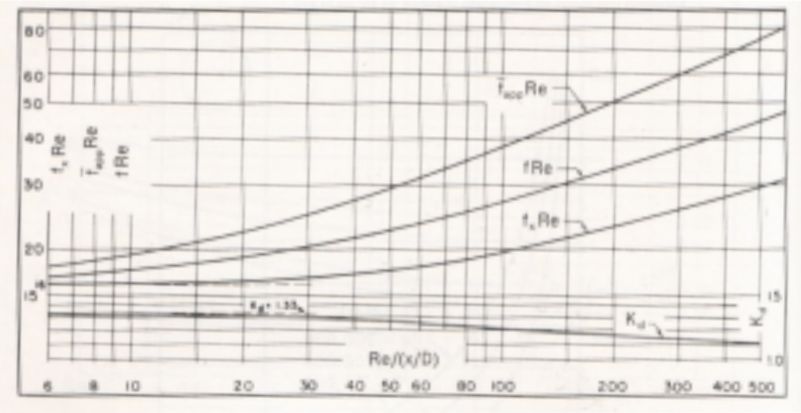

Figure 2.3: Local, mean and total apparent friction factors for laminar flow in the hydrodynamic entry length of a circular tube. The momentum flux correction factor for the hydrodynamic entry length is also plotted.

stress and the mean friction factor is based on the mean shear stress from 0 to x. At the beginning of the tube the velocity is assumed to be uniform, and a velocity profile is developed in the tube. This causes an increased axial momentum flux which results in an extra pressure drop, this is also taken into consideration in the apparent friction factor, f_{app}. It is based on the total pressure drop from 0 to x. In the entrance region of the pipe, where the boundary layers are still too small to meet each other in the middle, the friction can be calculated assuming external flow. The local friction factor for external flow along a flat plate is given in equation (2.20) and the mean friction factor in equation (2.23). The thickness of a laminar boundary layer is:

$$\delta_{lam} = 5x \cdot Re_x^{-1/2} \tag{2.42}$$

in which x is the distance along the plate or tube and Re_x the Reynolds number with x as characteristic length scale.
Due to the change in the velocity profile, an extra pressure drop is caused. If we assume that the velocity is uniform at the beginning of the tube and has a parabolic form at the end, it can be derived that: $< v_2^2 > - < v_1^2 >= \frac{1}{5} < v_1^2 >$ for flow between flat plates, with $< v^2 >$ the squared velocity, averaged over the height. .
These two effects cause a pressure drop over the tube of:

$$\Delta P_{tube} = -\frac{1}{2}\rho v^2 (4f \cdot \frac{L}{D_h} + \frac{1}{5}) \tag{2.43}$$

in which L is the length of the tube, D_h the hydraulic diameter and v the velocity of the fluid. This pressure drop is determined under the assumption that the velocity profile at the end is parabolic, but in reality it can be smaller when the profile is not yet laminar at the end of the tube.
An excellent curve-fit expression for f_{app} has been suggested by [Shah, 1978], [White, 1988].

$$f \cdot Re_D = \frac{3.44}{\zeta^{1/2}} + \frac{0.31/\zeta + 16 - 3.44/\zeta^{1/2}}{1 + 0.00021/\zeta^2} \tag{2.44}$$

In this equation is $\zeta = \frac{(x/D_H)}{Re_D}$. The mean Nusselt number also changes in a developing flow; for the Nusselt number with constant wall temperature an experimental correlation by Sieder and Tate is often used [Sieder and Tate, 1963], [White, 1988]:

$$\overline{Nu}_T = 1.86 * (\frac{x/D_H}{Re_D Pr})^{-1/3} \tag{2.45}$$

This correlation can be used if the difference between the wall temperature and the mean fluid temperature is not too large, $0.5 < Pr < 17000$ and $\frac{x/D_H}{Re_D Pr} \leq 0.125$.

2.7.3 Sudden expansion

A sudden expansion causes a pressure drop due to its friction, but also increases the pressure due to the decrease in velocity of the fluid. Again equations (2.9) and (2.10) are used in combination with the friction coefficient equation (2.46) (see also figure 2.2)[Janssen and Warmoeskerken, 1987].

$$K_w = (\frac{A_1}{A_2} - 1)^2 \tag{2.46}$$

For the resulting velocity we can use equation (2.40). Equation (2.9) is used to calculate the pressure difference.

$$\Delta P = -\frac{1}{2}\rho v_1^2 \cdot 2\frac{A_2}{A_1}(1 - (\frac{A_2}{A_2})) \tag{2.47}$$

2.8 Influence of transpiration of the surface

The term transpiration is a general description of blowing, suction, injection, mass transfer etc. at the surface. This can be the case with a porous surface through which part of the main stream is being sucked or blown, this might also be the case in this experiment. The applicable differential equations are the same, but the boundary condition of zero flow in y-direction has changed.

2.8.1 Transpiration in a laminar boundary layer

For the derivation of a laminar boundary layer with suction the normal velocity at the wall is assumed to be v_w; when $v_w > 0$ blowing from the wall occurs and when $v_w < 0$ there is suction. When the ratio between v_w and the core flow velocity U_∞ is small, only the fluid particles near the wall are sucked up.
The boundary layer momentum equation for constant-property, two-dimensional flow, becomes:

$$\nu\frac{\partial^2 u}{\partial y^2} = u\frac{\partial u}{\partial x} + v\frac{\partial u}{\partial y} + \frac{1}{\rho}\frac{dP}{dx} \tag{2.48}$$

The blowing (or suction) parameter, B, is defined as $\frac{v_w}{U_\infty}Re_x^{1/2}$, which is a measure for the amount of air that is blown through the wall. The equation can numerically be solved [Donoughs and Livingood, 1954], the results for the friction factor, f and for the heat transfer, depending on the blowing parameter are given in table 2.1. The most commonly used coefficient in the mean Nusselt number for laminar flow past a flat plate is 0.664 (see equation(2.24)), but this differs a little with different authors, therefore the value for the heat transfer without blowing from the table is slightly different.
The ratio between heat transfer and friction increases as the blowing parameter grows.

2.8.2 Transpiration in a turbulent boundary layer

Transpiration strongly affects the sublayer thickness of the boundary layer. According to [Kays and Crawford, 1980], the following expression holds for the friction factor of a turbulent flow along a plate:

$$\frac{f}{f_0} = \frac{ln(1 + B_f)}{B_f} \tag{2.49}$$

Table 2.1: The heat transfer and friction factor in laminar flow along a plate, depending on the blowing parameter.

$\frac{v_w}{U_\infty}Re_x^{1/2}$	f	$StPr^{2/3}$	$\frac{StPr^{2/3}}{f}$
0	$\frac{1.328}{\sqrt{Re_L}}$	$\frac{0.585}{Re_L^{1/2}Pr^{2/3}}$	0.441
0.5	$\frac{0.658}{\sqrt{Re_L}}$	$\frac{0.332}{Re_L^{1/2}Pr^{2/3}}$	0.505
1.0	$\frac{0.142}{\sqrt{Re_L}}$	$\frac{0.103}{Re_L^{1/2}Pr^{2/3}}$	0.725

In this equation the subscript 0 refers to the situation where no transpiration occurs, which means that $v_w = 0$. Here, the blowing parameter, B_f is the ratio of the transpired momentum flux to the wall shear force. A definition for B_f is:

$$B_f = \frac{v_w/U_\infty}{f/2} \tag{2.50}$$

Equation (2.49) can be solved by using equation (2.29).
It turns out that the same equation as equation (2.49) applies for the Stanton number if the blowing parameter for friction, B_f is replaced by the blowing parameter for heat transfer, B_h, as shown in the next equations:

$$B_h = \frac{v_w/U_\infty}{St} \tag{2.51}$$

$$\frac{St}{St_0} = \frac{ln(1+B_h)}{B_h} \tag{2.52}$$

As the blowing increases, both the friction and the heat transfer decrease with almost the same amount.

2.9 Analogies between heat and mass transfer

There are a few different derivations for the analogy between the friction and the heat flux. In this section the main analogies are discussed.

2.9.1 The Reynolds analogy for heat and mass transfer

Reynolds postulated a proportionality between friction and wall heat flux, which is called the Reynolds analogy. This provides a simple relationship and corresponds quite closely to the experimental results. To understand this analogy, see figure 2.4 and consider an element of fluid of mass δm with velocity u, in equilibrium with its surroundings that moves in y-direction over a distance l and comes into equilibrium with its new surroundings.
The distance l is called the Prandtl-mixing length. Physically, the mixing length is the distance that a particle has to travel in a direction perpendicular to the flow until the difference between its original velocity and the velocity of its new place is the same as the mean fluctuating velocity in the direction of the flow [Schlichting, 1951]. The net result of this event is the transfer of momentum and thermal energy in the y-direction, completely independent of that transferred by purely molecular processes. Assume that this process is taking place continuously and that the effective

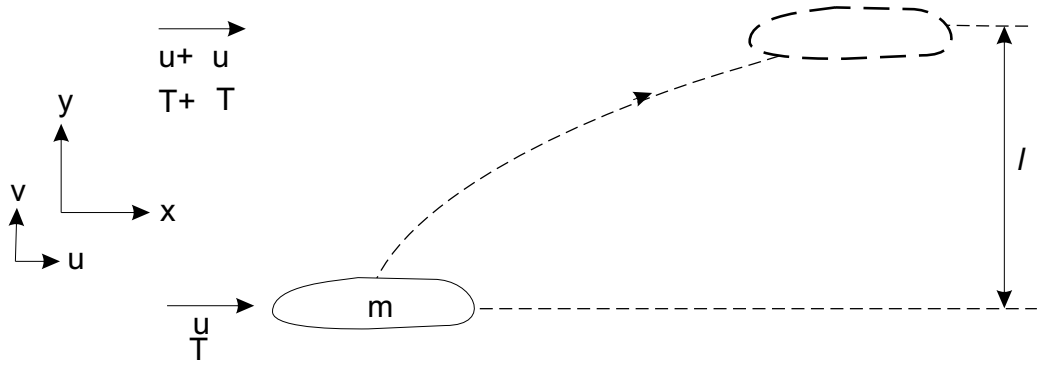

Figure 2.4: Turbulent exchange model on which the Reynolds analogy is based.

continuous velocity in the y-direction is $C\sqrt{\overline{v'^2}}$, with v' the instantaneous velocity component in the y-direction and C is a constant. The effective turbulent shear stress must be:

$$\tau_t = C\sqrt{\overline{v'^2}}\rho \cdot \delta\overline{u} \tag{2.53}$$

and the effective turbulent heat flux:

$$q_t'' = C\sqrt{\overline{v'^2}}\rho c \cdot \delta\overline{T} \tag{2.54}$$

c is the specific heat and $\overline{T}$ is the average temperature of the surrounding fluid.
If the Prandtl mixing-length is relatively small compared to the other dimensions of the system then: $\delta\overline{u} = l\frac{d\overline{u}}{dy}$ and $\delta\overline{T} = l\frac{d\overline{T}}{dy}$. By rearranging and using the definition for ϵ_M and ϵ_H: $\frac{\tau_t}{\rho} = \epsilon_M\frac{d\overline{u}}{dy}$ and $\frac{q_t''}{\rho c} = \epsilon_H\frac{d\overline{T}}{dy}$, this leads to:

$$\epsilon_M = \epsilon_H = C\sqrt{\overline{v'^2}}l \tag{2.55}$$

This Reynolds analogy is a considerable simplification of a very complex process. However it is a reasonable and convenient approximation for real fluids for $Pr > 0.5$. For the case of $Pr = 1$, constant core velocity U_∞ and constant wall temperature, the Reynolds analogy can also be expressed as:

$$St = \frac{f}{2} \tag{2.56}$$

The velocity and temperature profiles are as sketched in figure 2.5 [Kay and Nedderman, 1985; Kays and Crawford, 1980].

2.9.2 The film model

Some useful predictions can also be obtained by the film model. This film model assumes a laminar layer of thickness δ adjacent to the wall, the thickness of this laminar layer is much smaller than the diameter of the tube. In this laminar layer the transport takes only place by molecular processes. The central core is assumed to be perfectly mixed, so that the temperature and velocity are assumed to be constant in the turbulent core. The laminar boundary layer is so small compared to the tube, that a linear profile can be assumed for the velocity and the temperature, as shown in figure 2.6. The velocity gradient is then given by $\frac{U_\infty}{\delta}$ and the temperature gradient by $\frac{T_w - T_\infty}{\delta}$. The transport in the laminar layer is assumed to take place only by molecular processes, and so the wall shear stress, τ_w, becomes:

$$\tau_w = \eta\frac{U_\infty}{\delta} \tag{2.57}$$

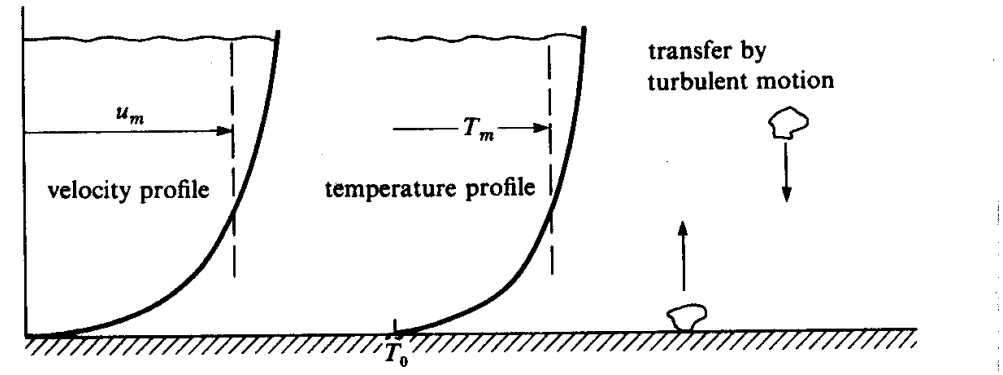

Figure 2.5: Velocity and temperature profile according to the Reynolds analogy [Kay and Nedderman, 1985]

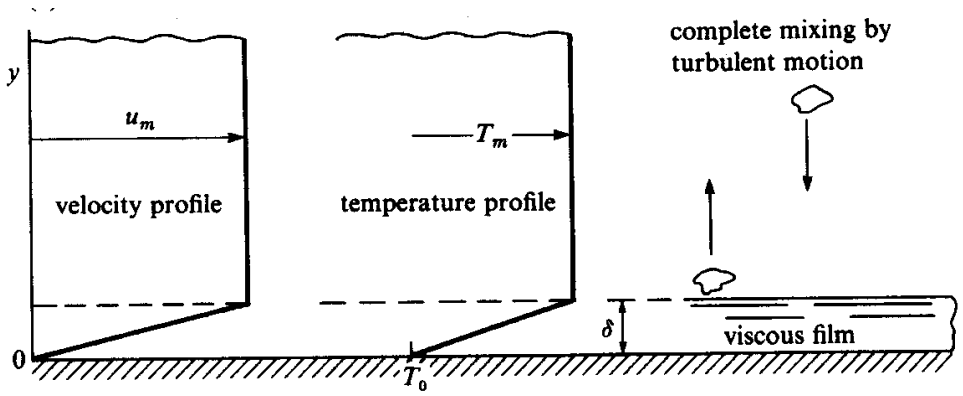

Figure 2.6: Velocity and temperature profile according to the film model according to [Kay and Nedderman, 1985]

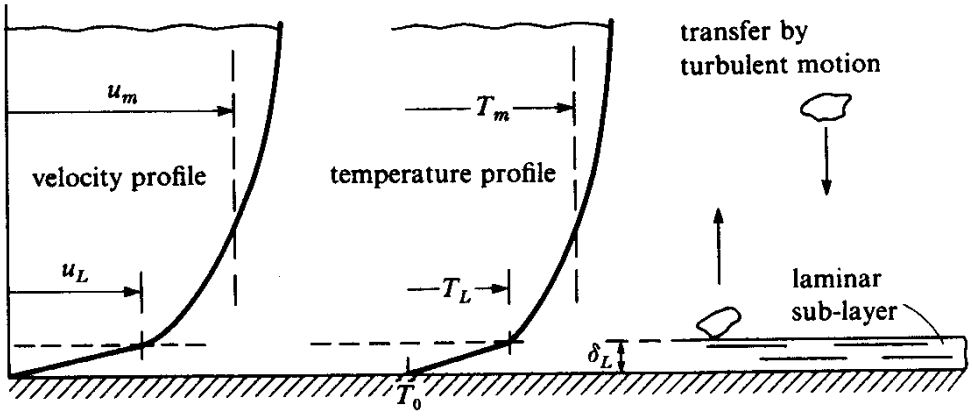

Figure 2.7: Velocity and temperature profile according to Prandtl-Taylor analogy

and for the rate of heat transfer per unit area we find:

$$q''_w = \lambda \frac{T_w - T_\infty}{\delta} \tag{2.58}$$

With these results the Nusselt- and Stanton number can be calculated, and finally we obtain:

$$StPr = \frac{f}{2} \tag{2.59}$$

In the case of $Pr = 1$ the film model and Reynolds analogy agree with each other. For other values of the Prandtl the models differ, but it is usually found that the experimental values lie between the two predictions. [Kay and Nedderman, 1985]

2.9.3 The Colburn analogy

In section 2.9.1 and 2.9.2 we considered two models that cannot both be correct, because they take opposite views of the nature of turbulent flow. If we recall the results obtained for the laminar boundary layer on a flat plate, we divide equation (2.22) on both sides by the product $Re_x Pr^{1/3}$ and obtain:

$$\frac{Nu_x}{Re_x Pr^{1/3}} = \frac{0.332}{Re_x^{1/2}} \tag{2.60}$$

This leads, together with equation (2.20) to the following expression:

$$StPr^{2/3} = \frac{f}{2} \tag{2.61}$$

Colburn applied this analogy to a wide range of data for flow and configurations. He found it to be quite accurate as long as there was no form drag and $0.5 < Pr < 50$. This analogy is therefore called the Colburn analogy.

2.9.4 The Prandtl-Taylor analogy

As can be seen in figure 2.7 the Prandtl-Taylor analogy is in effect the film model and the Reynolds analogy in series. In the laminar layer the transport is by molecular processes and in the turbulent

core eddy transport dominates. For the laminar layer we can use equations (2.57) and (2.58), but with the temperature, T_L and velocity, u_L at the edge of the laminar layer instead of that in the core. For the turbulent core the equations (2.53) and (2.54) are adapted into:

$$\tau_t = C\sqrt{\overline{v'^2}}\rho \cdot (U_\infty - u_L) \tag{2.62}$$

$$q''_t = C\sqrt{\overline{v'^2}}\rho c \cdot (U_\infty - u_L) \tag{2.63}$$

Rearranging of these equations results in:

$$\frac{f}{2} = St\{(Pr-1)\frac{u_L}{U_\infty} + 1\} \tag{2.64}$$

According to [Kay and Nedderman, 1985] an estimate for the ratio $\frac{u_L}{U_\infty}$ is: $\frac{u_L}{U_\infty} = 8.2\sqrt{f}$. This leads to:

$$St = \frac{\frac{1}{2}f}{1 + 8.2\sqrt{f}(Pr-1)} \tag{2.65}$$

In this estimation the thickness of the laminar layer is overestimated, for flow in a smooth pipe with $Re < 10^5$ the following, more accurate, expression may be used [Kay and Nedderman, 1985]:

$$\frac{u_L}{U_\infty} = 1.5Re^{-1/8}Pr^{-1/6} \tag{2.66}$$

This leads to:

$$St = \frac{\frac{1}{2}f}{1 + 1.5Re^{-\frac{1}{8}}Pr^{-\frac{1}{6}}(Pr-1)} \tag{2.67}$$

2.9.5 Comparison of the analogy models

For $Pr = 0.7$, as in air, the relation between the Stanton number and the friction factor is plotted in figure 2.8 for the different analogies that were presented in the preceding sections. We see in this figure that equation (2.65) agrees with the others only for small friction factors. The friction factor of tubes and plates is usually smaller than 0.02, but surfaces of heat exchangers can have friction factors up to 0.2. According to equation (2.67) the ratio between heat transfer and friction factor decreases when the Reynolds number increases.

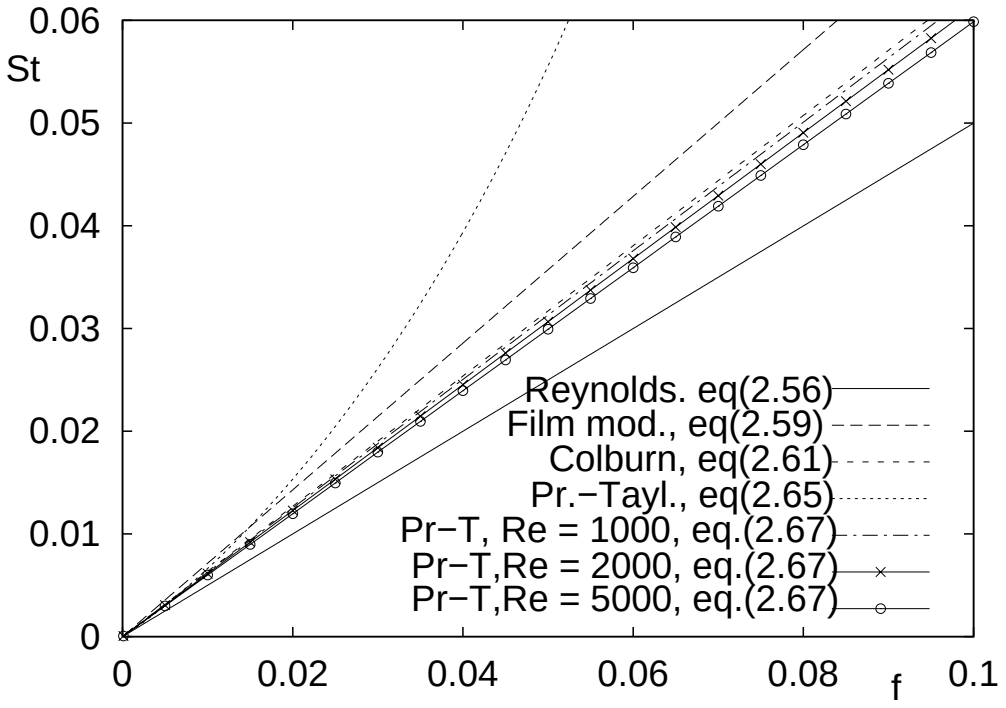

Figure 2.8: Comparison of the different analogies for the relation between the Stanton number and the friction factor. The Prandtl number is assumed to be 0.7.

Chapter 3

Friction measurements with a mass balance

The first plan to measure the friction of the wire cloths was to use a mass balance. Measuring the force that is exerted by the air on the wire cloth with a mass balance is the most direct way. In this chapter the results of these measurements are described. The theory of friction along a flat plate has already been discussed in section 2.5. In a perfect experiment the object would be placed in an infinite flow field to measure the friction. In the present experiments the object was placed in a tube through which air was blown, see also figure 3.4. To validate the experimental method and set-up the drag coefficient of two cylinders and a sphere was measured also, so that the experimental results could be compared with the theoretically expected values.
In section 3.1 the theory of the influence of a non-infinite flow field is given. The set-up for these experiments are described in section 3.2 and the results of the measurements are given in section 3.3.

3.1 Theory on the influence of a non-infinite flow field

The drag on an object is not the same for an object in a bounded fluid as in an infinite fluid.

1. The enclosure walls change the boundary conditions for the equations of motion and continuity of the surrounding fluid. Instead of the condition of uniform flow remote from the particle, containing walls impose conditions which must be satisfied at definite boundaries.
2. Another aspect is that when the cross-section of the flow is partially blocked by the object, the velocity increases with increasing blockage and separation of vorticity occurs from the channel walls.
3. The impermeability of the wall gives an irrotational constraint to the object wake which cannot spread without limit.

The effect of the walls can be expressed with a correction factor, k, so that: $F_D = k \cdot F_\infty$, in which F_∞ is the drag force on the object in an infinite fluid, whereas F_D is the drag force on the same object in the bounded fluid. The reason that in this relation the drag force is used instead of the

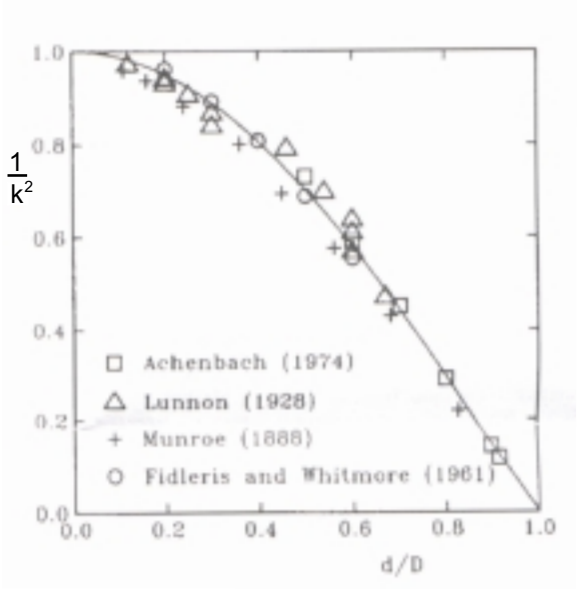

Figure 3.1: The correction for a sphere in a bounded fluid, expressed as $1/k^2$, experimental and theoretical results.

drag coefficient is that the latter can be based on the mean approach velocity or on the velocity at the minimum free flow area, which creates ambiguity.
The problem of a sphere falling through a fluid has already been treated by Newton [Newton, 1687]. He conducted experiments with spheres in circular, square and rectangular containers. The result of these experiments and an extensive theoretical reasoning led to:

$$k = (\frac{A}{A - \frac{\pi d^2}{4}})^2 (\frac{A}{A - \frac{\pi d^2}{8}}) \tag{3.1}$$

In this equation is A the cross-section of the tube and d the diameter of the sphere. The first term is the correction for the increase in velocity due to partial blocking of the container.
There is an excellent agreement between this expression and experimental data, as shown in figure 3.1 [Di Felice et al., 1995]. However, this equation was derived for the case of a sphere moving through a stagnant fluid.
According to [Clift et al., 1978] the results of investigations for different configurations (free settling spheres in an undisturbed fluid, fixed spheres in a moving fluid, spheres in an upward-flowing fluid) are in remarkably good agreement. For Re in the range from roughly 100 to 10^4, k seems to be independent of Re and given within 6% by equation (3.2) for $\lambda \leq 0.6$:

$$k = \frac{1}{1 - 1.6\lambda^{1.6}} \tag{3.2}$$

in which the blockage ratio $\lambda = \frac{d}{D}$ is the diameter of the sphere divided by the diameter of the tube. For particles in ducts of noncircular sections, one usual defines D as the conventional hydraulic diameter, but the accuracy of this approximation does not appear to have been seriously assessed. Similarly according to [Feng et al., 1994] the flow around a cylinder fixed between two parallel walls is equivalent to steady settling of a cylinder through a quiescent fluid in a vertical channel.

Achenbach [Achenbach, 1974] studied the effects of tunnel blockage on the flow past spheres. His problem was to determine whether, for high blockage ratios, a critical Reynolds number existed, above which the drag considerably drops. In his experiments he used a sphere in a cylindrical tube, the sphere was mounted onto a balance to measure the force. In figure 3.2 the drag coefficient f

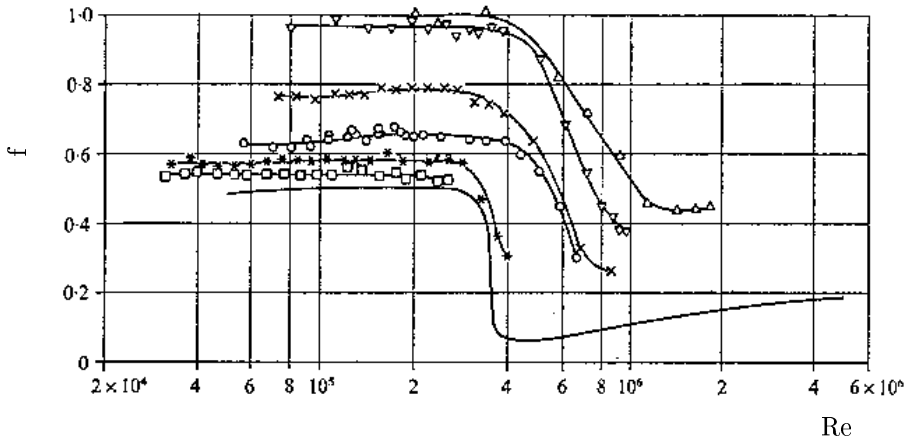

Figure 3.2: Drag coefficient versus Reynolds number for a sphere at various blockage ratios. −, d/D = 0; □, d/D= 0.5; ∗ d/D = 0.6; ∘, d/D = 0.7; ×, d/D = 0.8; ▽, d/D = 0.9; △, d/D = 0.916

is plotted as a function of the Reynolds number. In this figure $f = \frac{F}{\frac{1}{2}\rho U_f^2 \frac{\pi}{4} d^2}$, in which F is the force that is exerted on the object, ρ is the density of the air, U_f is the velocity at the minimum free flow area and d is the diameter of the sphere. The Reynolds number is based on the diameter of the sphere and the velocity at the minimum free flow area, U_f. The friction factor is calculated by dividing it by the velocity at the minimum free flow area, and therefore the correction factor for the increase in velocity is not taken into account in figure 3.2.

The curve that provides the best fit to the experimental results is given by equation (3.3). In this equation the correction factor for the higher velocity is taken into account, so that this correction factor can be compared with equation (3.1) and (3.2).

$$k = \frac{1 + 1.45(\frac{d}{D})^{4.5}}{(1 - (\frac{d}{D})^2)^2} \tag{3.3}$$

This equation is experimentally confirmed for the blockage range $0.5 < \frac{d}{D} < 0.92$.

The results of [Clift et al., 1978] (eq.3.2), [Newton, 1687] (eq.3.1) and [Achenbach, 1974] (eq.3.3) are plotted in figure 3.3. In this figure some experimental data are plotted from an experiment in which the drag exerted by the walls of a cylindrical vessel was measured. The drag is given for Reynolds number between 0.05 and 20000 [Fidleris and Whitmore, 1961].

3.2 Experimental set-up

The experimental set-up was designed and constructed to measure only the friction on the wire cloths. The original plan was that it would be modified later to allow measurements of the heat transfer as well. The most direct way to measure the friction factor is by measuring the force that is exerted on the wire cloth. Therefore a mass balance was used to measure the mass of a wire cloth in an airstream at several air velocities. By measuring the apparent weight of the wire cloth with and without air flowing along it, the force that is exerted on the cloth by the air can be calculated.
In figure 3.4 a sketch of the front view of the set-up is drawn.
Pressurized air flows via a tube to the set-up; it enters the set-up in a barrel and flows via two

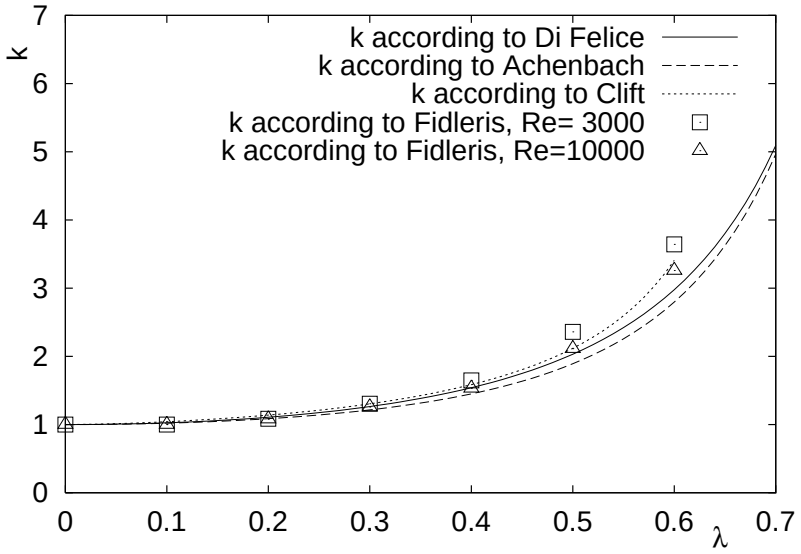

Figure 3.3: The wall correction factors according to equations (3.1), (3.2) and (3.3)

.

sinterplates into the measurement section. The purpose of the sinterplates is to equalize the flow field, so that it enters the set-up almost homogeneously, see for this section 3.2.1. The barrel could be used in future measurements when particles might have to be added to the air for flow visualization or LDA. The wire cloth, of which the drag force has to be measured, is suspended in the tube and is hitched onto the mass balance, so that its weight can be measured.
The wire cloth cannot be hitched onto the mass balance directly, because then the mass balance should be placed straight above the tube. That is why the wire cloth is hitched via a wire onto a small bar, that is connected to the mass balance. In the first measurements this bar hinges around a fulcrum to pass on the force from one end of the bar to the other. After some unexpected measurement results the set-up was changed to be sure that the resistance of the fulcrum did not have any influence on the measurements: the bar was kept in equilibrium by a counterweight on the other side. The weight of the wire cloths, and of the counterweight, the bar and the wire are measured first without airflow and subsequently for different values of the velocity of the air along the cloth.
As the air flows along the cloth, a force is exerted on the cloth and its weight seems to be lower. From the mass difference, Δm, that is measured by the mass balance the force of the air on the cloth, F_D can be calculated as well as the friction factor, f.

$$f = \frac{F_D}{\frac{1}{2}\rho v_f^2 \cdot A_{cloth}} = \frac{\Delta m \cdot g}{\frac{1}{2}\rho v_f^2 \cdot A_{\perp}} \tag{3.4}$$

The velocity that is used is the velocity at the minimum flow area. The area of the cloth, A_{cloth} is used as characteristic area.
The setup is also used to measure the drag force on cylinders and spheres, suspended in the set-up in a similar way. In the calculation of the drag coefficient of a cylinder or a sphere the same equation is used, but with the cross-sectional area instead of the longitudinal surface and for the velocity the mean approach velocity, v_0. Also the dimensionless number that is calculated is called drag coefficient instead of friction factor.

$$C_D = \frac{F_D}{\frac{1}{2}\rho v_0^2 \cdot A_{obj}} \tag{3.5}$$

In the measurements where a hevel is used to pass on the force to the mass balance, the measured

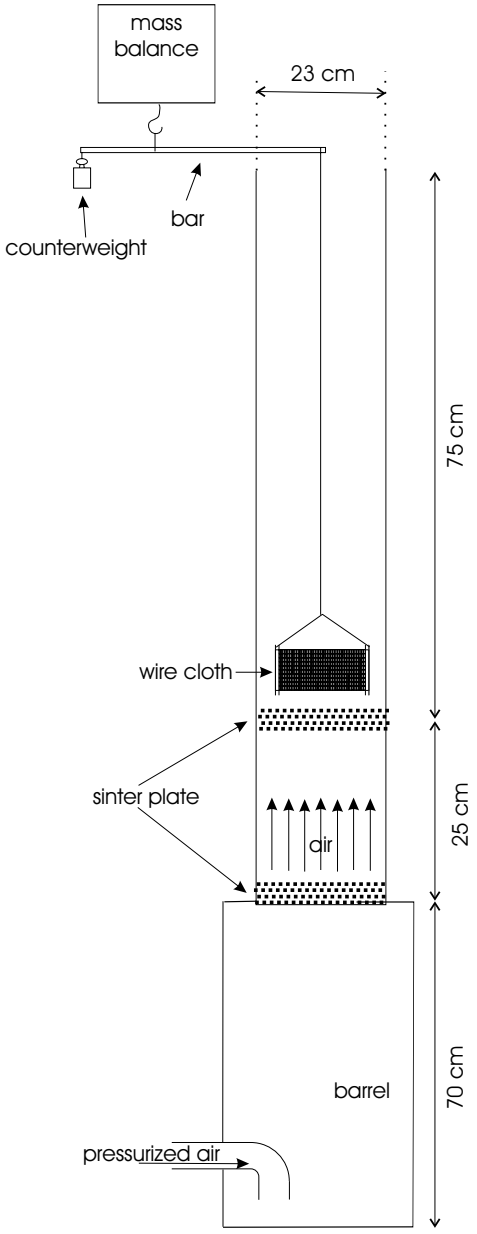

Figure 3.4: Sketch of the set-up with the mass balance.

mass difference at the mass balance should logically be multiplied by the ratio of the lengths of the arms.
The airflow is measured with a mass flow meter before the air enters the set-up. The unhindered velocity of the air, v_0 is calculated by dividing the mass flow, ϕ_m, by the density, ρ and the cross-sectional area of the tube, A_{tube} as in equation(3.6).

$$v_0 = \frac{\phi_m}{\rho A_{tube}} \tag{3.6}$$

In most cases the bar which holds the object should also be taken into account, since the air from the tube flows also against this bar; this causes an extra drag force. Only in a few measurements where the tube was half covered at the top, this extra force could be left out of calculation. The length of the bar above the tube is 10.0 cm and its diameter is 4.0 mm. The drag coefficient for a cylinder with this ratio between length and diameter is $C_{D,bar0} = 0.97$. The force on the bar becomes:

$$F_{bar} = C_{D,bar0} \cdot \frac{1}{2}\rho v_0^2 \cdot L_{bar} \cdot d_{bar} \tag{3.7}$$

in which $C_{D,bar0}$ is the drag coefficient in an infinite flow field, based on the area of the bar. The total force that is measured is the sum of this force, F_{bar} and the drag force on the object, F_{obj} and this total force is used to calculate the apparent drag coefficient of the object with equation (3.8):

$$C_D = \frac{F_{bar} + F_{obj}}{\frac{1}{2}\rho v_0^2 A_{obj}} \tag{3.8}$$

in which A_{obj} is the characteristic area of the object: the cross-sectional area in the case of a cylinder or sphere, the longitudinal area in the case of a wire cloth. The drag coefficient that is calculated in this way can in fact be split into $C_{D,obj}$ and $C_{D,bar}$. The drag coefficient due to the drag on the bar is:

$$C_{D,bar} = C_{D,bar0} \cdot \frac{L_{bar} \cdot d_{bar}}{A_{obj}} \tag{3.9}$$

This elaboration is described for the drag coefficient, but is also valid for the friction factor, f. In table 3.1 the extra term in the drag coefficient due to the friction on the bar is given for the different objects that are used.

object	object area (m^2)	$C_{D,bar}$
cylinder (small)	$1.2.10^{-3}$	0.33
cylinder (large)	$2.7.10^{-3}$	0.21
pingpong ball	$1.1.10^{-3}$	0.36

Table 3.1: The term in the apparent drag factor that is due to the force on the bar above the tube.

3.2.1 Sinterplates

The function of a sinterplate is to equalize pressure differences in the flow. With axial flow onto the plate, the highest pressure is expected to be in the middle. The deviation of the mean pressure is given by:

$$p_{max} - \bar{p} = \frac{1}{2}\rho v_{as}^2 \tag{3.10}$$

[Remery, 1997] The air flows into the barrel (see figure 3.4) from a round nozzle and forms a circular turbulent jet. Experimentally, for the maximum velocity, u_{max}, in the middle of a jet, the

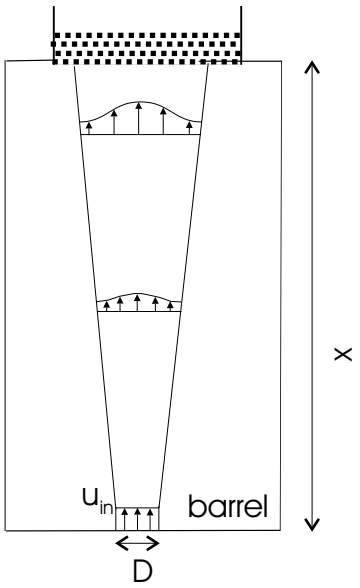

Figure 3.5: Sketch of the jet that is used for the calculation of the pressure difference.

following was found:

$$\frac{u_{max}}{u_{in}} = 6.3\frac{D}{x} \tag{3.11}$$

u_{in} is the velocity of the air at the outlet of the nozzle, D is the nozzle diameter and x is the distance from the nozzle in the direction of flow [Akker, 2000]. If the velocity in the measurement section should be 3.5 m/s, the air leaves the nozzle with a velocity of 17 m/s. In the calculation the jet is assumed to enter the barrel vertically in the direction of the sinterplate (see figure 3.5, in reality the velocity is slowed down more, because of the change in direction it has to make). The length of the jet is taken to be 70 cm and the nozzle diameter 6 cm. The maximum velocity in the center of the plate becomes 10 m/s which corresponds to a pressure difference of 50 Pa. The pressure drop over the plate should be larger than this pressure difference [Remery, 1997]. In the set-up two sinterplates of 3mm thickness are used, that each have a pressure drop of 300 Pa at a mean velocity in the tube of 3.5 m/s.

3.3 Results

In this section the results of the experiments are presented. In the beginning only a few test measurements were done with the wire cloths. Because this led to unexpected results, subsequently most measurements were done with cylinders or a pingpong-ball. In this way the results could be compared with values from literature to determine the reliability of the measurements. The results for the cylinders are discussed first in section 3.3.1 and the results for the sphere in section 3.3.2. To determine the influence of the bar which holds the object in the tube, the drag on the bar was also measured without an object in the tube, in section 3.3.3. Because of the also unexpected and unexplained results for the friction of the cylinders and sphere, this set-up was not used any further to measure the friction of the wire cloths.

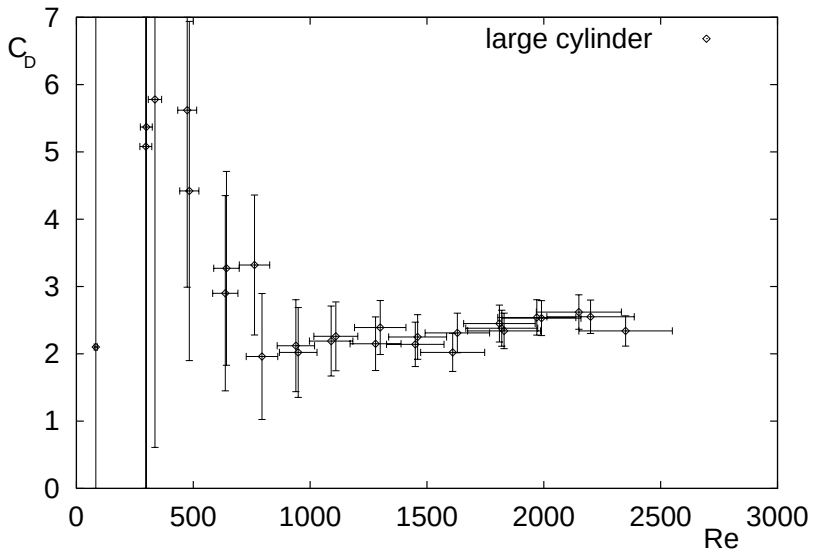

Figure 3.6: The drag coefficient of a cylinder plotted against the Reynolds number

3.3.1 Drag coefficient of a cylinder

Two cylinders were used for this measurements, a larger and a smaller one with almost the same length to diameter ratio. The larger measured 12.3 x 2.2 cm, the smaller measured 7.9 x 1.5 cm. Note that the cross-sectional area of the measurement section was 23.0 x 6.0 cm. The experiments were done at different circumstances: the placement of the cylinder higher or lower in the tube, while the upper exit of the tube tube was half covered etc. In figure 3.6 the drag coefficient of the cylinder is plotted against the Reynolds number for one of the measurements. The latter is based on the diameter of the cylinder. The drag coefficient is based on the mean approach velocity.
At the low Reynolds numbers the value of the drag coefficient is very high, but the uncertainty in the measurements is also high, since the force and the friction are both very small, so that the relative uncertainty becomes this high. They are plotted anyway to give a complete image of what is measured.
According to the theory the drag coefficient should be constant for $10^3 < Re < 10^5$. In the next table 3.2 therefore the averaged measured drag coefficients are given for $Re > 10^3$ in different experiments as well as their 1 σ-uncertainties, $u(C_D)$.

size cylinder	lever	details	dragcoefficient, C_D	$u(C_D)$
large	x	·	2.3	0.3
large	x	·	2.4	0.3
large	x	sides of cylinder were open	2.0	0.2
large	x	·	2.4	0.3
small	x	placed low and left in the tube	3.1	0.2
small	x	placed low in the tube	3.8	0.4
small	x	placed high in the tube	3.6	0.6
small	x	placed high in the tube	3.0	0.3
small	·	·	3.1	0.3
small	·	tube half covered at the end	2.5	0.3
small	·	tube made smaller	3.3	0.3

Table 3.2: Drag coefficients, C_D, and uncertainties $u(C_D)$, from the experiments with the cylinders

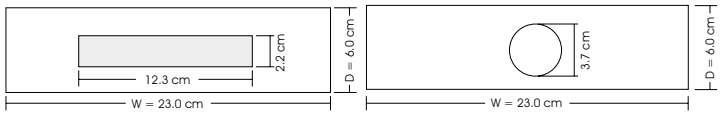

(a) Large cylinder (b) Ping-pong ball

Figure 3.7: Horizontal cross-section of an object in the tube

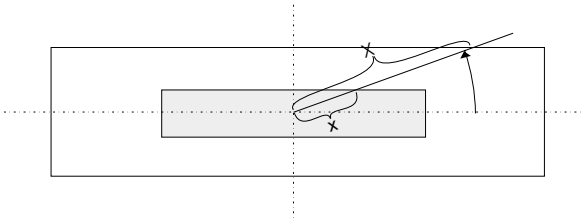

Figure 3.8: Horizontal cross-section of the cylinder in the tube with the direction of view

The drag coefficient of a cylinder depends on the ratio between the length and the diameter. The ratio of the length and the diameter is for both cylinders about the same, their theoretical drag coefficient has therefore also the same value, $C_D = 0.8$. [Janssen and Warmoeskerken, 1987]
This value is for a cylinder in an infinite flow field which is not the case here. To adapt this theoretical value to be valid for flow in a finite tube, the equations from section 3.1 are used. In the table 3.3 an overview is given of the correction factors and theoretically expected drag coefficients that are obtained in this way. The equations for the correction factors that are used in this table are meant for the drag coefficient on a sphere. When these equations are used to describe the drag force on a cylinder, the variable in the equations to calculate the correction factor is the ratio between the characteristic horizontal length scale of the cylinder and that of the tube, but which length should be taken for the characteristic horizontal length scale is not clear.
In spite of all this, the correction equations for bounded flow are still used to give an idea of what we can expect from the influence of the boundaries. For the diameter ratio, λ, different values are used: the ratio of the hydraulic diameters, the ratio of the diameter of the cylinder and the depth, D, of the tube and the ratio of the length of the cylinder and the width, W, of the tube, see table 3.2.
In figure 3.7 (a) a horizontal cross-section is drawn of the large cylinder in the tube.
Clearly, the precise choice of the value of λ has a large influence on the value of the correction factor k. In order to estimate what would be the best correction factor, it is integrated over the angle of the direction in which the ratio of the lengths of the cylinder and tube are taken. Figure 3.8 makes this more clear, where x is the length of the cylinder and X the length of the tube. The mean correction factor can then be expressed, with $\lambda = \frac{x}{X}$, as:

$$k = \int_0^{\frac{\pi}{2}} k(\lambda) d\phi \tag{3.12}$$

The correction factors and drag coefficients that were obtained in this way are also given in table 3.3.

From the results in table 3.2 the mean measured drag coefficient can be calculated. For the large cylinder the mean measured drag coefficient is 2.3. The drag coefficient from the measurement in which the sides of the hollow cylinder were open, is slightly lower than in the other measurements. The correction factor, from table 3.3, varies between 1.4 and 2.4 for the large cylinder, but according

correction equation	λ	large cylinder		small cylinder	
		k	C_D	k	C_D
$k = \frac{1}{1-1.6\lambda^{1.6}}$ (3.2)	$\frac{D_{H,cyl}}{D_{H,tube}}$	1.6	1.2	1.2	1.0
	$\frac{d_{cyl}}{D}$	1.5	1.2	1.2	1.0
	$\frac{L_{cyl}}{W}$	2.4	1.9	1.4	1.1
	acc. to (3.12)	1.6	1.2	1.4	1.1
$k = \frac{1+1.45(\frac{d}{D})^{4.5}}{(1-(\frac{d}{D})^2)^2}$ (3.3)	$\frac{D_{H,cyl}}{D_{H,tube}}$	1.4	1.1	1.2	0.9
	$\frac{d_{cyl}}{D}$	1.4	1.1	1.1	0.9
	$\frac{L_{cyl}}{W}$	2.1	1.7	1.3	1.0
	acc. to (3.12)	1.5	1.2	1.3	1.0
$k = (\frac{A}{A-A_{cyl}})^2(\frac{A}{A-\frac{A_{cyl}}{2}})$ (3.1)		1.7	1.4	1.3	1.0

Table 3.3: The correction factors and theoretically expected drag coefficients for a cylinder in a bounded fluid

to equation (3.12) between 1.5 and 1.6. The drag on the bar above the tube increases the apparent drag coefficient of the cylinder with 0.21 (see table 3.1). The total measured drag coefficient of the large cylinder, inclusive the correction for the bar and the correction factor for the walls, is therefore expected to be: $1.3 < C_D < 2.2$ (i.e. $0.8 * 1.4 + 0.21 < C_D < 0.8 * 2.2 + 0.21$) , but probably between 1.4 and 1.5. The average measured value of 2.3 lies above these two ranges.
The mean measured drag coefficient for the small cylinder is 3.3 (the measurement of the small cylinder while the tube was half covered is left out of consideration), but they lie between 3.0 and 3.8. The two measurements just above the sinterplate give a drag coefficient of 3.0 left in the tube and 3.8 in the middle of the tube. Drag coefficients measured higher in the tube differ from 3.0 to 3.6. The theoretical drag coefficient is also 0.8, but the influence of the bar above the tube is now 0.33. The correction factor lies between 1.1 and 1.4. When the drag coefficient is calculated with equation(3.12) the correction factor lies between 1.3 and 1.4. This leads to a theoretically expected measured drag coefficient between 1.2 and 1.5, but probably between 1.3 and 1.4. The measured drag coefficient is about two times as high as this value.
The drag coefficient for the small cylinder when the tube was covered at the end (so that the air could not flow against the bar) was 2.5, also about two times as high as expected after correction for the finite tube dimensions. The difference between this measurement and the average of the other measurements is 0.8, while the influence of the friction on the bar should only be 0.33.

3.3.2 Drag coefficient of a sphere

The sphere in this experiments was a pingpong-ball. A pingpong-ball is almost spherical, but has a seam where its two halves are joined. It is filled with gas and therefore very light. When the air velocity became too high, the ball began to swing. In most measurements therefore a pingpong-ball was used that was filled with water to prevent it from swinging at low velocities.
In figure 3.9 the results are shown of two measurements of the drag coefficient of the pingpong-ball against the Reynolds number. As characteristic diameter in the Reynolds number the diameter of the sphere is used. In the calculation of the drag coefficient the mean approach velocity is used.
The same remarks as for the drag coefficient around a cylinder can be made for the drag coefficient around a sphere at low Reynolds numbers. The theoretical curve of the drag coefficient of a sphere looks slightly different from that of a cylinder. It tends to decrease until $Re \approx 2500$, stays more or less constant and begins to increase slightly again at $Re \approx 9000$. When we look at figure 3.9 we could say this is how the measured drag coefficient also behaves, but this is highly doubtful. The Reynolds range is too small to draw conclusions concerning the form of the curve of the drag

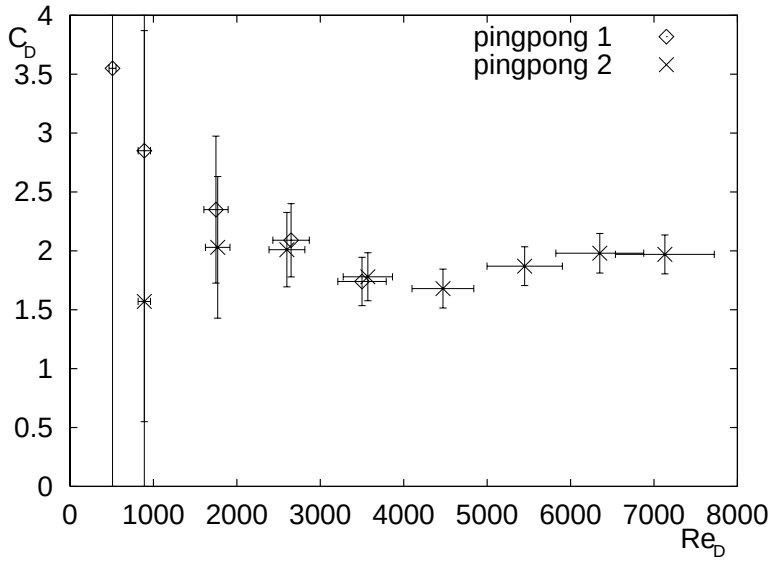

Figure 3.9: Drag coefficient of two measurements of pingpong-balls

coefficient. Apart from this the theoretical drag coefficient of a sphere is much lower than the results of this measurement.
The averaged experimental values of the drag coefficient in this Reynolds-region are given in table 3.4. The averaged drag coefficient is 2.2, but the result of the measurement with a smaller tube is 1.8 and the result when the tube was covered is 1.4.

weight	details	dragcoefficient, C_D	$u(C_D)$
light	one side of balance was open	2.1	0.3
heavy	one side of balance was open	1.9	0.2
heavy	·	2.0	0.2
heavy	tube half covered at the end	1.4	0.2
heavy	·	2.5	0.3
heavy	extra tape on the pingpong ball	2.3	0.3
heavy	tube made smaller	1.8	0.2

Table 3.4: Experimental drag coefficients, C_D, and uncertainties $u(C_D)$, from the experiments with the pingpong-ball

The drag coefficient is not the same for a sphere in bounded flow as for a sphere in an infinite flow field. The correction factors and drag coefficients for flow in a bounded fluid that were obtained with the equations from section 3.1 are given in table 3.5. Equations (3.2) and (3.3) are meant to be used with a sphere in a circular tube. The tube in this experiment is rectangular, with quite a large ratio between the long and the short side. The correction factors are therefore given for different values of λ, in which as diameter of the tube the hydraulic diameter, the width of the tube and the horizontal length of the tube are used. The correction factor of the walls for the drag coefficient of a pingpong-ball is also calculated using equation(3.12).
The theoretical drag coefficient of a sphere between $Re = 10^3$ and $Re = 3 \cdot 10^5$ is approximately $C_{D,pp} = 0.47$ [Janssen and Warmoeskerken, 1987]. After multiplying this value with the correction factors and adding 0.36 as the influence of the bar, the theoretically expected value of the drag coefficient of a pingpong-ball measured in the present set-up lies between 0.8 and 2.2, but according to equation(3.12) between 1.2 and 1.3. The averaged measured drag coefficient coincides with the upper boundary of the first range, but is too high according to the last range of correction factors. The difference in drag coefficient for the measurement with and without flow against the bar is

correction equation	λ	pingpong-ball k	pingpong-ball C_D
$k = \frac{1}{1-1.6\lambda^{1.6}}$ (3.2)	$\frac{D_{pp}}{D_{H,tube}}$	1.6	0.73
	$\frac{D_{pp}}{D}$	3.9	1.9
	$\frac{D_{pp}}{W}$	1.0	0.47
	acc. to (3.12)	2.1	0.99
$k = \frac{1+1.45(\frac{d}{D})^{4.5}}{(1-(\frac{d}{D})^2)^2}$ (3.3)	$\frac{D_{pp}}{D_{H,tube}}$	1.4	0.67
	$\frac{D_{pp}}{D}$	3.1	1.5
	$\frac{D_{pp}}{W}$	1.0	0.47
	acc. to (3.12)	1.8	0.86
$k = (\frac{A}{A-A_{cyl}})^2(\frac{A}{A-\frac{A_{cyl}}{2}})$ (3.1)		1.2	0.60

Table 3.5: The correction factors and drag coefficients for a pingpong-ball in a bounded fluid

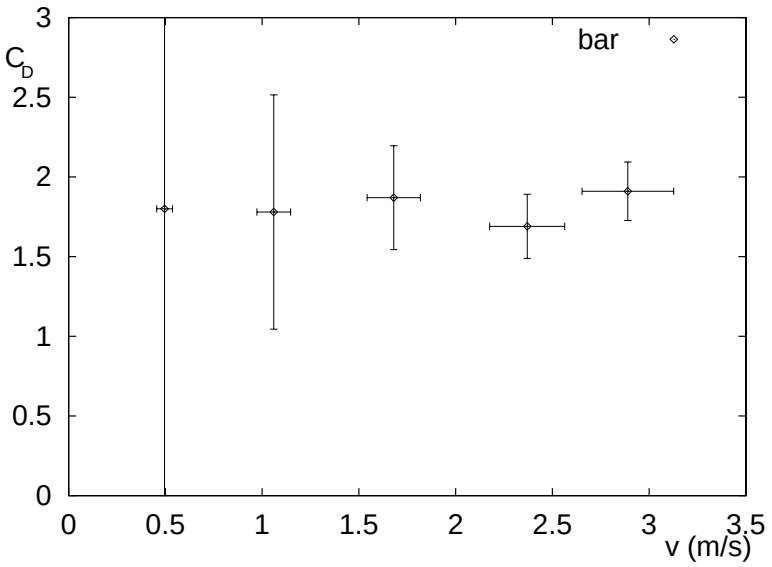

Figure 3.10: Drag coefficient the bar above the tube

0.8.

3.3.3 Drag coefficient of the bar above the tube

This measurement was done to determine the drag force of the air on the bar only. This force influences the measurement, because the balance measures a smaller mass when the air exerts a force on the bar. The measured drag coefficient of this bar is given in figure 3.10: The drag coefficient in this figure is based on the area of the bar, whose length is 10 cm and its diameter is 4 mm. The average drag coefficient on the bar is 1.8. The theoretically expected drag coefficient, based on the area of the bar, is 0.97. In the experiments the total force that is measured by the mass balance is used to calculate the measured drag coefficient. When the force on the bar is divided by $\frac{1}{2}\rho v^2 \cdot A_{obj}$, the influence of the bar on the drag coefficient is: 0.3 for the large and 0.6 for the small cylinder, and 0.7 for the pingpong-ball, as opposed to the theoretically expected influence as given in table 3.1.

3.3.4 Overview of the results

In this section the main results are summarized in table 3.6. In this table the averaged measured drag coefficients are given for the drag force on the object, inclusive the drag on the bar above the tube. Also, the results for an object in a covered tube are given, where there is no force on the bar. The range of correction factors are given, the theoretical drag coefficient for the object, inclusive the drag on the bar and the drag coefficient of the object only.

object	average measured C_D	av.meas. C_D (corrected for bar)	av.meas. C_D (corr. for bar and wall influence)	theoretically expected C_D
large cylinder	2.3	2.1	0.86 - 1.5	0.8
small cylinder	3.3	3.0	2.1 - 2.6	0.8
small cylinder (with cover)	2.5	2.5	1.8 - 2.2	0.8
pingpong-ball	2.2	1.8	0.47 - 1.7	0.47
pingpong-ball (with cover)	1.4	1.4	0.36 - 1.43	0.47
bar above tube	1.8	-	-	0.97

Table 3.6: Overview of the average measured drag coefficients and the theoretically expected value

3.4 Conclusions

The drag coefficients that result from the measurements are (much) higher than expected according to the theory. To find out what the reason is of this difference, the measurements were done with different configurations, for example a smaller tube, a different object, or the tube was covered to prevent the air from flowing against the bar above the tube.
The data from the measurements with the pingpong-ball are not in contradiction with the theoretical values, and the range of theoretically expected values for the large cylinder overlaps the uncertainty-range of the measurement. Other measurements, for example of the drag coefficient of the small cylinder are in contradiction with the theoretically expected values. But even if they would coincide with the theoretical expected values, this set-up can not be used for the experimental determination of the friction of the wire cloths. The influence of the wall is too uncertain, even while the friction on the wire cloth is less influenced by the wall, because of the smaller horizontal dimensions of the wire cloth.
Because of the necessity to connect the object to the balance and because of the accuracy of the balance, the object can not be made so small that its dimensions are negligible compared to the dimensions of the tube. The force on it would become too small compared to that on the bar and for the balance to measure. On the other hand, the tube cannot be made larger, because of the limited air flow that could be generated and the desired velocities.
Another aspect that makes it difficult to measure the force of the flow on the object, is that is has the tendency to start to swing if the velocity is getting higher.
There are still results that can not be explained. The measured, uncorrected drag coefficient of the smaller cylinder is higher than that of the large one. This is in contradiction with the expectation that the measured C_D of the large cylinder must be higher, because the effect of the confinement would be larger. As expected, the influence of the force on the bar on the apparent drag force on a cylinder is higher for a small than for a large cylinder, but this influence should not be as high

as measured.

Chapter 4

Second experimental set-up

Because the experimental set-up described in the previous section led to unsatisfactory results, a new second set-up was designed to measure two things: the friction factor of the air around the wire cloths and the heat transfer of the cloths to the air. The friction and heat transfer of flat plates were also measured to be able to compare experimental values with those from literature. Another reason for these flat plate measurements was that to substantiate the claim that the wire cloths have a better heat transfer to friction ratio than flat plates. The set-up that was used for the experiments with flat plates was the same as for the wire cloths and is described in this chapter, most of the time the word 'cloths' is used, were also 'plates' could have been meant.

In the fine wire heat exchanger itself, the cloths are placed around the fan, in such a way that the air flows along the cloths as can be seen in figure 1.4. In the experiment two types of wire cloths are used. These wire cloths are the same as the cloths in the Fiwihex prototypes and are described in section 4.1. The distance between the wire cloths can be adjusted. In the experiments the heat transfer and friction of both types of wire cloths is compared at a fixed distance between both wire cloths. For one type of wire cloths these measurements are also done at different distances between the cloths. The cloths are placed parallel to each other, see figure 4.1, and the airflow is made homogenous along the cloths. The experimental set up has to make sure that the flow flows between and parallel to the cloths.
The cloths are placed in a stack in a rectangular tube, with equal distance between them, so that they fill the whole tube. The splits between this bank of cloths and the tube wall are filled up, so that all the air has to pass between the cloths. At the end of the tube, a fan is placed to suck the air through the tube. The power of this fan can be regulated by regulating the voltage over it.
At the entrance of the tube and before the mass flow meter a kind of gauze is placed to make the airflow homogenous.
Warm water flows through the cloths to heat the air. The temperature difference of the air before and after the cloths is measured. The waterflow is also measured, see section 4.3.
The airflow is measured by a mass flow meter at the end of the tube. This mass flow meter is described in 4.4.
The preceding measurements are used to calculate the heat transfer. In section 4.5 this calculation is explained. For the calculation of the friction factor a pressure difference meter is used as can be read in section 4.6.

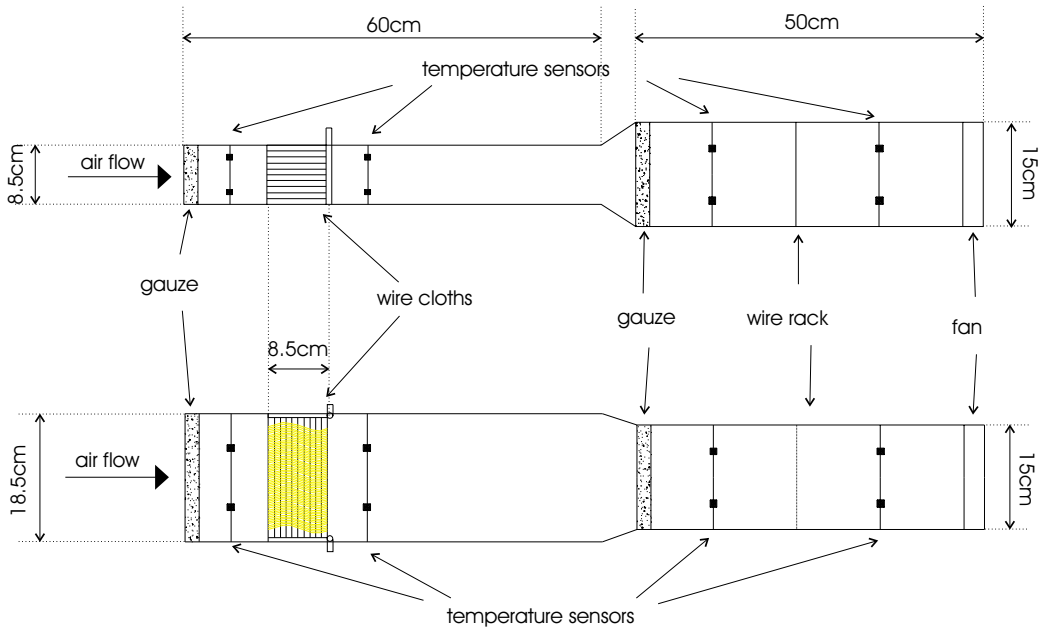

Figure 4.1: Sketch of the set-up

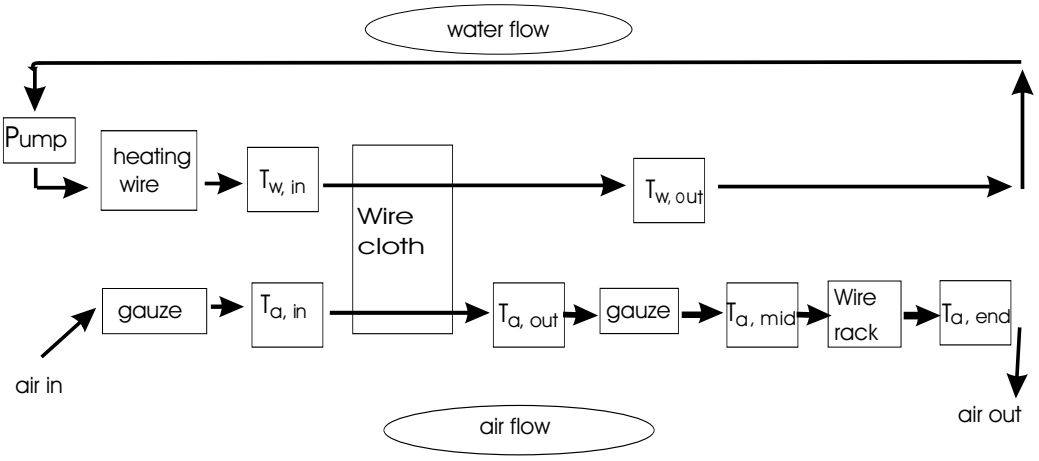

Figure 4.2: Schematic overview of the experimental set-up to measure the heat transfer

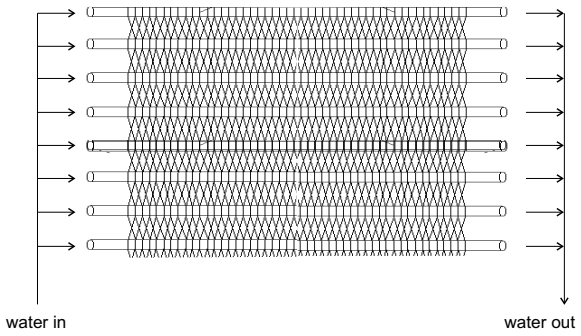

Figure 4.3: Sketch of the lay-out of one wire cloth.

4.1 Wire cloths

The heat transfer takes place in the wire cloths. These wire cloths are heated by warm water and transfer their heat to the air that flows along them. In figure 4.3 a part of the wire cloth is drawn schematically, in which eight capillaries can be seen (the horizontal tubes). The vertical wavy lines are copper wires of 100 μm diameter that are woven around the capillaries and soldered to them for a good heat transfer. The two types of wire cloths that are used in the experiments have the same size: 8.5 x 15 cm is the surface of the woven copper. They differ in the distance between the capillaries; this is 8 mm or 12 mm. Both ends of the capillaries are soldered to a tube of 6.8 mm diameter. Warm water flows into this tube via the capillaries to the other tube and heats the capillaries and the copper wires. This in turn heats the air that flows along the cloths.
The cloths have to be soldered to the tube by hand, therefore they are not always placed perfectly parallel to each other, only after soldering they could be bent a little, but this had to be done very carefully to prevent leakage. The cloths themselves are also not perfect: not all the wires are soldered to the capillaries, some have gone loose. For the measurements the best wire cloths were used, but they were not identical to each other.

4.2 Flat plates

The flat plates are similar to the wire cloths in as many aspects as possible. They have the same size, the same number of capillaries as the 8mm wire cloths and are made out of the same materials, see also figure 4.4. The flat plates consist of the same framework of capillaries as the wire cloths, with a flat thin ($0.1mm$) copper plates soldered onto the capillaries on both sides. The ten plates that were made, were used in two measurements: one with 8 plates and one with 10 plates.

4.3 Waterflow

Water flows through the capillaries of the wire cloth. This water is pumped round by a little pump. The water is heated by a copper wire, through which a current flows. The water flows via this copper wire into a header on which the smaller headers of the wire cloths are soldered. It then splits again to flow through all the capillaries and flows in the same way back to the water reservoir, from which it can be pumped round again. This can be seen in the upper part of figure 4.2. As reservoir a small, thermally insulated glass is used.

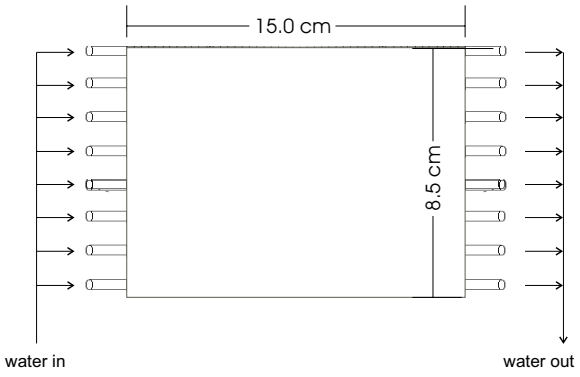

Figure 4.4: Sketch of the lay-out of one flat plate.

The pump that pumps the water can be regulated by the voltage over it. The velocity of the water however depends not only on the power of the pump, but also on the resistance of the wire cloths. In the first measurements the flow could not be measured during the measurement of the heat transfer, so that it had to be measured separately. To measure the velocity of the water flow that is obtained at a certain voltage over the pump, the water is led via the wire cloths to a measuring cup, instead of being pumped round. For different voltages over the pump the time is measured that it took to fill a certain part of the measuring cup. During the last measurements a water volume meter was available, so that the water flow could be measured at the same time as the friction and heat transfer.

4.4 Airflow

The airflow is measured by a mass flow meter in the tube. This meter consists of two sets of four temperature sensors and a wire rack. The air first passes four temperature sensors to determine the begin temperature, $T_{a,mid}$. After this the air flows through the wire rack. This wire rack is a kind of barred window in which the 'bars' of this window consist of copper wire, through which a current flows to heat the wire rack. The power, P_c, of this current is measured by a power meter. At the end, after the wire rack, the temperature of the air, $T_{a,end}$ is measured again by four temperature sensors. The mass flow, $\phi_{m,a}$ is calculated by equation (4.1):

$$\phi_{m,a} = \frac{P_c}{c_a(T_{a,end} - T_{a,mid})} \tag{4.1}$$

where c_a is the specific heat of the air. In order to calculate the air velocity through the stack of cloths, we have to divide ϕ_m by the density of air, ρ_a, and the minimum free flow area, A_f. The minimum free flow area is indicated in figure 4.5.
With this data, the Reynolds number can also be calculated:

$$Re = \frac{\rho_a v_a D_h}{\eta_a} \tag{4.2}$$

in which ρ_a is the density and η_a is the dynamic viscosity of the air. The hydraulic diameter, D_h is defined in equation(2.2).

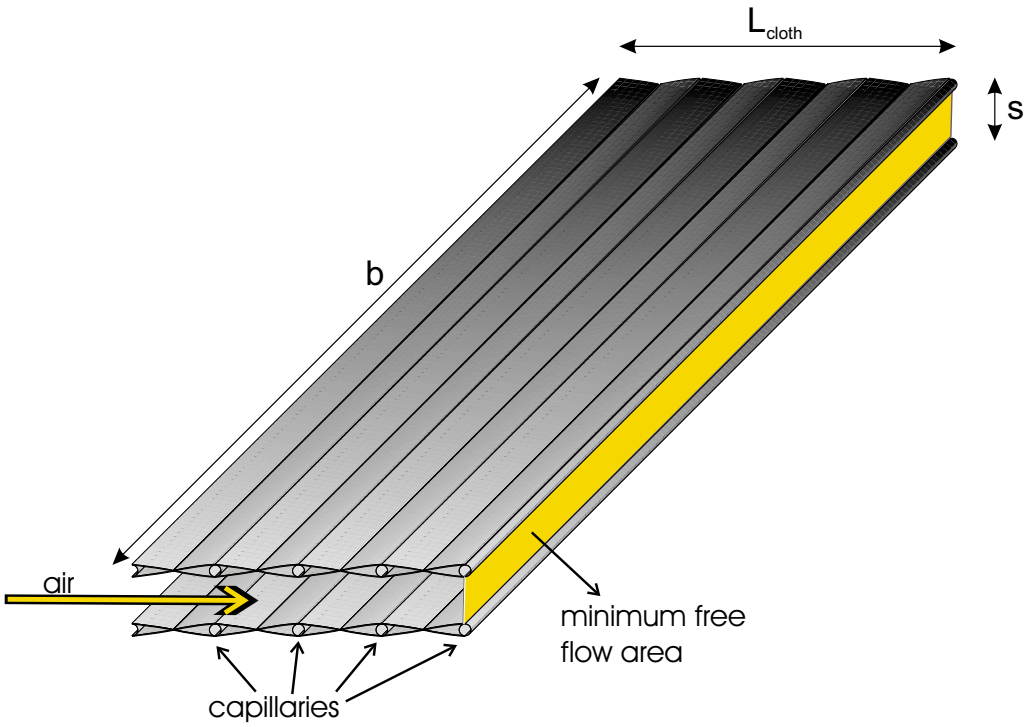

Figure 4.5: The minimum free flow area between the wire cloths

4.5 Heat transfer

As described in section 4.3, the water that is pumped through the capillaries of the wire cloth is heated by a copper wire. A power meter measures the power of this current, P_w. Heat is transferred from this warm water to the capillaries, from the capillaries to the wires of the wire cloth and from the wires to the air that flows along the cloth. The power of the copper wire is used to heat the water or to keep the temperature of the incoming water at a certain temperature. The water cools down during its flow trough the capillaries. The water temperature is measured before and after it flows through the cloths. The air that flows along the cloths is heated; the temperature of the air is measured before and after the wire cloths. These temperatures are measured by temperature sensors that are read by the computer. It takes about 2,5 second for every sensor, so that every 40 seconds all the temperature sensors in the set-up are read and saved to a file.

4.5.1 Calculation of the heat transfer coefficient

The heat transfer can in principle be calculated in three ways.
The first way is by measuring the power that is used to heat the water. The water reservoir and the tubes are isolated, so that the heat losses are limited. In steady state all the power that is put into the water is used to heat the air and to compensate for the remaining heat losses. The problem with this method is that it takes some time for the water to reach constant temperature (steady state situation). When the environment has no constant temperature the water also heats and it is not possible to say then whether this is due to the heating of the environment or that steady state is not yet reached.

The second way to calculate the heat transfer is by measuring the temperature difference between

the inflow and outflow of the water. To calculate the heat that is transferred to the air per second, P_a, equation (4.3) can be used:

$$P_a = \phi_{m,w} \cdot c_w \cdot (T_{w,in} - T_{w,out}) \tag{4.3}$$

The temperature difference of the water is quite small, about 0,3 K and the resolution of the temperature sensors is 0,1 K so that using this method gives an enormous uncertainty in the results.

The heat transfer should therefore be calculated by using the heating of the air. The heat per second that is transferred to the air is:

$$P_a = \phi_{m,a} \cdot c_a \cdot (T_{a,out} - T_{a,in}) \tag{4.4}$$

Using P_a from equation (4.4) the overall heat transfer coefficient can be calculated by dividing by the temperature difference between water and air. For this the logarithmic temperature difference, ΔT_{ln} is used:

$$\Delta T_{ln} = \frac{(T_{w,in} - T_{a,in}) - (T_{w,out} - T_{a,out})}{\ln(\frac{(T_{w,in} - T_{a,in})}{(T_{w,out} - T_{a,out})})} \tag{4.5}$$

And for the overall heat transfer coefficient:

$$h_{overall} = \frac{P_a}{A_h \cdot \Delta T_{ln}} \tag{4.6}$$

This overall heat transfer coefficient however is not the heat transfer coefficient that we are looking for. We are looking for the heat transfer coefficient from the wire cloth to the air, $h_{wire \to a}$. This can be calculated with equation (4.7):

$$\frac{1}{h_{overall}} = \frac{1}{h_{wire \to a} \cdot \eta_{fin}} + \frac{1}{h_w} \tag{4.7}$$

The fin efficiency, η_{fin}, is the efficiency of the heat transport from the capillaries to the wires and h_w is the heat transfer coefficient from the water in the capillaries to the capillaries themselves [Bird et al., 2002].
To be able to calculate $h_{wire \to a}$ we look first at the calculation of h_w. For the Nusselt number of forced convection in a tube, equation (4.8) is given:

$$Nu = 1,62 \cdot Gz^{-\frac{1}{3}} \qquad if \quad Gz < 0.05 \tag{4.8}$$

in which Gz is the number of Graetz and is given by:

$$Gz = \frac{a_w L_{cap}}{d_{cap}^2 v} \tag{4.9}$$

In equation (4.9) a_w is the thermal diffusion coefficient, L_{cap} the length of a capillary, d_{cap} is its diameter and v is the velocity of the fluid. The thermal diffusion coefficient a is for water at $20°C$: $a = 0.143.10^{-6} m^2/s$, the length of the capillaries is 18.5 cm and their internal diameter 1.1 mm. When the velocity of the water is larger than 0.43 m/s the Graetz number is small enough to use equation (4.9). After calculating the Nusselt number, h_w can also be calculated, with equation (4.10) in which λ_w is the thermal conductivity of the water:

$$h_{w,cap} = \frac{\lambda_w Nu}{d_{cap}} \tag{4.10}$$

This $h_{w,cap}$ is expressed in W/m^2K and is related to the surface of the capillaries, but the $h_{wire \to a}$ that we are looking for is related to the surface of the wire cloth, $A_{cloth} = 2 \cdot \frac{\pi}{2} \cdot b \cdot L_{cloth}$ (the area of the cloth is the width, b times its length, L_{cloth}; the $\frac{\pi}{2}$ comes from the fact that the surface of

the cloth is not flat, but consists of copper wires and the factor 2 is for both sides of the cloth). After recalculation h_w related to the surface of one wire cloth becomes:

$$h_w = \frac{\lambda_w Nu \cdot n_{cap}}{L_{cloth}} \tag{4.11}$$

in which n_{cap} is the number of capillaries per cloth. Now that both the heat transfer coefficient of the water and the overall heat transfer coefficient are known, we only have to determine what the fin efficiency, η_{fin} is, to obtain $h_{wire \to a}$. The actual rate of heat loss from the fin is not the same as the rate of heat loss from an isothermal fin at T_w. The fin efficiency is the ratio between these two and can be calculated with these equations [Bird et al., 2002]:

$$\eta_{fin} = \frac{\tanh N}{N} \tag{4.12}$$

$$N = \sqrt{\frac{h_{wire \to a} \cdot L_{fin}^2}{\lambda_c \cdot d_{wire}}} \tag{4.13}$$

L_{fin} is the length of the fin, which is half the distance between the capillaries in this case, λ_c is the heat conductivity coefficient of the material. So we have to iterate with equations (4.7), (4.12), (4.13) to calculate the heat transfer coefficient from wire to air. The heat transfer from the wires to the air is not very different from the overall heat transfer, because $h_w >> h_{wire \to a}$ and $\eta_{fin} \approx 1$.

4.5.2 Calculation of $StPr^{2/3}$

It is common to present the heat transfer as $StPr^{2/3}$ plotted against the Reynolds number. In this way the data is comparable for the different measurements. The Prandtl number is not a test variable, but $Pr^{2/3}$ is included as an approximation over a moderate range of Prandtl numbers [Kays and London, 1984]. The Prandtl number depends on the kind of fluid and its temperature and is 0.713 for air at room temperature and atmospheric pressure. The Stanton number is the heat transferred divided by the heat capacity of the fluid:

$$St = \frac{h}{\rho c v} = \frac{Nu}{Re \cdot Pr} \tag{4.14}$$

in which h is the heat transfer coefficient, ρ is the density of the fluid, c the heat capacity and v the velocity, see also section 2.2.

4.6 The friction factor

The energy that is needed to make the air flow along the cloths, depends on the friction factor, f, of the cloth. This friction factor is a function of flow geometry and the Reynolds number and is for most of the surfaces a combination of viscous shear and pressure force. The total force that the air exerts on the wire cloth consists of the entrance- and exit effects and the friction of the cloth itself through wall shear. Since we are only interested in the latter, we could not just measure the pressure difference over the cloth. Instead, one of the exits of the pressure difference meter was placed before the wire cloths, the other was moved along the cloths to measure the pressure difference with the pressure at the front, at different mutual distances. This is sketched in figure 4.6.
The pressure meter consisted of two pressure measurement tubes that are connected to two rooms,

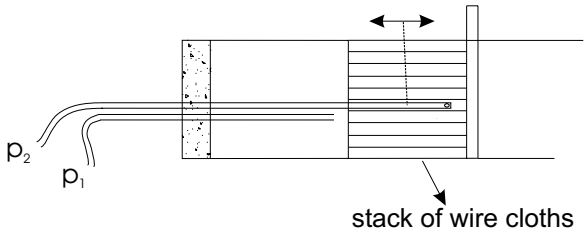

Figure 4.6: The pressure measurement

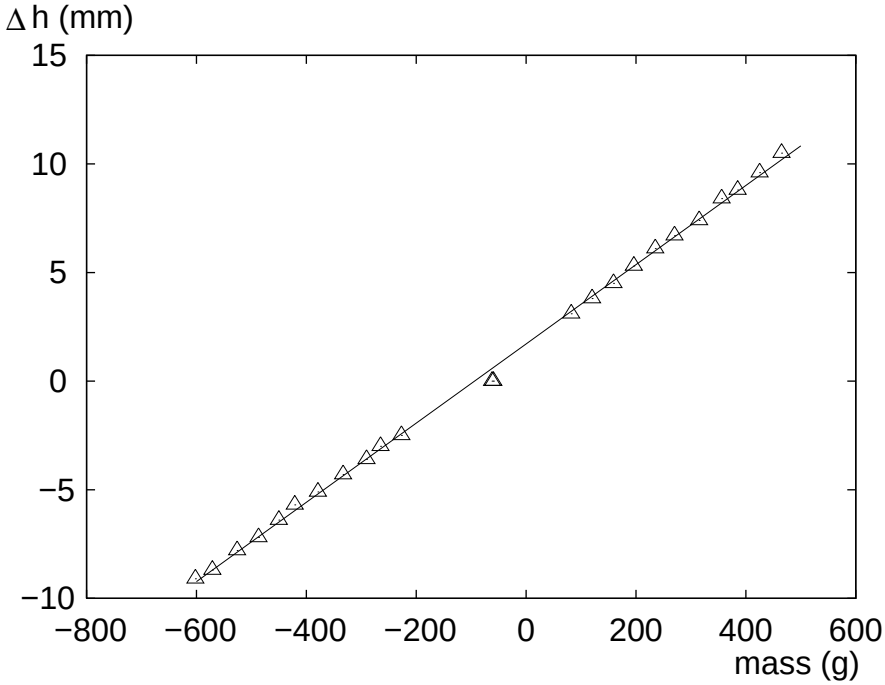

Figure 4.7: Calibration of the pressure meter

the pressure difference between those rooms is measured with a electronic mass balance. It was calibrated using a oil-manometer. The difference in height for the two legs of this manometer is plotted against the mass that was displayed by the pressure meter in figure 4.7: The mass balance seemed to work non-linear around 0, therefore the pressure difference measurements were not done around m=0.

The measured pressure difference, ΔP was plotted against the distance between the both ends of the pressure difference meter, Δx, as in figure 4.8. In this figure is also shown how the gradient of the pressure difference against the mutual distance is measured. From the gradient of this line, $\frac{d(\Delta P)}{\Delta x}$, the overall pressure drop, ΔP_{tot} , except for the entrance and exit effects could be calculated, as in equation (4.15)

$$\Delta P_{tot} = L_{cloth} \cdot \frac{d(\Delta P)}{d(\Delta x)} \tag{4.15}$$

This value for the pressure drop is used to calculate the shear stress:

$$\tau = \frac{(\Delta P) \cdot bs}{\pi b L_{cloth}} \tag{4.16}$$

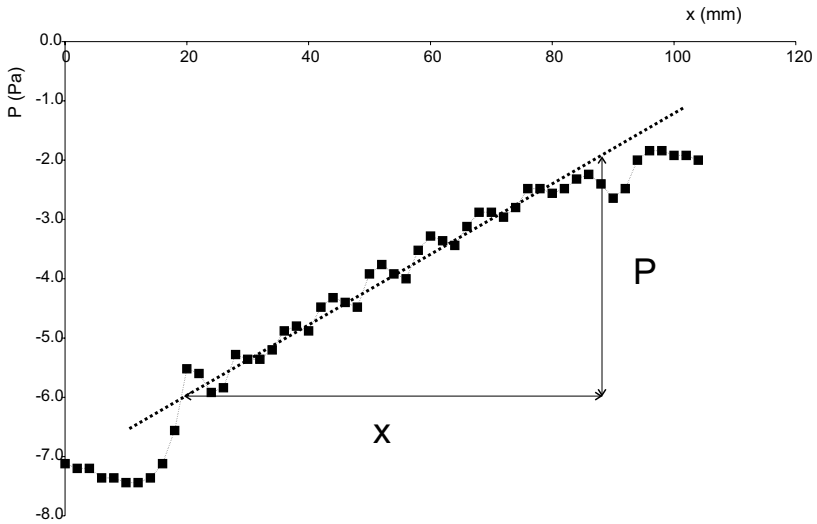

Figure 4.8: The pressure difference between the pressure probe ends against the distance between them. The air velocity is 2.6 m/s.

(see figure 4.5)
Finally with equation (4.17) the friction factor, f can be calculated:

$$f = \frac{\tau}{\frac{1}{2}\rho < v >^2} \tag{4.17}$$

4.7 Variance and uncertainty

In an experiment like this it is important to look at the uncertainty in the measurement results to see how reliable a result is. The uncertainty of a measured value gives an idea of the extent of accuracy and reproducibility of a measurement. The uncertainty can be determined in two ways: statistical and non-statistical. A non-statistical determination of the uncertainty checks all things that can possibly influence the measurement and determines subsequently the uncertainty in the result. For a statistical determination it is necessary that measurements are repeated several times, so that the uncertainty can be determined from the difference between the measured values and the mean measured value.

For the non-statistical determination of the uncertainty an estimation was made of the uncertainty in measuring devices. Subsequently the influence of these uncertainties on the end results was calculated. This calculation is not very difficult, but quite extensive; it is given in appendix A. More details on the non-statistical determination of the uncertainty can be found in [Chatfield, 1970]. This method led to an relative uncertainty in the friction factor of about 13%. The uncertainty in the heat transfer expressed as $StPr^{2/3}$ is about 6%.

The uncertainty is determined again statistically after the measurements. The standard deviation, s, of n measurements of x is calculated as:

$$s = (\frac{1}{n-1}\sum_{i=1}^{n}(x_i - \overline{x})^2)^{1/2} \tag{4.18}$$

in which $\overline{x} = \frac{1}{n}\sum_{i=1}^{n} x_i$. The friction factor was measured between two and six times for a certain configuration. The uncertainties that were determined in a statistical way differ much for

each measurement; the uncertainty in the friction factor differs from 1 to 45% and in the heat transfer from 3 to 44%. In the figures of chapter 5 and 6 a combination of the statistically and non-statistically determined uncertainties is used as explained in appendix A.

Chapter 5

Experiments with flat plates

In this chapter the experiments with flat plates, using the set-up described in chapter 4, are described. The goal of these experiments was to validate the experimental set-up, because theoretical values are known for both the friction and heat transfer at flat plates. These theoretical values are described in chapter 2. The results of the experiments are described in section 5.1 and some conclusions are given in section 5.2.

5.1 Results for the flat plates

In this section first the results for the heat transfer are given and after this the results for the friction. These results are compared with theoretical values.

5.1.1 Heat transfer

The results for the measurement with 8 flat plates are plotted in figure 5.1 together with the theoretical results from equation (2.45), for $3000 < Re_D < 5500$. For the measurements with 10 flat plates, the same kind of figure is drawn in figure 5.2. The heat transfer, $StPr^{2/3}$, of 8 flat plates decreases with increasing Reynolds number from 0.018 to 0.016. The measurement at $Re = 4200$ is very low, about 0.014, but its uncertainty is also very high, so that it is still possible to draw a descending line within the uncertainties of the measurements. The heat transfer of 10 flat plates decreases more: from almost 0.025 to 0.014. The first measurement, at $v_a = 2.1 m/s$ is quite high, but its uncertainty is also quite high.

5.1.2 Friction

The most convenient way to compare the results from the flat plates for the friction would be to plot their friction factor against the Reynolds number. The plots of the pressure against the displacement of the sensor however did not show a straight curve between the plates. In figure 5.3 and 5.4 the pressure difference between the two ends of the pressure meter is given as a function of the displacement of the sensor, for different velocities. For each specific set of experimental conditions, the results of four reproduction experiments are shown, as well as the theoretical

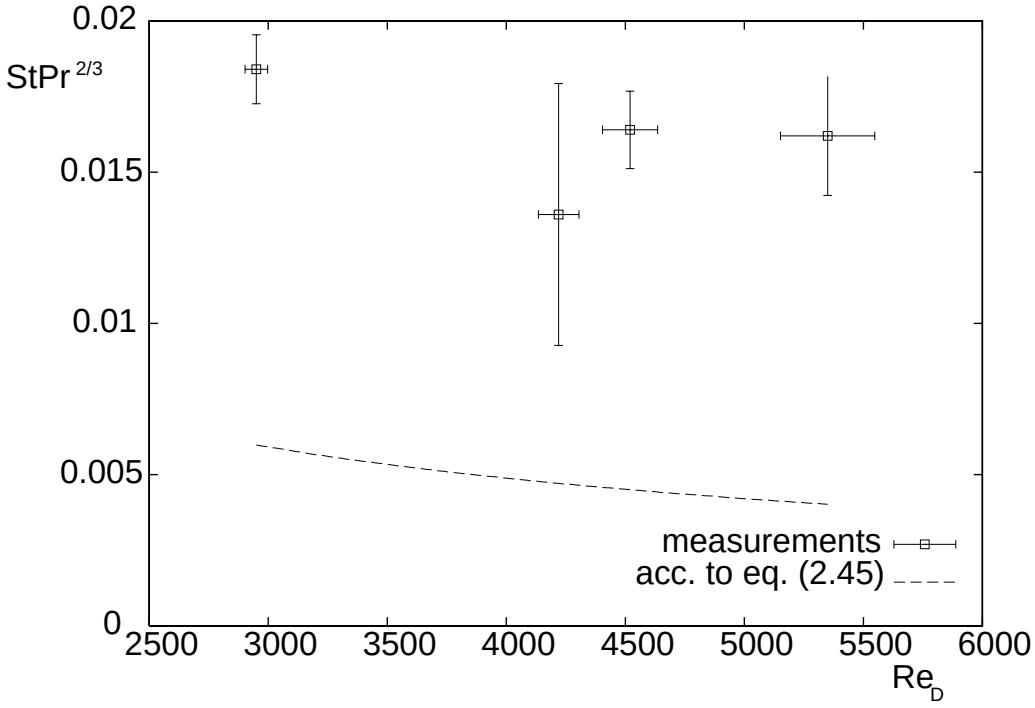

Figure 5.1: Heat transfer of 8 flat plates compared with values from literature

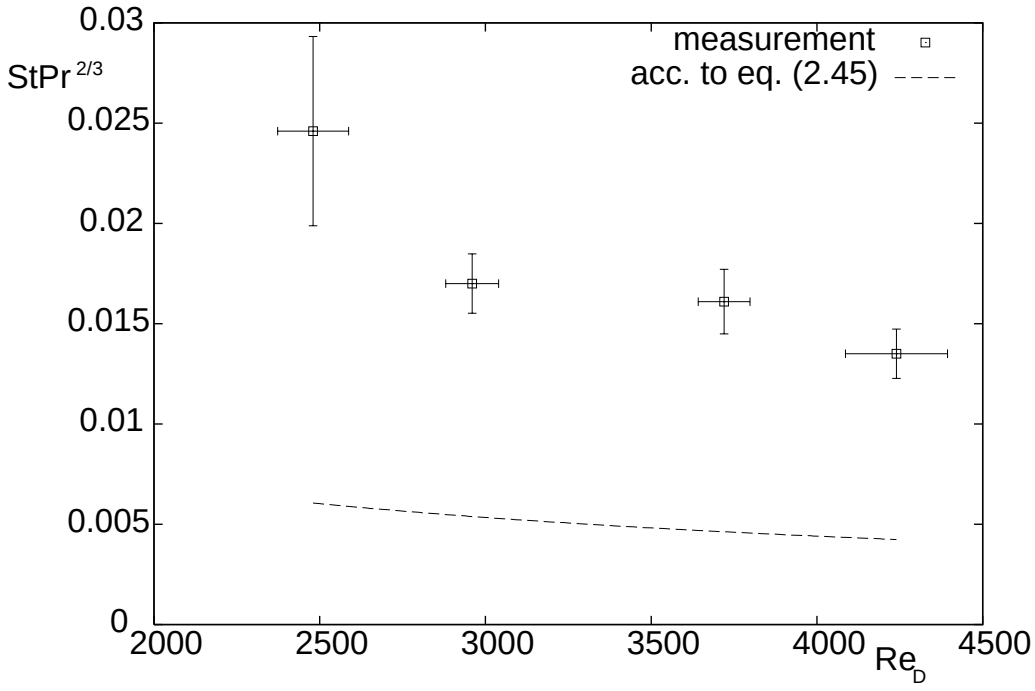

Figure 5.2: Heat transfer of 10 flat plates compared with values from literature

pressure drop curve, calculated from equation (2.44).
CFD simulations have been performed to see what could be expected from the measurements of the pressure curve between flat plates and how the pressure measurement tube would influence the measurement. These simulations are described in appendix B. A conclusion from these simulations was that the flow between the pair of plates with the pressure meter tube was about 10 % lower than the mean velocity between the other pairs of plates. The theoretical curves in figure 5.3 and 5.4 are therefore also calculated for a velocity of 90 % of the mean velocity between the plates.
The theoretical curves differ from the experimental ones in certain aspects:
The entrance effect starts later than expected. The sudden pressure drop exact at the edge of the plate in the theoretical curve is of course not what really should happen. According to the CFD simulations the pressure drop at the entrance takes place between 0.5 cm before and after the edge of the plate. In the experimental results the pressure drop takes place between 0.5 and 1.5 cm after the edge of the plate.
The same kind of difference, but more pronounced, can be seen at the end of the plates. According to the theory and simulations, the pressure gain should take place between about 0.5 cm before and after the edge of the plates. In the experimental results however, the pressure starts to rise again much earlier, from about 3.5 cm before the edge in some cases. The experimental pressure gain has the same 'S' form as the curve that resulted from the simulations (see appendix B).
It is difficult to see wether the steepness of the theoretical curve is about the same as the measured curve. For the measurements with the 10 flat plates it seems that for $0.02 < x < 0.04$ the inclination of the lines is about the same. The reason to look especially at this region, is that this region is most likely between the region with the entrance pressure drop and the region with the exit pressure gain, so that it can be compared with the theoretical curve. When we look at the experimental results of the 8 flat plates, almost nothing can be said, because of the strange peaks in the lines.
These strange peaks are almost absent in the curves of the 10 flat plates, but ruin the results for the 8 flat plates, because almost nothing can be said on the steepness of the line, or the start of the exit pressure gain. The smallest peaks seem to occur at lower velocities and at the beginning of the plates.
A possible explanation for this could be the disturbances by the pressure meter tube. From the CFD simulations it can be seen that the pressure meter caused a negative peak at the measurement point (see section B.1 and for example figure B.3), because of the stagnation point before the tube and the low pressure after it. This negative peak is expected to be larger when the velocity is larger, so that we expect the disturbances in the pressure curves to become larger with growing velocity. This is seen in the experiments.
The flow that enters the channel is almost uniform, in the channel a velocity profile is developed that at the end almost is parabolically shaped with a larger maximum velocity. This could be the explanation for the fact that the disturbances seem to increase at the end of the tube. It is surprising that this can not be seen in the pressure curves of 10 flat plates.

5.2 Conclusions from the experiments with flat plates

The main conclusion is that the set-up has not been validated by these flat plate measurements. The results are not in all aspects in agreement with the theory and simulations.
The measured heat transfer from the flat plates is much higher than expected according to the theory. This might be due to the fact that the flat plates are not completely flat.
The friction factor can not be determined from the measurements with the flat plates because of the irregular pressure curve. In the measurement with 8 flat plates the overall pressure drop is in some measurements quite different from the theoretically expected value. In the results from the

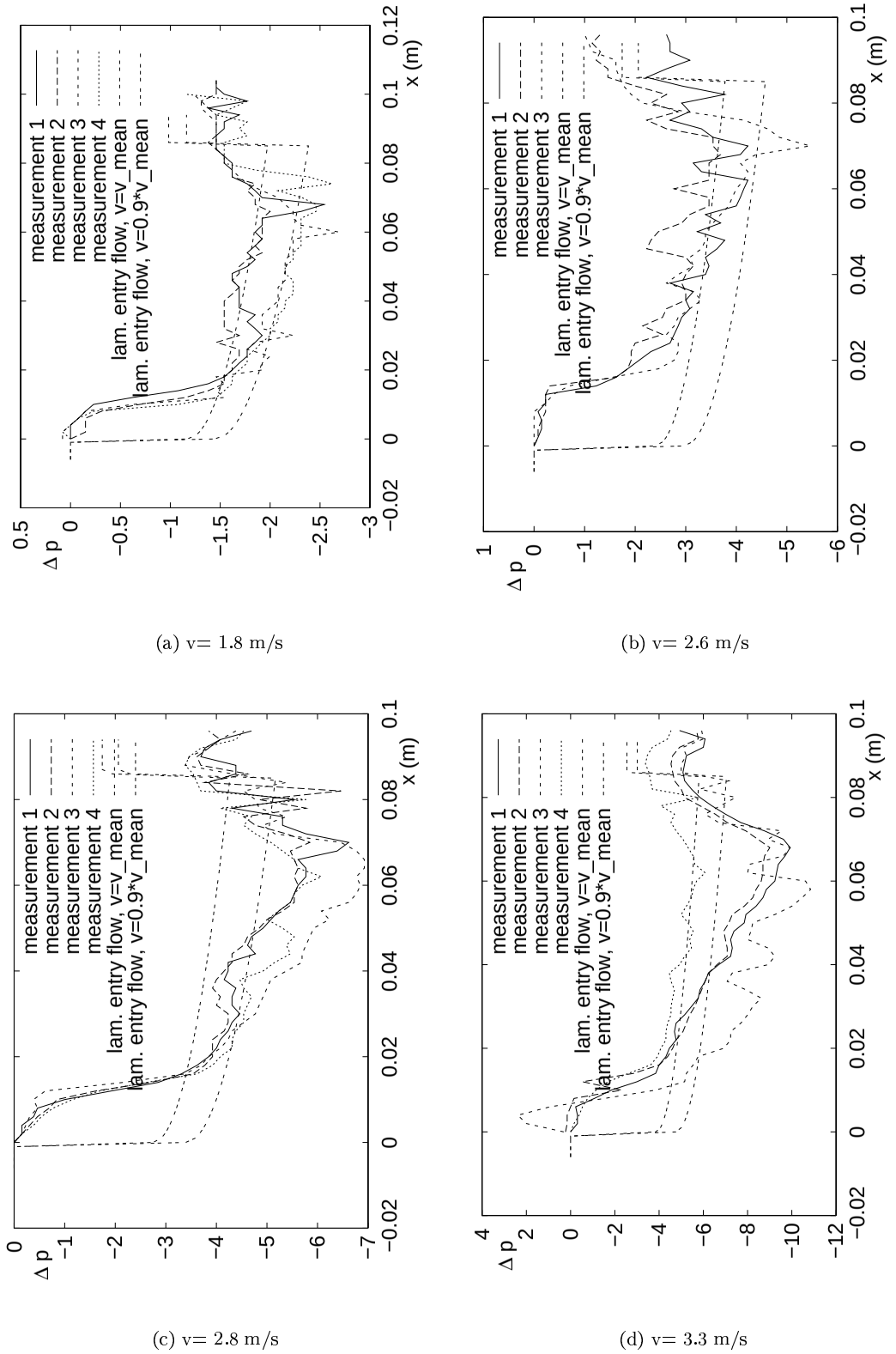

(a) v= 1.8 m/s

(b) v= 2.6 m/s

(c) v= 2.8 m/s

(d) v= 3.3 m/s

Figure 5.3: Measured pressure and theoretical curves of 8 flat plates.

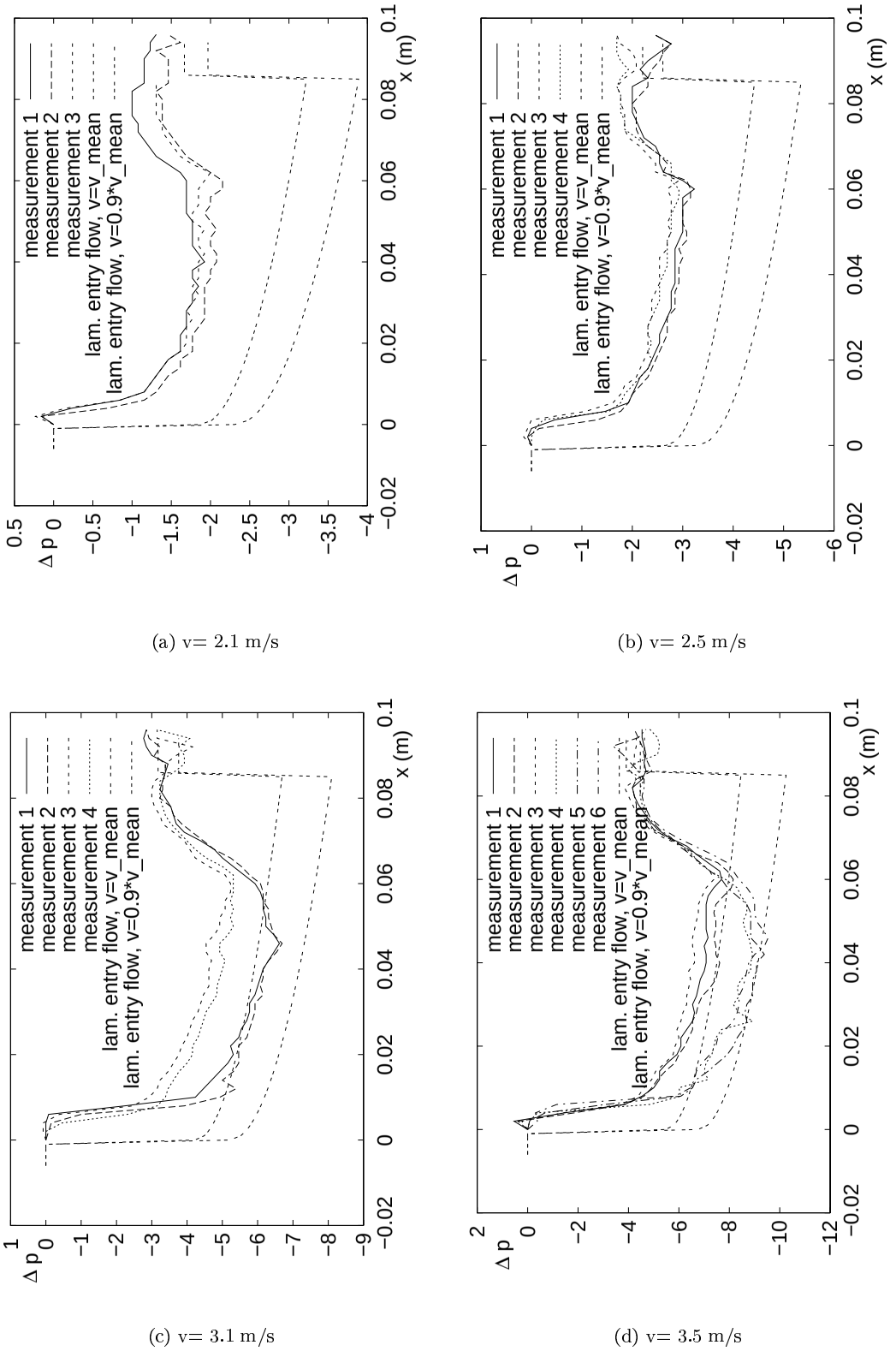

(a) v= 2.1 m/s

(b) v= 2.5 m/s

(c) v= 3.1 m/s

(d) v= 3.5 m/s

Figure 5.4: Measured pressure and theoretical curves of 10 flat plates.

measurements with 10 flat plates can be seen that the measured overall pressure drop is not very different from the theoretically expected value.
The heat transfer per area heat exchanging surface does not differ much for 8 or 10 flat plates. The irregularities in the pressure curve for 8 flat plates are larger than those for 10 plates. This is in contradiction with the expectation that larger irregularities would occur when the relative dimension of the pressure tube to the thickness of the channel is larger. The Reynolds number however of the measurement with 8 flat plates is higher for the same velocity than for 10 flat plates, because of the larger hydraulic diameter. A smaller tube also holds the pressure measurement tube better in position in the middle of the channel.

Chapter 6

Experimental results for the Fiwihex wire cloths

In this chapter, the results from the measurements on the heat transfer and friction of the wire cloths are presented.
The first section describes the measurements that are done. In section 6.2 the results are given for the heat transfer. These results are compared with the theoretical values from chapter 2. The next section, 6.3, deals with the friction factors that are measured and compares these friction factors with those from literature. The last section, 6.4 describes the measured relations between the friction and the heat transfer.

6.1 Wire cloths

As described in chapter 4, the measurements were done with two types of wire cloths and at different mutual distances. The dimensions of the tube in which the cloths were placed are fixed, so that there is a direct relationship between the number of cloths and the distance between them, see also figure 4.1. The wire cloths with 12 mm between the capillaries were measured in a stack of ten cloths, that corresponds to a mutual distance of 8.5 mm. The wire cloths with 8mm between the capillaries were measured in a stack of eight, ten and twelve cloths, corresponding to mutual distances of 10.6, 8.5 and 7.1 mm respectively.

6.2 Heat transfer

In this section the results of the measurements on heat transfer are described. These results are calculated as described in section 4.5. The heat transfer is measured at different airflows, the range of possible airflows was limited at the upper side by the fan, which broke down if it was turning too fast and on the other side by the accuracy of the temperature sensors that were used to measure the airflow. The velocities that were obtained depended on the configuration of the cloths, but they lie all between 1.1 and 3.5 m/s along the wire cloths. With each type of cloth the heat transfer was measured for 6 or 7 different velocities. When the measurements seemed to give unexpected results the measurement was repeated. Especially with the 10 wire cloths of 8mm, the

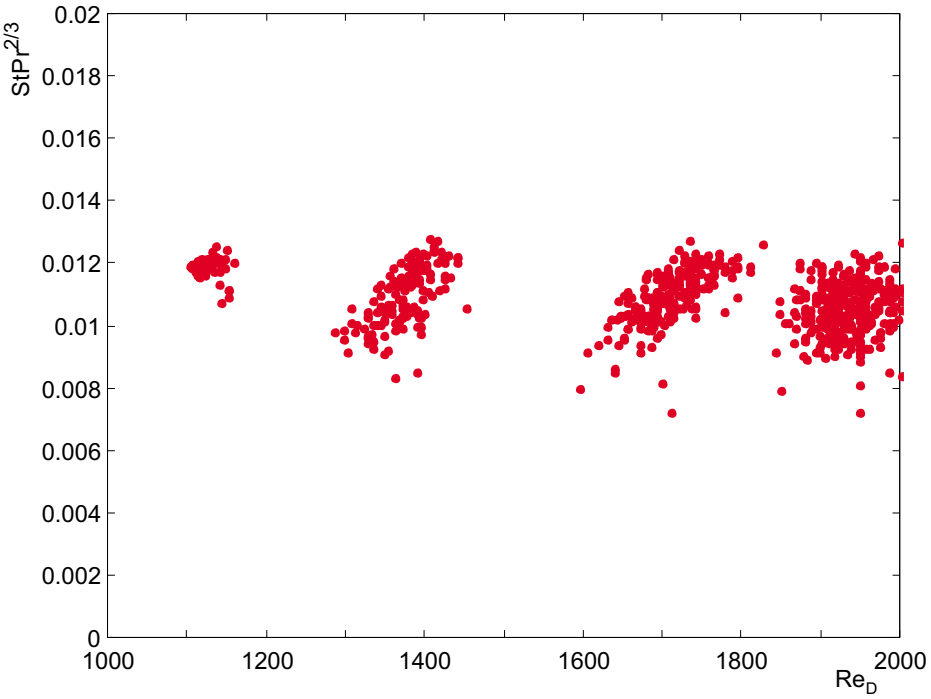

Figure 6.1: $StPr^{2/3}$ plotted against the Reynolds number. The measurement is done with twelve 8mm-cloths.

values were unexpectedly high, so that the stack of tubes was measured again. Between those two series of measurements the cloths were a bit bent so that they were more horizontal. The fact that the cloths can not be placed perfectly horizontal restricts the precision of the measurements, it can not be guaranteed that all the air flows along the cloths, instead of through them.

6.2.1 Experimental results

During a measurement the heat transfer was determined several times. Temperature sensors measured the temperatures roughly every 40 seconds. In figures 6.1, 6.2, 6.3 and 6.4 of the heat transfer against the Reynolds number all these points are drawn. This gives an indication of the precision with which the measurements could be done. From these figures it can be seen that the size of the 'clouds' of points differs strongly for the different measurement series. This size is a measure for the uncertainty in the measurement. From each cloud the mean Reynolds number and the mean heat transfer is calculated and also a variance is statistically derived, as explained in section 4.7.

Two series of measurements for the ten 8-mm cloths differ much from each other as can be seen in figure 6.2. In figure 6.2 the upper series of measurements is measured first. In the first measurement the cloths were not quite parallel placed, which gives a higher heat transfer. This seems logical: a part of the air travels trough the cloths instead of along it and therefore the heat transfer is higher. After trying to make the cloths a bit more parallel and straight the lower points were measured. It can be seen that the clouds of the upper series are less dense, and that the density of the clouds decreases with increasing Reynolds number. In the second measurement the heat transfer was much lower. This large difference means that the configuration of the cloths is important

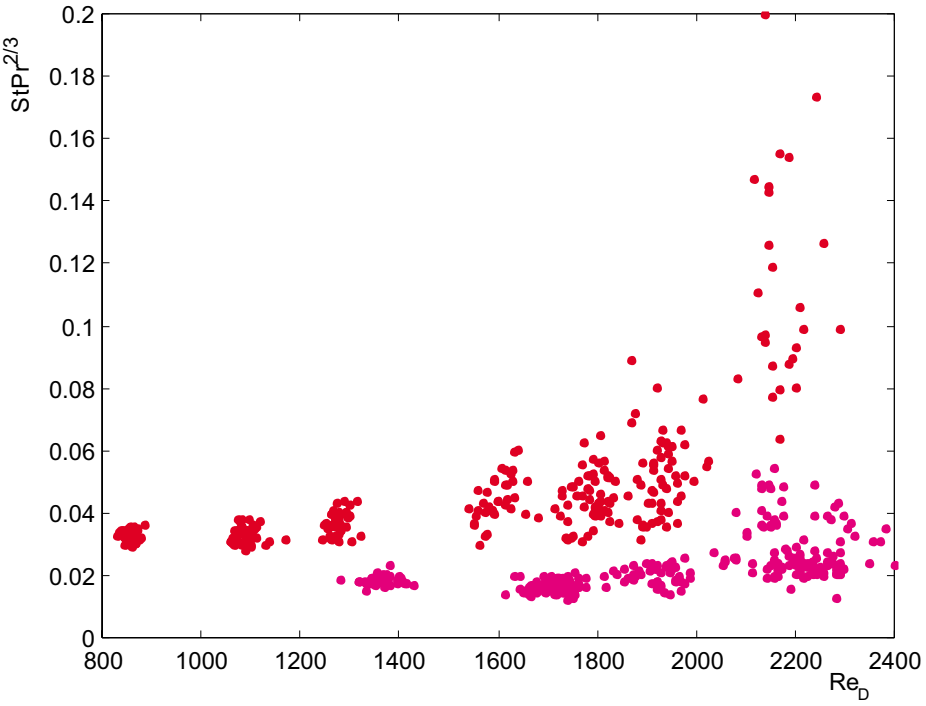

Figure 6.2: $StPr^{2/3}$ plotted against the Reynolds number. The measurement is done with ten 8mm-cloths.

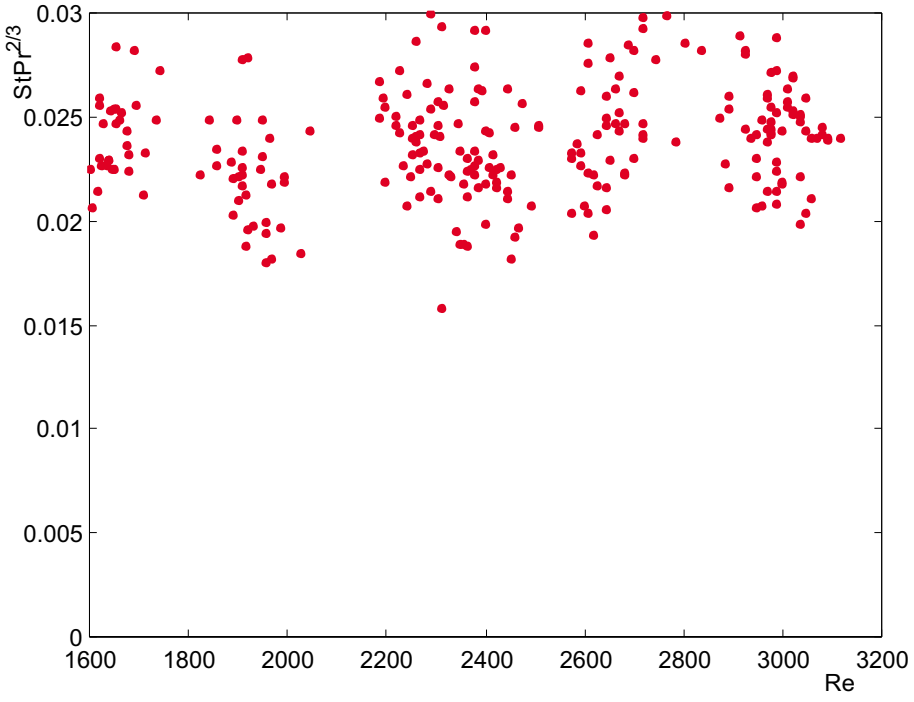

Figure 6.3: $StPr^{2/3}$ plotted against the Reynolds number. The measurement is done with eight 8mm-cloths.

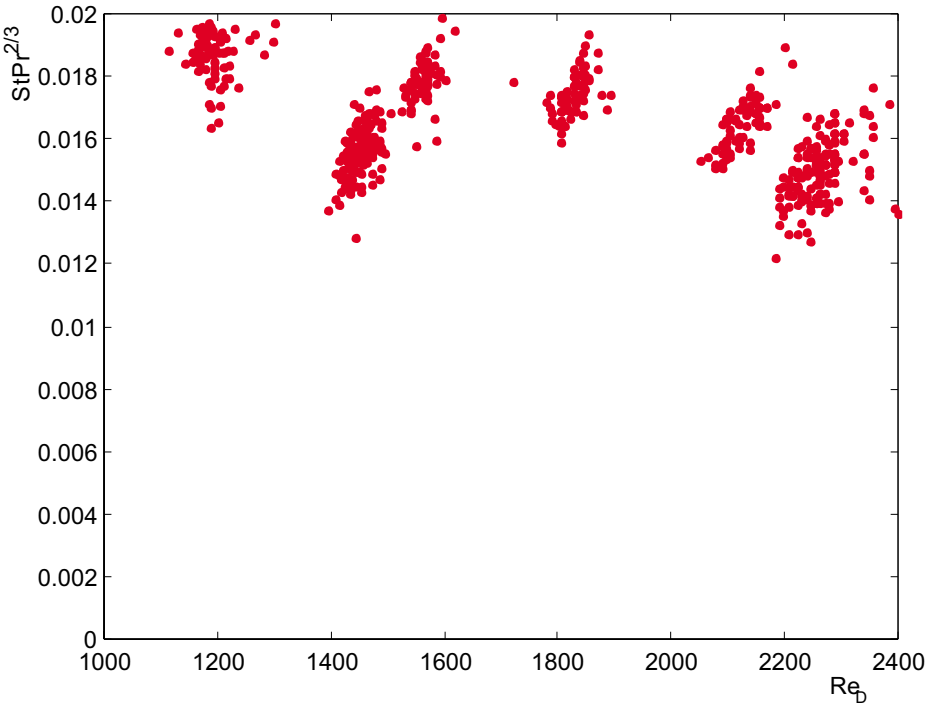

Figure 6.4: $StPr^{2/3}$ plotted against the Reynolds number. The measurement is done with ten 12mm-cloths.

for the results. In the other measurements the cloths were visually parallel, so that the results would be not very different if the measurements were repeated with a new stack of cloths. This large dependency of the heat transfer on the configuration of the cloth means that in order to be able to predict the heat transfer of a Fiwihex it is necessary to place the cloths very precisely in the required direction.

The data clouds of the eight 8mm cloths in figure 6.3 are also not very dense, so that the uncertainty in the measurements is higher. This can also be seen in figure 6.5, where all the measurements are plotted into one figure, inclusive error bars. The error bars are the square root of the statistically derived variances. In this figure the upper series from figure 6.2 is left out, because the cloths were not placed quite parallel in this measurement and the uncertainty became very high at higher Reynolds numbers. The lowest values for the heat transfer are measured with twelve 8mm-cloths, see figure 6.1.

The heat transfer of the second measurement of the ten 8mm-cloths and of the ten 12-mm cloths is comparable in size, and larger than the heat transfer of the twelve 8mm-cloths, see figure 6.5. The results of the eight 8mm-cloths give the highest heat transfer.

When we look at the Reynolds number dependence, we see a slight decrease in heat transfer with increasing Re for the twelve 8mm cloths and the ten 12mm cloths. For the ten 8mm cloths heat transfer seems to increase with Re, whereas for eight 8mm cloths it is almost constant. However, all observed Re-dependencies are small compared to the experimental uncertainties. Therefore, it seems more justifiable to look at average values of $StPr^{2/3}$, averaged over the measured range of Reynolds numbers. These averages, as a function of the distance between the cloths, are shown in figure 6.6. The lowest heat transfer is measured for the cloths with the smallest mutual distance, the highest heat transfer for the cloths with the highest mutual distance. The heat transfer of the 12mm wire cloths is smaller than that of the same number of 8mm wire cloths.

If the wire cloths have to be placed in a certain volume, the mutual distance between the wire

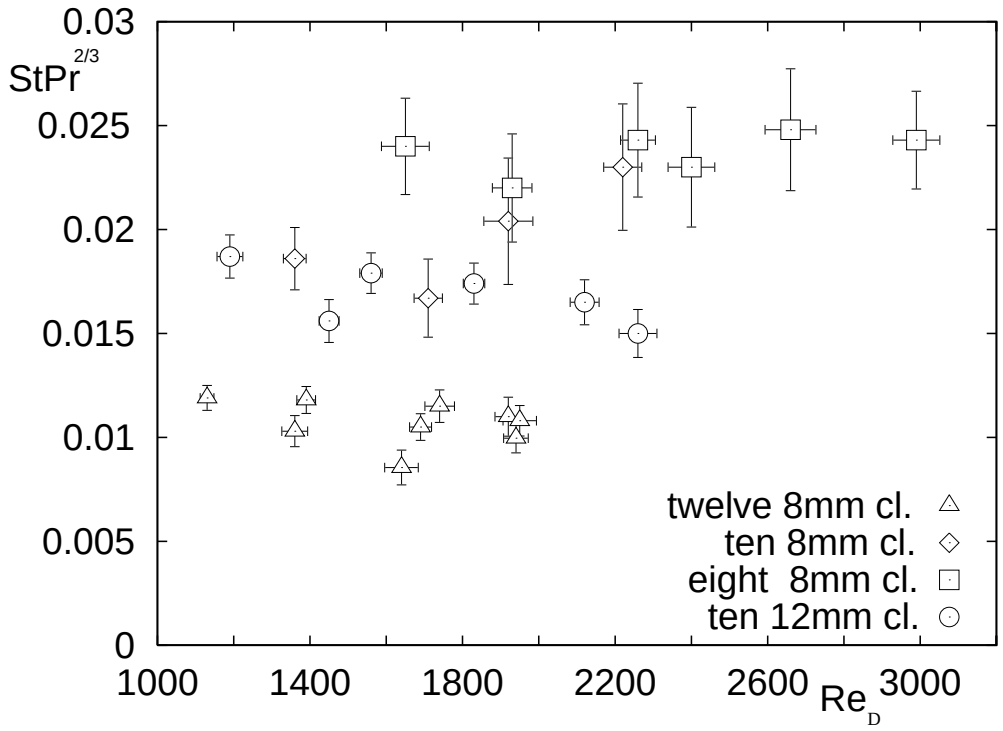

Figure 6.5: $StPr^{2/3}$ plotted against the Reynolds number, inclusive the error bars.

cloths influences the number of cloths that fit into this volume. In figure 6.7 the heat transfer, expressed in $StPr^{2/3}$, multiplied by the number of cloths that fit in a stack of 1 m high is plotted against the mutual distance between the cloths. The heat transfer of the eight 8mm cloths is larger, but less cloths fit into a certain volume, because of the larger mutual distance. The highest heat transfer can be seen for the ten 8mm cloths.

6.2.2 Comparison with theoretically expected values

In the present experiments the flow is not yet developed, so that we use the theory from section 2.7 for non-developed flow to compare the experimental results with. In the comparison of these calculations with the experimental results, two properties are important: the shape of the $StPr^{2/3}$ vs. Re curve and the height of this curve. The calculated heat transfer for flat plates is plotted in the same figure as the experimentally obtained values for the different stacks of cloths in figures 6.8, 6.9, 6.10 and 6.11. It is remarkable that the heat transfer of the wire cloths is much higher than would be expected from the theory. The measured heat transfer is between 1.3 and 4.2 times higher than the expected theoretical heat transfer.
The range of Reynolds numbers is small, so that it is almost impossible to define the shape of the relation between the heat transfer and the Reynolds number. The heat transfer of the 12x8mm and 10x12mm cloths seems to decrease with increasing Reynolds number, the heat transfer of 10x8mm cloths seems to increase and the heat transfer of the 8x8mm cloths stays more or less the same. However, as noted earlier, variations with Re one small compared to the experimental uncertainty.

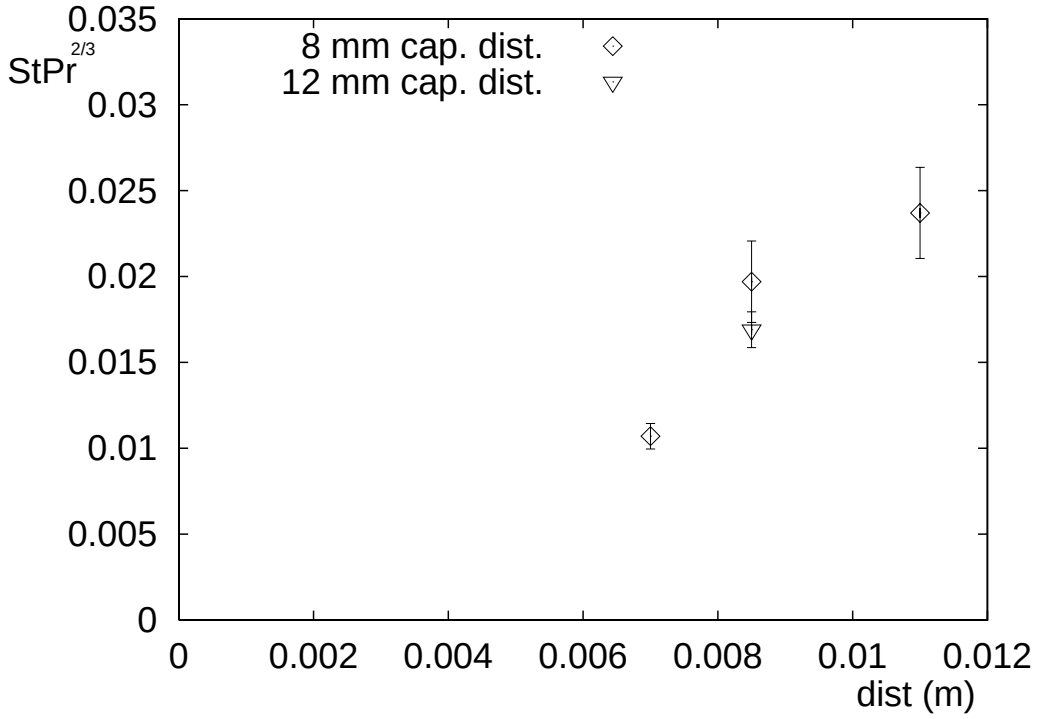

Figure 6.6: $StPr^{2/3}$ plotted against the distance between the cloths

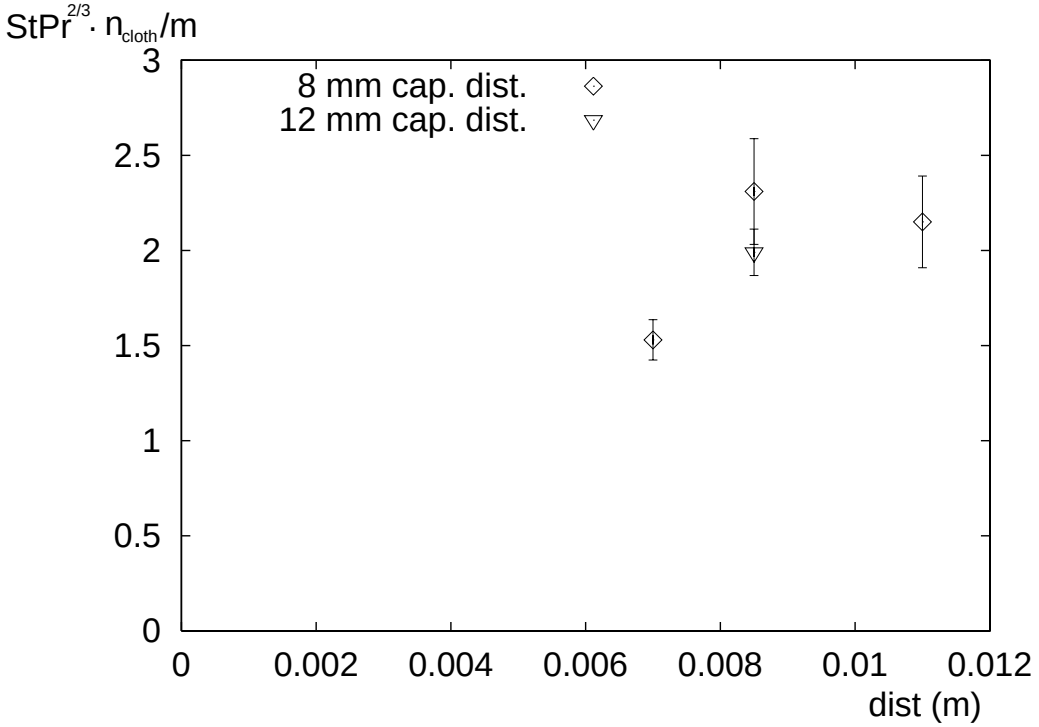

Figure 6.7: $StPr^{2/3}$ for a 1 m high stack of wire cloths, plotted against the distance between the cloths

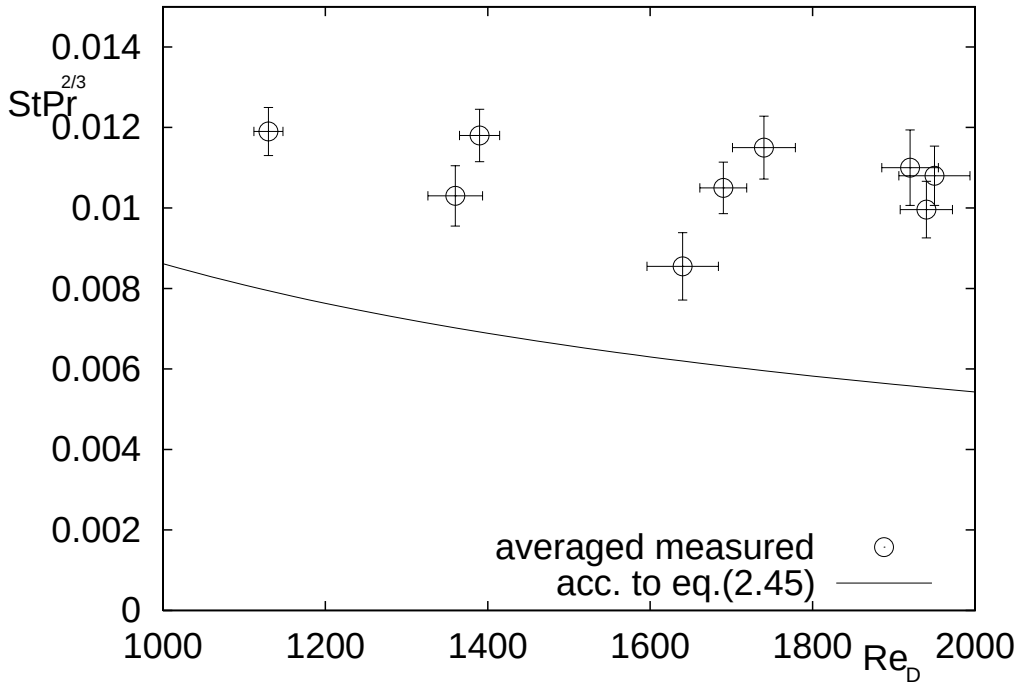

Figure 6.8: $StPr^{2/3}$, from the experiments and expected from the theory for laminar flow along a wire cloth plotted against the Reynolds number. The measurement is done with 12 8mm-cloths.

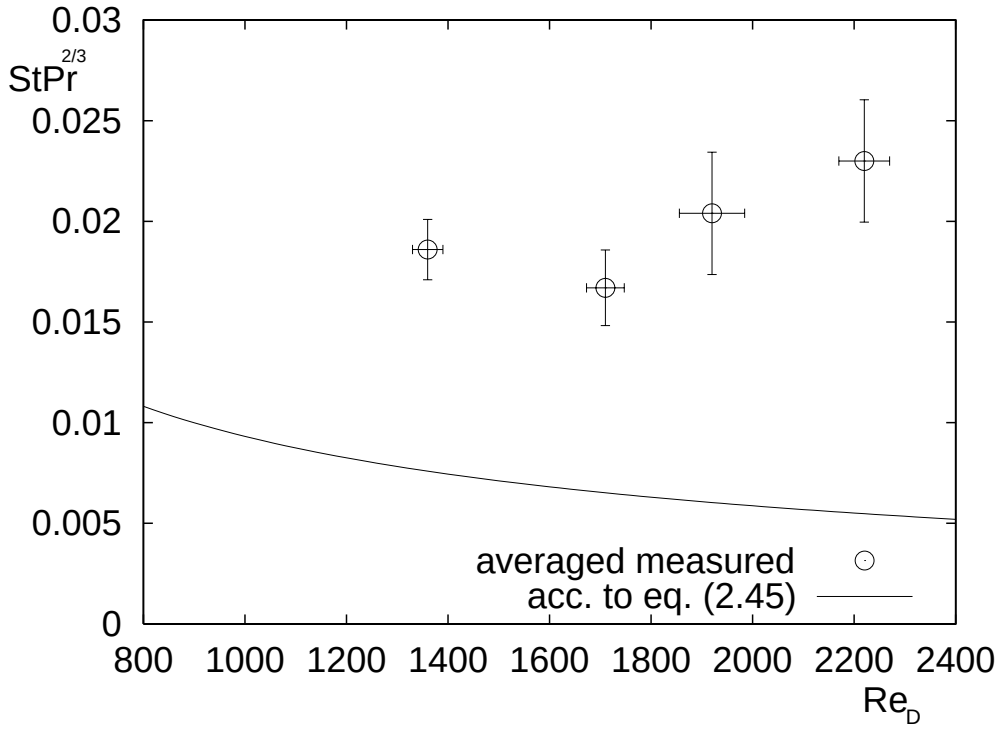

Figure 6.9: $StPr^{2/3}$, from the experiments and expected from the theory for laminar flow along a wire cloth plotted against the Reynolds number. The measurement is done with 10 8mm-cloths.

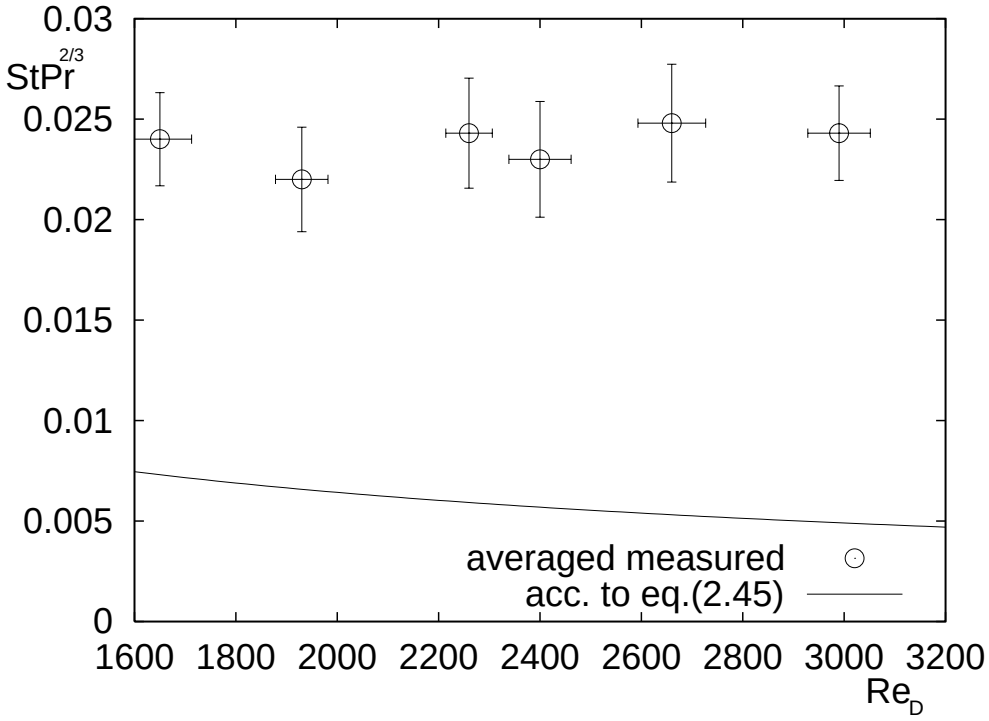

Figure 6.10: $StPr^{2/3}$, *from the experiments and expected from the theory for laminar flow along a wire cloth plotted against the Reynolds number. The measurement is done with 8 8mm-cloths.*

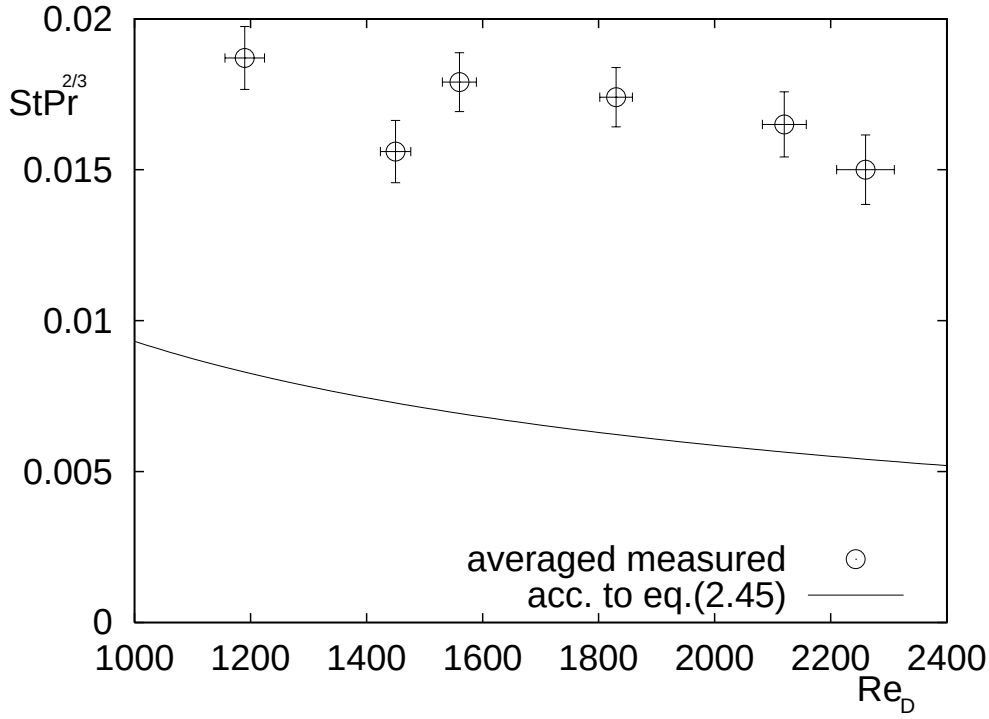

Figure 6.11: $StPr^{2/3}$, *from the experiments and expected from the theory for laminar flow along a wire cloth plotted against the Reynolds number. The measurement is done with 10 12mm-cloths.*

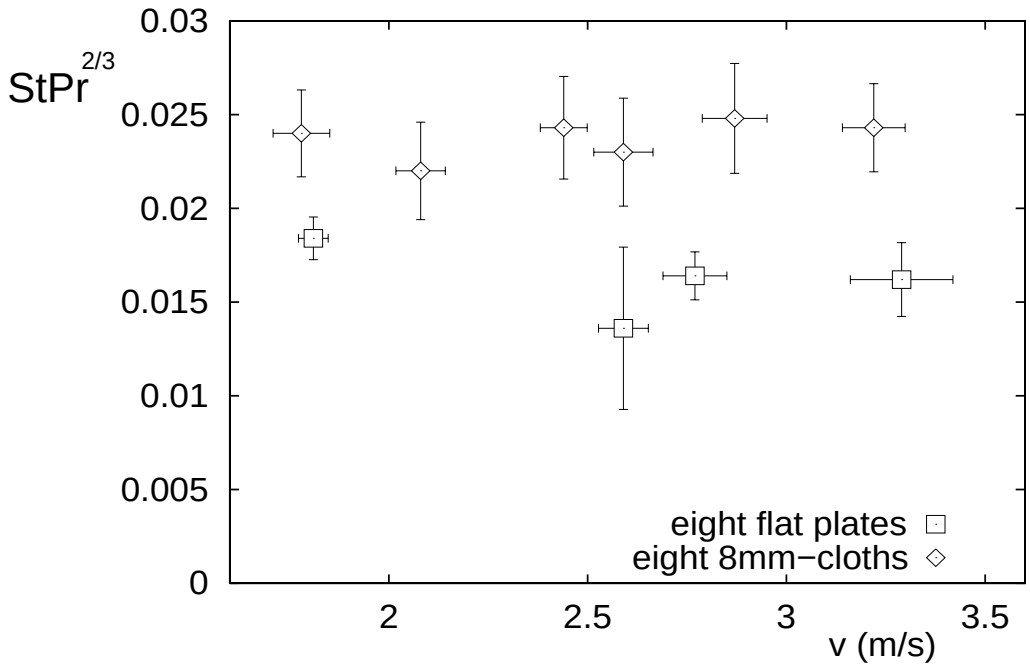

Figure 6.12: Heat transfer of eight flat plates and of eight wire cloths

6.2.3 Comparison with measurements on flat plates

To compare the heat transfer of the wire cloths with that of the same number of flat plates, both of these are plotted in figure 6.12. In figure 6.12 the heat transfer is plotted against the air velocity. This is because the air velocity in both measurements is almost the same, while the Reynolds numbers differ. The hydraulic diameter, as defined in equation (2.2), of the cloths namely is much smaller, its heat transfer area is much larger since it consists of wires instead of a flat plate.
In figure 6.13 the heat transfer of ten plates and of the same number of wire cloths can be seen. The heat transfer of the 8 wire cloths is about 1.5 times as large as that of the 8 flat plates. The heat transfer of 10 flat plates is comparable to the heat transfer of ten 12mm or 8mm wire cloths. The heat transfer of the ten flat plates around $v = 2.1m/s$ is quite high, but its uncertainty is also very high. The heat transfer of the 8mm wire cloths increases beyond $v_a = 2.4m/s$, so that the heat transfer of the 8mm cloths is higher than that of the flat plates for $v_a > 2.5m/s$.
When the heat transfer is expressed in $StPr^{2/3}$ it is corrected for the surface of the heat exchanging area. The heat exchanging area of the wire cloth is $\pi/2$ times larger than that of a flat plate with the same width and length. Therefore the total heat transfer of the set-up is also plotted, to compare the total heat transfer per wire cloth with that of a flat plate. The results for the measurement with 8 plates or cloths are given in figure 6.14 and those for 10 plates or cloths in figure 6.15. In figure 6.14 it can be seen that the total heat transfer of the plates is about twice as low as that of the 8mm wire cloths. From figure 6.15, the total heat transfer per wire cloth is between one and twoandahalf times as high as that of a flat plate.

6.3 Friction

The friction coefficient could not as easily be measured as the heat transfer. As described in section 4.6 the pressure difference had to be measured for different mutual distances before the friction

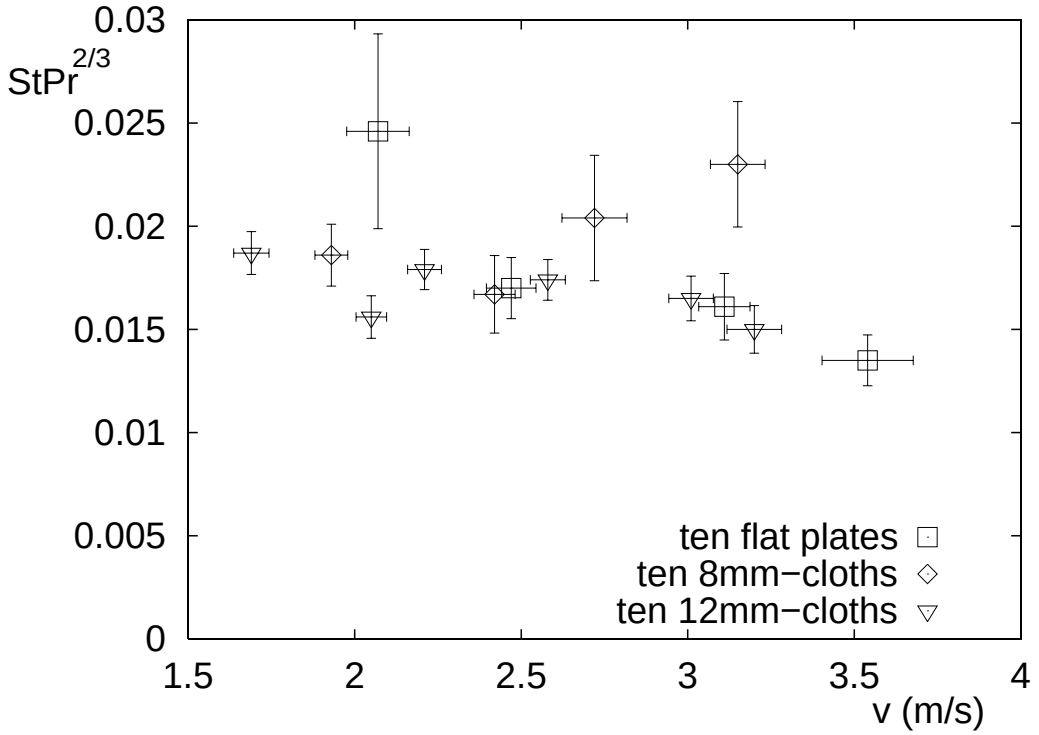

Figure 6.13: Heat transfer of ten flat plates, ten 12mm- and ten 8mm wire cloths

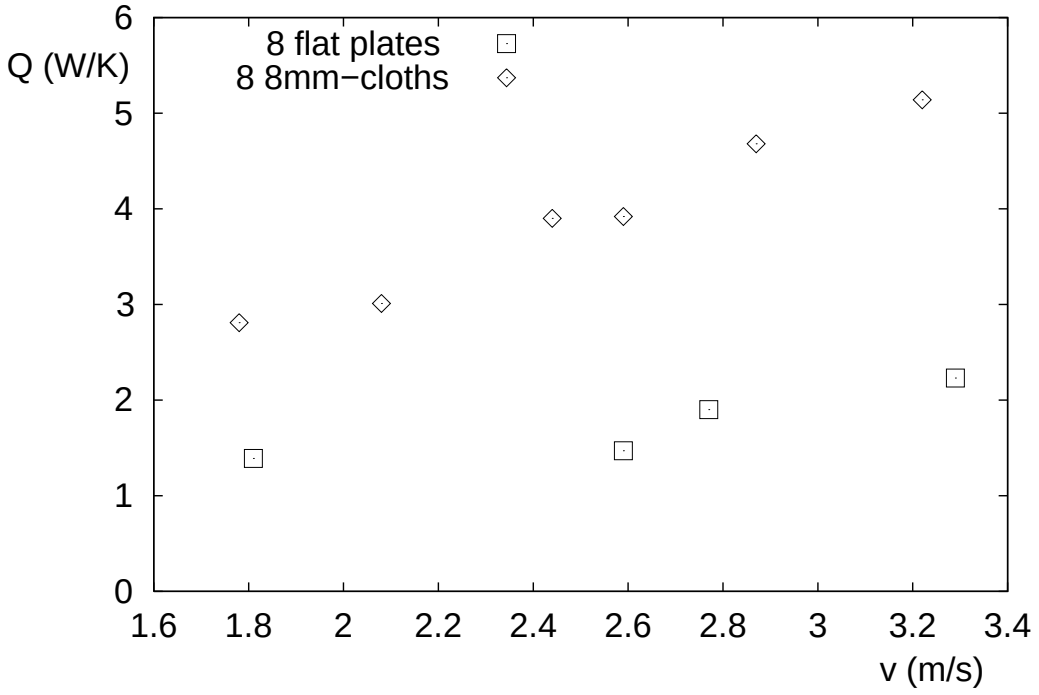

Figure 6.14: Total heat transfer of eight flat plates and eight 8mm wire cloths

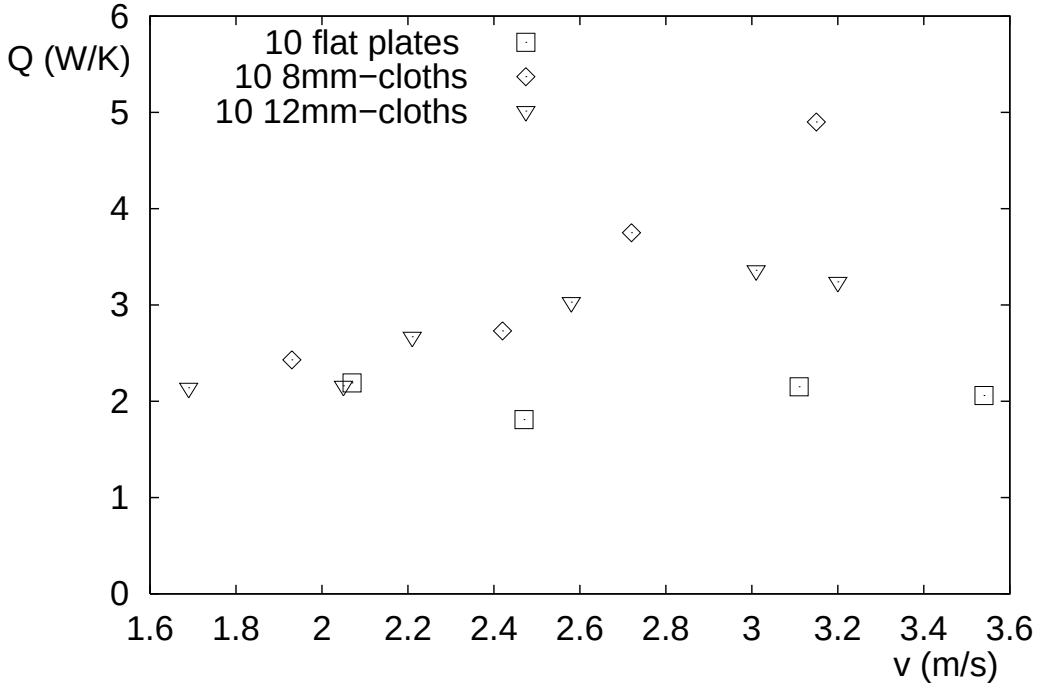

Figure 6.15: Total heat transfer of ten flat plates, ten 12mm- and ten 8mm wire cloths

factor could be calculated. For this reason the friction factor was not measured as many times as the heat transfer, but still a few times for each configuration and air velocity.
Although the results of the measurements with the flat plates did not validate this set-up it is used anyhow. The reason to do this was that the measurements with the wire cloths looked much better than those with the flat plates: the lines were more smooth, the entrance and exit effect took place around the edge of the cloth and the exit effect was much smaller. The pressure meter was even sensible enough to measure the pressure differences due to the capillaries. Apart from this the calibration of the pressure meter showed good agreement with the pressure according to a manometer, see figure 4.7. From these measurements also the friction factor could be calculated.

6.3.1 Experimental results

A typical graph of the pressure difference against the distance between both ends of the pressure meter was plotted in figure 4.8 in section 4.6. This is a measurement of twelve 8mm wire-cloths. In the figure the entrance and exit effects are easy to see. Another aspect that strikes the attention is that the points do not lie on a straight line, but on a line with bumps. These bumps occur every 8mm, which indicates that the pressure difference meter is so sensible that it 'sees' the capillaries in the cloth. At the capillaries the flow area is about 20% smaller, so that the velocity is higher than between the capillaries. This can be seen in figure 4.5.
To compare the friction between the different configurations it would be easy to plot all the data into one figure. The friction factors however lie so close together that by plotting the data into one figure it is impossible to distinguish the different points. Therefore the friction factors are plotted in four separate graphs at the same scale in figure 6.16.
The curves of the friction factor are not as smooth as the curves of the heat transfer. The friction factor of the 12 8mm-cloths increases strongly around Re=2000. In the measurement at Re=1690 the power of the fan was set at about the same value as in the measurement at Re=1920. There

was probably an error in the determination of the velocity, which also gives an explanation for the high value for the friction factor.
The results of the friction factor for the measurements of the ten 8mm-cloths showed again the same effect as the results for the heat transfer. The friction of the first series of measurements (not shown here) were almost two times as high, which can again be explained by the air that travels through the cloths instead of along them.
The friction factor of the eight 8mm cloths is higher than those of the twelve 8mm-cloths and of the second measurement of the 10 8mm-cloths.
The highest friction can be seen with the ten 12mm-cloths. The friction factor is even more than two times higher than that of the ten 8mm-cloths, where the heat transfer was comparable in size.
The uncertainties in the friction factors are higher than in the heat transfer. This can be explained by the small pressure differences that had to be measured: the total pressure difference (without entrance and exit effects) was between 1 and 10 Pa. The sensibility of the pressure difference meter was 0.16 Pa. Apart from that are the pressure differences so small that a little disturbance could have a large influence on the measurement.
The friction factor averaged over the measured range of Reynolds numbers is plotted against the distance between the wire cloths in figure 6.17.

6.3.2 Comparison of friction factor with theoretical expected values

The friction factor is plotted against the Reynolds number for the four measurements in figures 6.18, 6.19, 6.20 and 6.21. In the same figures also the friction factors are plotted that are calculated according to the theoretical curve for the friction factor, that is described in section 2.7.2, see equation (2.44). In all measurements the friction factors seems to increase with increasing Reynolds numbers, in contrast with the theoretically expected results. The theoretical curves for the friction decrease with increasing Reynolds number, while the experimental values seem to increase or stay the same. The experimental values for the friction are lower than the theoretically expected values. The highest friction factors can be seen in the experimental results for the 10x12mm wire cloths and the lowest results are for the 10x8mm wire cloths.

6.3.3 Comparison with measurements on flat plates

The experiments on the flat plates did not make it possible to calculate a friction factor, which could be compared easily to the friction factor of the wire cloths. Plotting the pressure curves of the plates and cloth in the same graphs seems to be a good solution, but is only possible if the air velocity is about the same. These pressure curves are plotted in figure 6.22. It is difficult to draw general conclusions from these figures. The pressure drop at the edge seems to be larger for the plates than for the cloths. The pressure drop per meter between the cloths or plates seems to be slightly larger for the plates than for the cloths. The overall pressure difference however seems to be larger for the wire cloths than for the plates. It is strange that the pressure gain at the end of the plates can not be seen in the pressure curves for the wire cloths.

6.4 Heat transfer and friction compared

As described in section 2.9, there are theories on the relation between heat transfer and friction. This is an important relationship for a heat exchanger, because it has to have a heat transfer

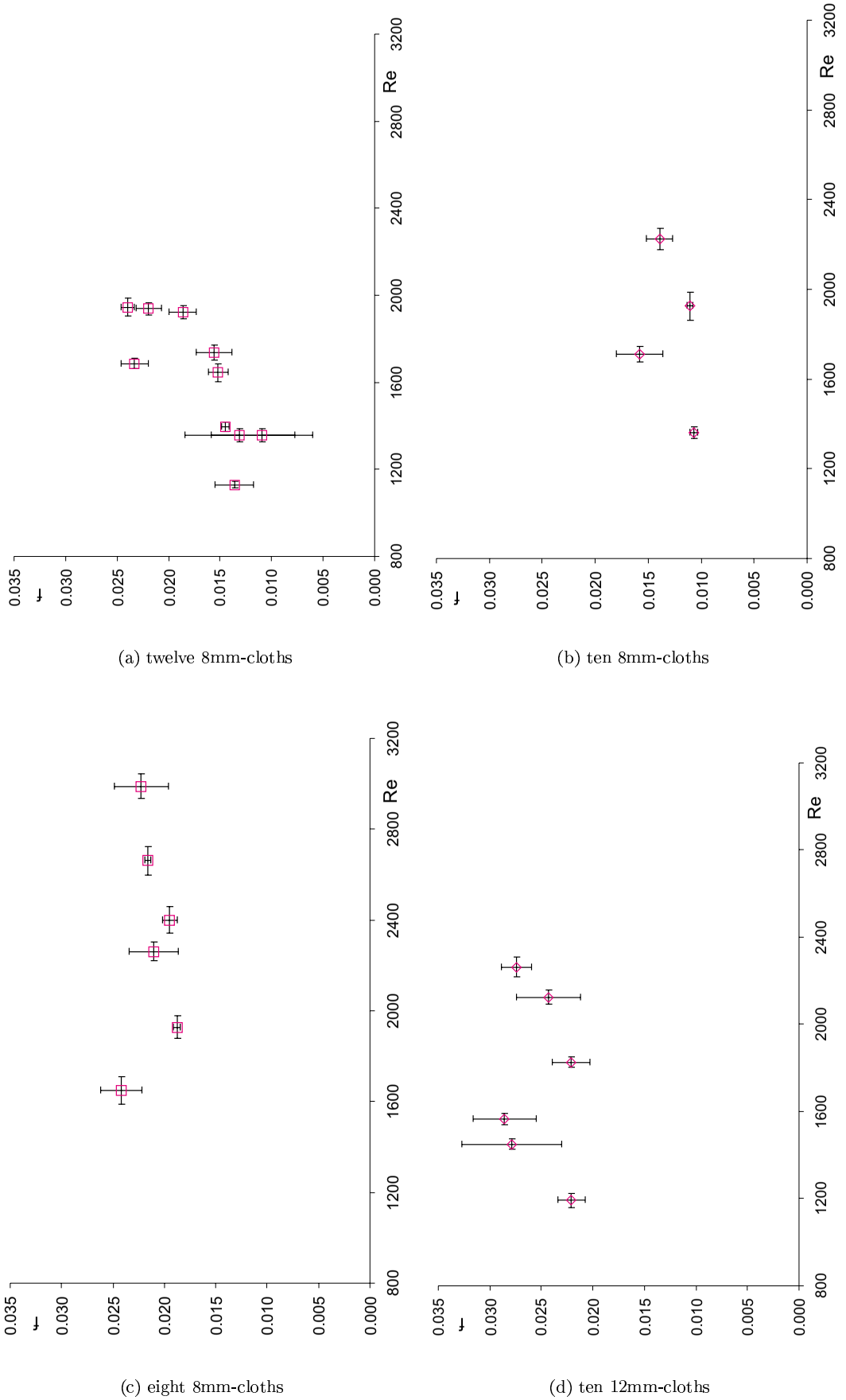

(a) twelve 8mm-cloths

(b) ten 8mm-cloths

(c) eight 8mm-cloths

(d) ten 12mm-cloths

Figure 6.16: The friction factor and its uncertainty for the different configurations.

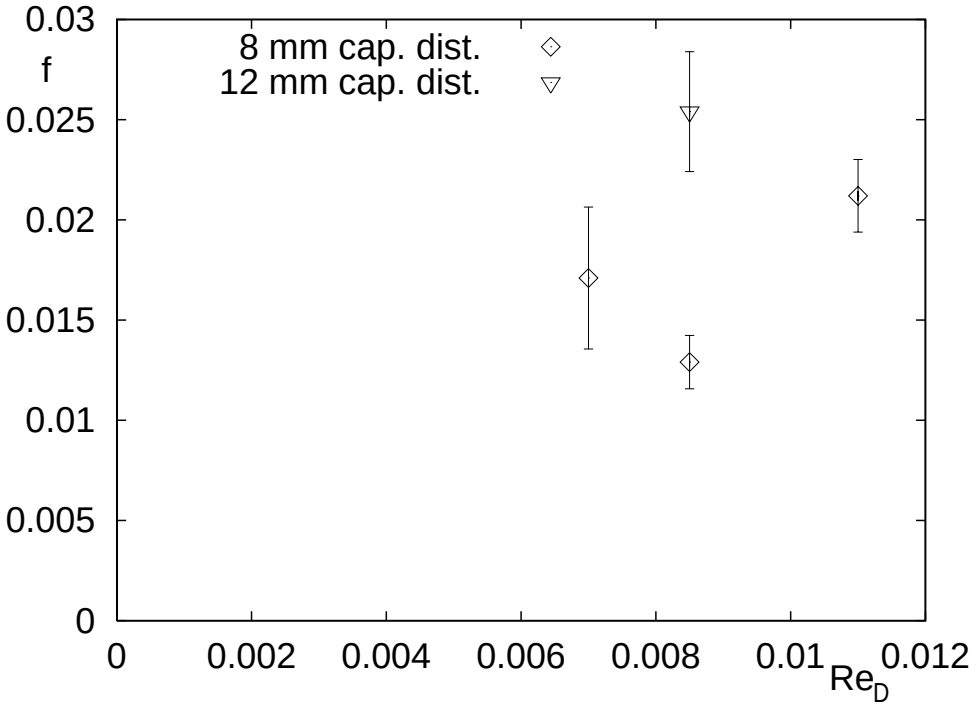

Figure 6.17: f plotted against the distance between the cloths.

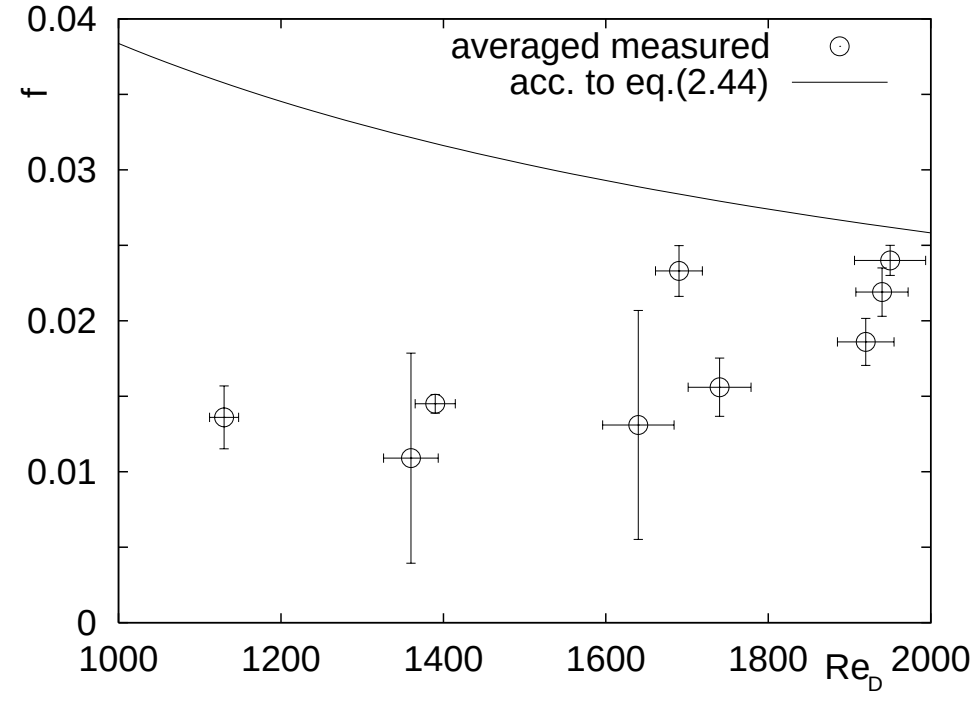

Figure 6.18: f, from the experiments and according to the theory plotted against the Reynolds number. The measurement is done with 12 8mm-cloths.

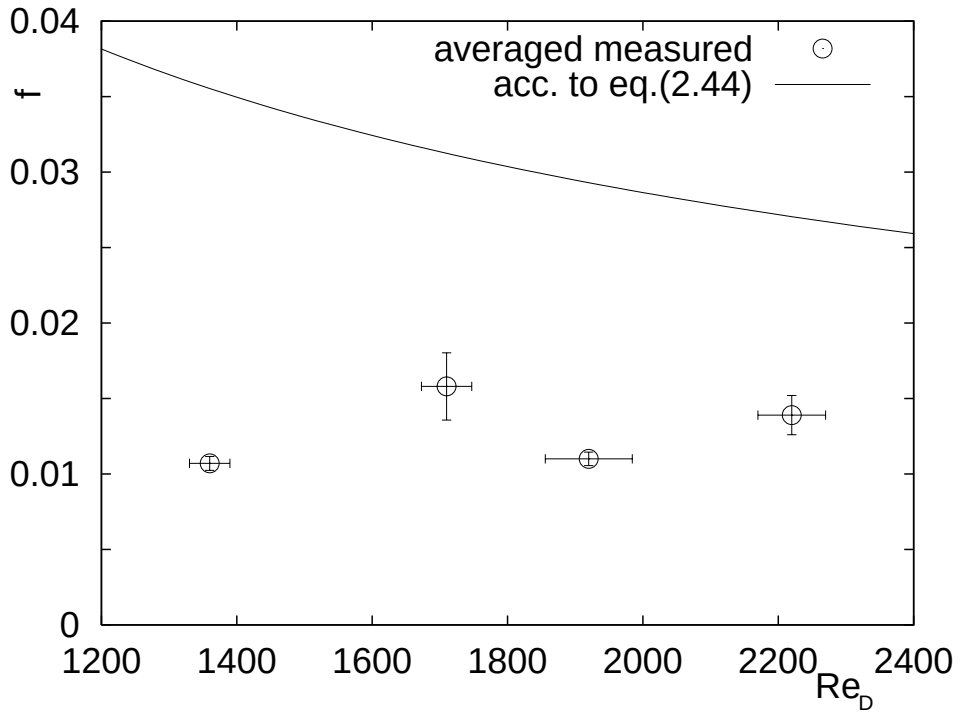

Figure 6.19: f, from the experiments and according to the theory plotted against the Reynolds number. The measurement is done with 10 8mm-cloths.

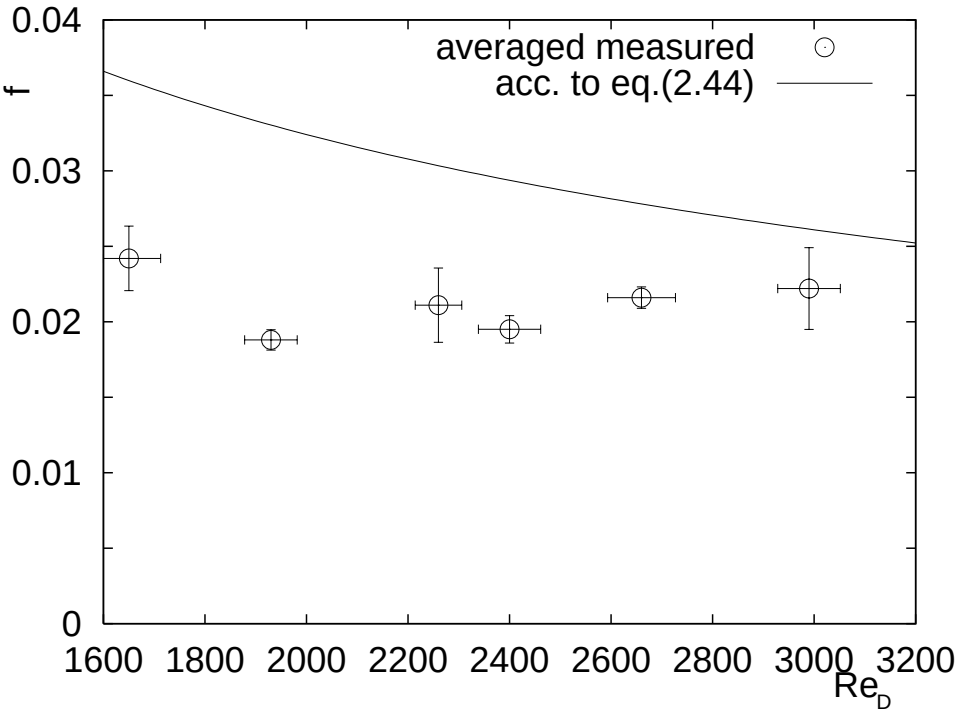

Figure 6.20: f, from the experiments and according to the theory plotted against the Reynolds number. The measurement is done with 8 8mm-cloths.

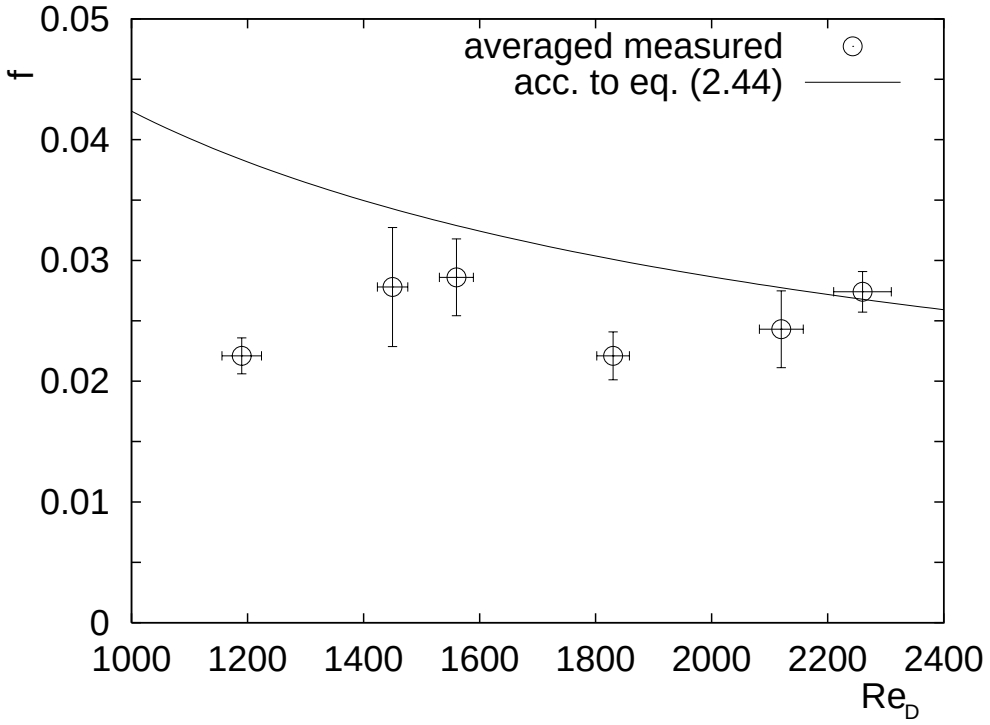

Figure 6.21: f, from the experiments and according to the theory plotted against the Reynolds number. The measurement is done with 10 12mm-cloths.

that is as high as possible with a friction that is as low as possible. In other words the ratio of heat transfer and friction should be as high as possible. In the figures in this section this ratio is expressed in $\frac{StPr^{2/3}}{f}$. This ratio is also used in [Kays and London, 1984], it makes it possible to compare our data with the data of other heat exchangers.
A comparison of the ratio of heat transfer and friction is given in figure 6.23. The ten 8mm-cloths give the best results. The lowest ratio of heat transfer and friction is measured with the twelve 8mm-cloths and the ten 12mm-cloths.
In the next figures the ratio is plotted for each configuration separately. The theoretically expected curve is calculated by dividing the theoretically expected curve for the heat transfer by the theoretically expected curve for the friction factor. In all cases, the measured ratio exceeds the theoretically predicted values by a factor 2-8.
When these ratios are plotted into figure 6.28 from [Kays and London, 1984] we see that the wire cloths have a much higher heat transfer-to-friction ratio than more commonly used heat exchangers.
The measurement of the ten 8mm-cloths gives the best results, but the eight 8mm-wire cloths give also a good result and the values for both heat transfer and friction factor do not show strange bumps.

6.5 Conclusions from the experiments with wire cloths

For the three series of measurements that were done on the 8mm cloths at various mutual distances, the heat transfer expressed in $StPr^{2/3}$ increases with increasing distance between the cloths. If this heat transfer is multiplied by the number of cloths that fits in a stack of 1 m high, the cloths with a mutual distance of 8.5mm (which was the case in the measurement with ten cloths) show

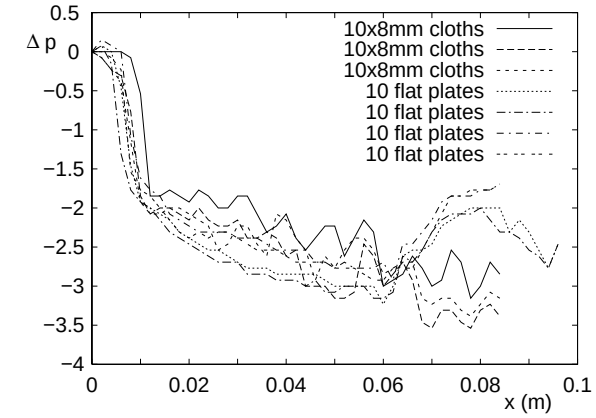

(a) n=10,$v_a = 2.4m/s$

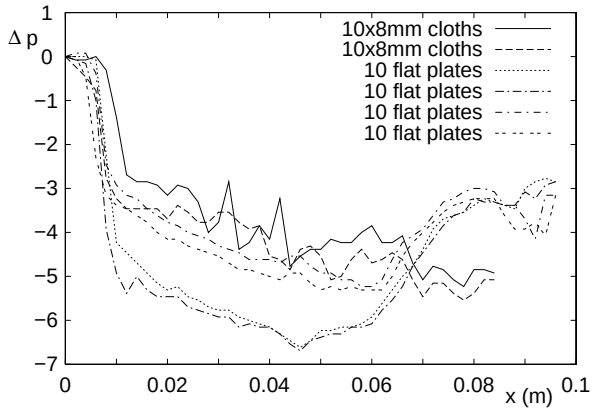

(b) n=10,$v_a = 3.1m/s$

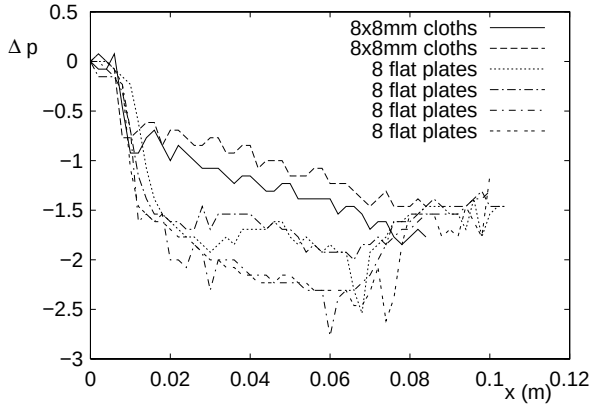

(c) n=8,$v_a = 1.8m/s$

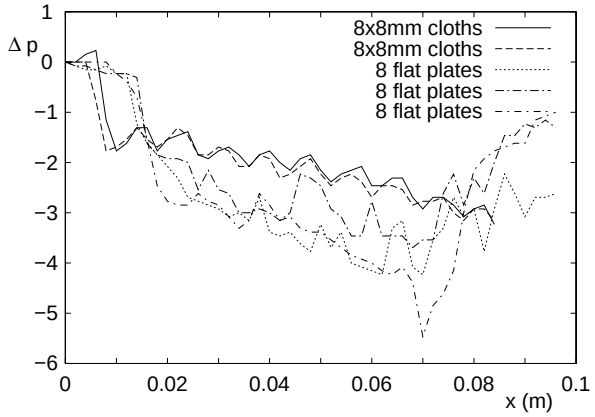

(d) n=8,$v_a = 2.6m/s$

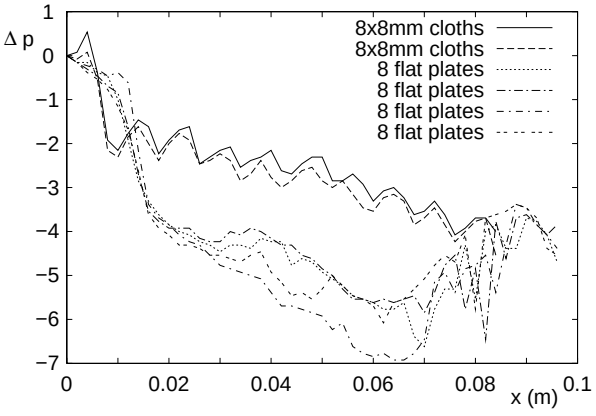

(e) n=8,$v_a = 2.8m/s$

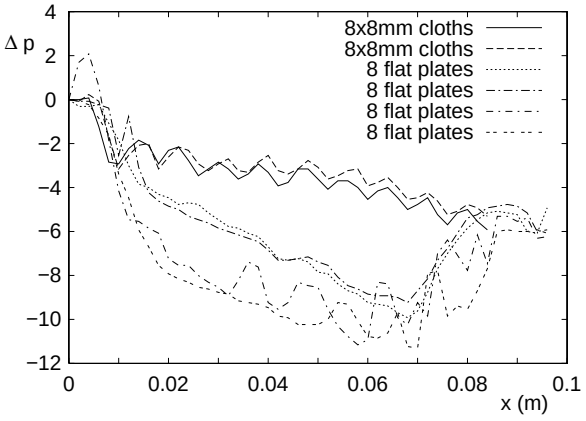

(f) n=8,$v_a = 3.2m/s$

Figure 6.22: Pressure curves of n cloths at different velocities of the air

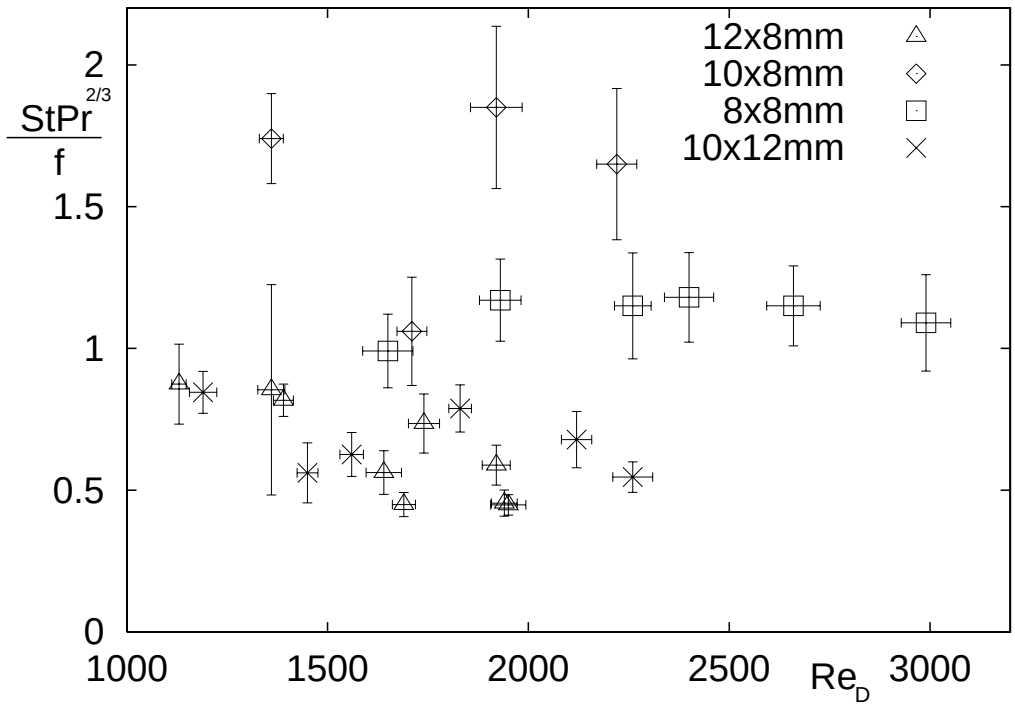

Figure 6.23: The ratio between heat transfer and the friction expressed as $StPr^{2/3}/f$ for the different cloths

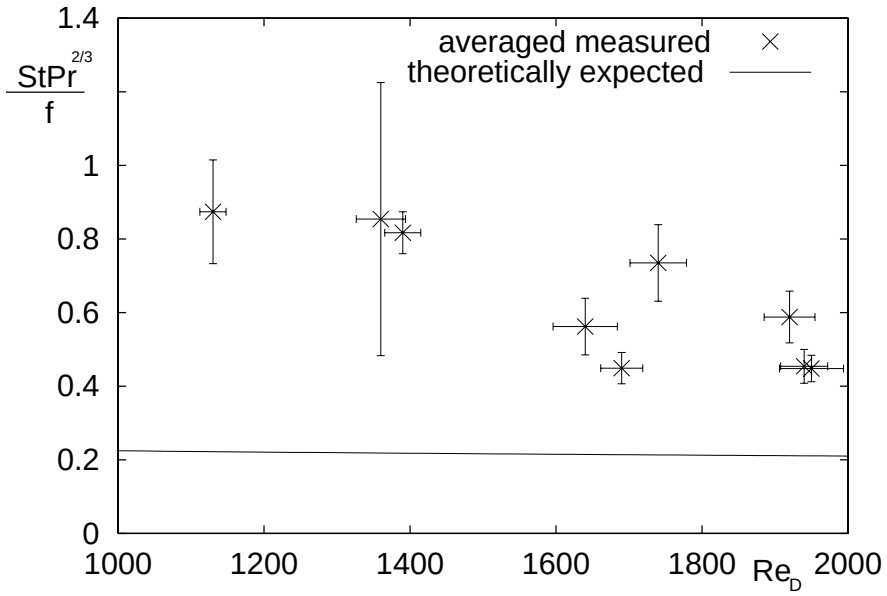

Figure 6.24: The ratio between heat transfer and the friction expressed as $StPr^{2/3}/f$. The measurement is done with 12 8mm-cloths.

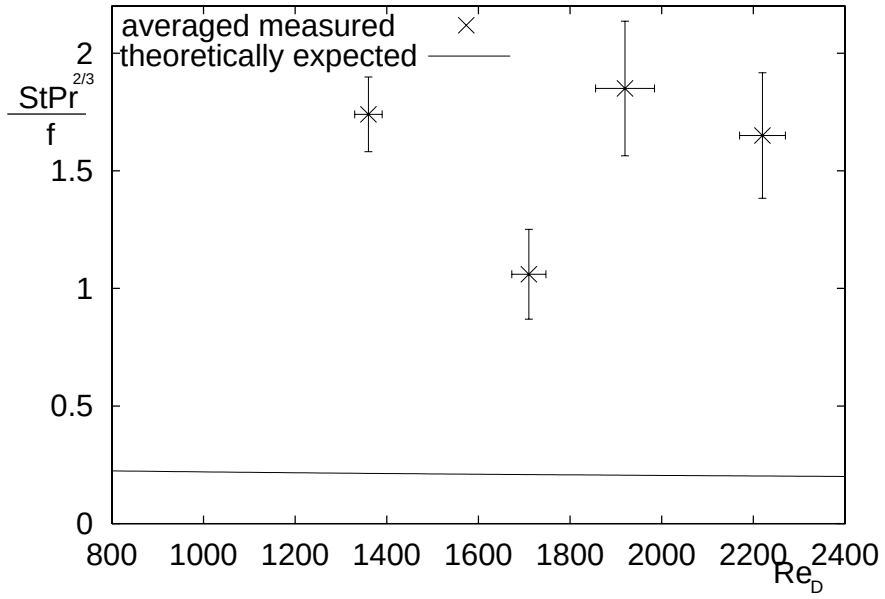

Figure 6.25: The ratio between heat transfer and the friction expressed as $StPr^{2/3}/f$. The measurement is done with 10 8mm-cloths.

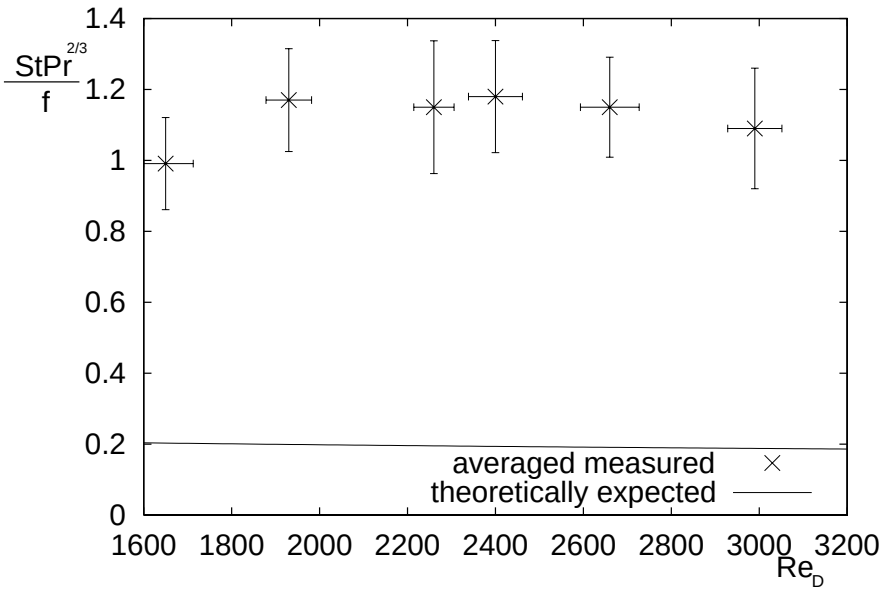

Figure 6.26: The ratio between heat transfer and the friction expressed as $StPr^{2/3}/f$. The measurement is done with 8 8mm-cloths.

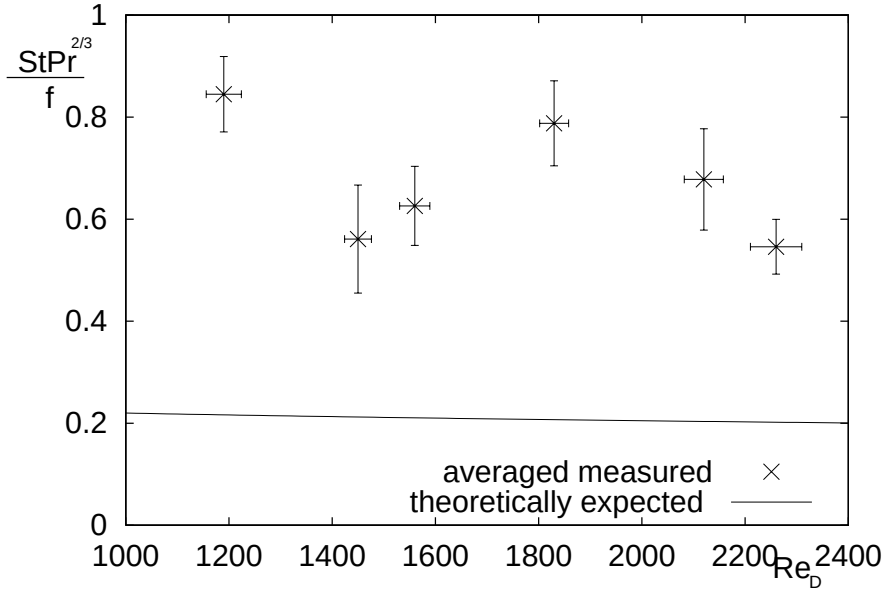

Figure 6.27: The ratio between heat transfer and the friction expressed as $StPr^{2/3}/f$. The measurement is done with 10 12mm-cloths.

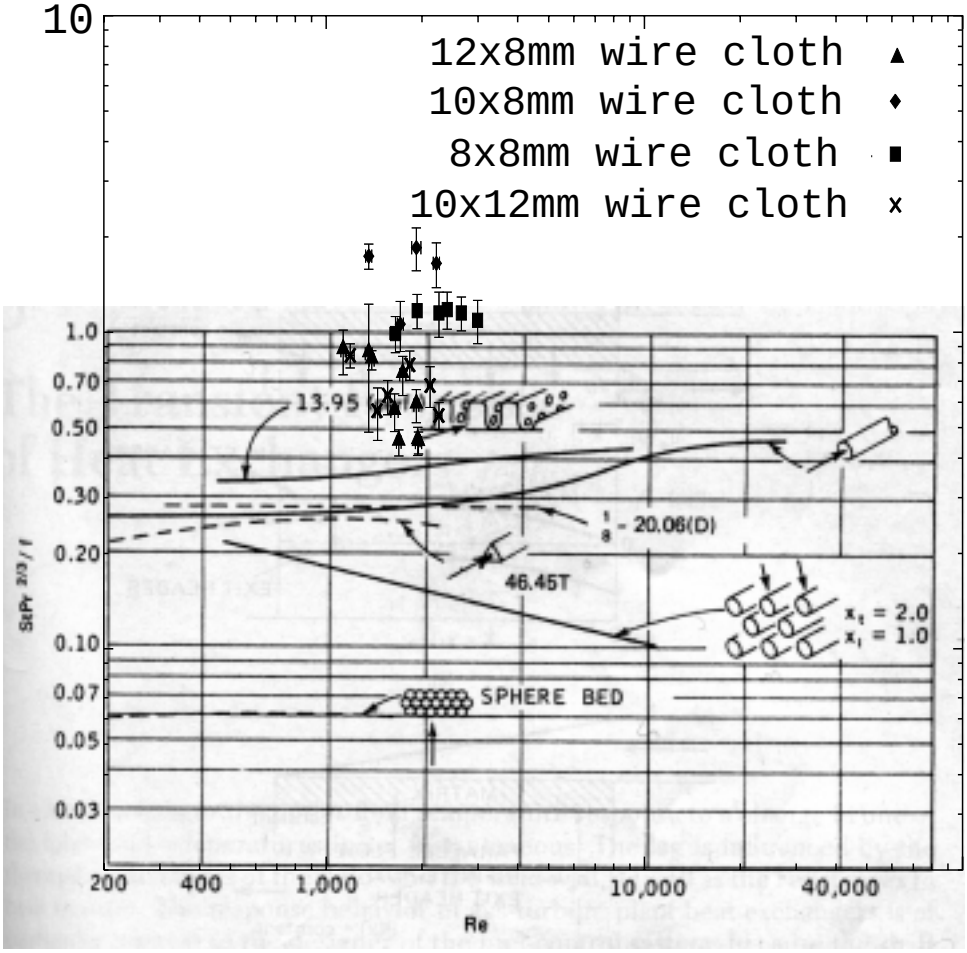

Figure 6.28: The ratio between heat transfer and the friction for different heat exchangers

the highest heat transfer.
The influence of the Reynolds number is so small compared to the experimental uncertainties that no conclusion can be drawn from these measurements.
The measured heat transfer is between 1.5 and 4 times higher than the theoretically expected value according to equation (2.45). The heat transfer in $StPr^{2/3}$ of the eight wire cloths is about 1.5 times as large as the heat transfer of the flat plates, but the heat transfer of the ten wire cloths is comparable to that of the ten flat plates.

The pressure curve between the wire cloths was approximately linear, so that the friction factor could be determined. The smallest friction factor was measured for ten 8mm cloths, the highest friction factor for ten 12mm cloths.
The friction factor is between 0.3 and 1.0 times lower than the theoretically expected friction according to equation (2.44), [Shah, 1978]. The highest friction factor is found for the 10x12mm wire cloths and the lowest for the 10x8mm wire cloths. The friction factor varies between 0.01 and 0.03. According to the theory, the friction was expected to decrease with increasing Reynolds numbers. This can not be seen in the measurements, but the range of Reynolds numbers and the difference in friction factor is too small to draw conclusions.

The ratio of the heat transfer and friction, expressed as $\frac{StPr^{2/3}}{f}$ is measured to be between 0.45 and 1.8. The highest ratio of the heat transfer and friction is measured for the 10x8mm cloths. This ratio is between 1.1 and 1.8, while usual heat exchangers do not reach more than 0.5. The theoretically expected value, calculated by dividing the theoretically expected values for heat transfer and friction, was about 0.2.

Chapter 7

Conclusions and recommendations

The goal of this thesis was to investigate the ratio between heat transfer and friction in a Fiwihex fan, to compare this ratio with that of flat plates and to investigate what the reason is of this high heat transfer. Different types of wire cloths were studied, viz. wire cloths with a distance of 8 and 12mm between the capillaries. In this section the conclusions from the measurements are described and recommendations are given for further research.

7.1 Conclusions

Measurements with a mass balance
A first attempt was made to measure the friction on a wire cloth with a mass balance. In these measurements the object was suspended to the mass balance in a tube through which air flowed. To validate this set-up the friction on cylinders and spheres was measured. The results for the measurements on the cylinders and the sphere could not be explained satisfactorily, so that no measurements were done on the wire cloths themselves. Therefore no conclusion can be drawn from these measurements on the properties of the wire cloths, but it can be said that it is very difficult to measure the drag coefficient by using a mass balance. This is probably due to wall effects.

Friction and heat transfer of flat plates
The friction and heat transfer of flat plates were measured to validate the second set-up in which the friction was measured with a pressure difference meter and the heat transfer with temperature sensors. The main conclusion from these measurements with flat plates was that there are too many differences between the measured and theoretically expected pressure so that the set-up was not validated by these measurements. The entrance- and exit effects seem to take place inside the channels instead of at the edge of them.

Friction and heat transfer of wire cloths
The heat transfer of the wire cloths is higher than that of the theoretically expected values for flat plates.
The heat transfer per cloth, i.e. the transferred heat divided by the logarithmic temperature difference, is measured to be between 1 and 2.5 times higher for the wire cloths than measured for the flat plates.
For the three measurements with the 8mm cloths at varying mutual distances, the heat transfer

expressed in $StPr^{2/3}$ increases with increasing mutual distance. However, if a stack of cloths has to be placed in a limited space, the highest total heat transfer can be reached with the cloths at a mutual distance of approximately 8.5mm. The heat transfer for the 12mm cloths is smaller than the heat transfer of the 8mm cloths.
The friction of the wire cloths is between 0.3 and 1.0 times lower than the theoretically expected friction for a flat plate. The highest friction factor is found for the 12mm wire cloths and the lowest for the 8mm wire cloths. The friction factor varies between 0.01 and 0.03.
The highest ratio of the heat transfer and friction, expressed as $\frac{StPr^{2/3}}{f}$ is measured for the 8mm cloths at a mutual distance of approximately 8.5mm. This ratio is between 1.1 and 1.8, while usual heat exchangers do not reach more than 0.5.

The ratio between heat transfer and friction that was measured, was considerably higher than that of flat plates or other heat exchangers. The reason why the ratio between heat transfer and friction is so large is not found. For this purpose more heat transfer and friction measurements would have to be done, and visualisation of the flow or velocity measurement techniques, like Laser Doppler Anemometry, should be used, to unravel the particular nature of the turbulent flow along the cloths.

7.2 Recommendations

Measurements with a mass balance
It is very difficult to measure the real friction coefficient of the wire cloths by using a mass balance. With a mass balance it is only possible to measure the drag force including entrance- and exit effects, but the advantage above measurements with a pressure meter is that it is easier to measure small mass differences than such a small pressure difference. A friction measurement with a mass balance is therefore expected to be more accurate, if the walls would not influence the drag. This influence of the wall can be minimized by increasing the size of the tube through which the air flows or by decreasing the size of the object of which the drag is measured. If the size of the object is decreased, the attachment of the object to the mass balance should be very small, so that the drag on the object is not negligible compared to the drag on the attachment.
More measurements are needed to find out what the causes were for the unexplained results and what the correct drag-coefficient is for a cylinder or sphere in a container. It would be interesting to do more measurements with cylinders, spheres and channels of different sizes to know the influence of the walls of a rectangular channel on an object.

Friction and heat transfer of the flat plates
Further measurements should be done on the heat transfer of flat plates and the friction, because of the strange and unexpected results obtained in the present research. When also measurements are done with plates that are longer than the expected entrance length, the friction factor can be determined by taking the steepness of the pressure curve when it has become straight. To determine what causes this large entrance and exit effects, the plates can be rounded to see what happens if the change in free flow area is not so abrupt. The pressure curve should be measured in every channel to see if there are large differences between the different channels.

Friction and heat transfer of the wire cloths The main recommendation is that more measurements should be done. Below some recommendations are listed as complement to the measurements that are done.

- To compare the theoretically expected shape of the curve of the heat transfer, $StPr^{2/3}$ or

the friction factor, f, as a function of Reynolds with the experimentally found shape, a larger measurement region is necessary. In the measurements, described in this report, the Reynolds region does not even cover a decade, so that it is impossible to give the relation between the heat transfer and the velocity.

- The friction of the 12mm wire cloth was larger than that of the 8mm wire cloths. The 12mm wire cloths can also be measured at different mutual distance, so that these results can also be compared with the results of the 8mm wire cloths. The influence of the distance between the capillaries on the friction can be investigated by measuring the friction factor of a wire cloth with a different number of capillaries.

- In the Fiwihex itself the cloths are placed around the fan, see figure 4.6. They are therefore not parallel to each other. The influence of the direction in which the cloths are placed with respect to each other should also be measured.

The recommendations above are especially needed to gain more data on the functioning of the Fiwihex, but the purpose of this project was also to gain more insight in the heat transfer and friction of the wire cloths, so that the optimal placement of the wire cloths around the Fiwihex fan could be found. Several recommendations are given below for further research on the wire cloths. First of all, visualisation of the flow field or velocity measurements with Laser Doppler Anemometry can give a picture of how the air flow really moves along the cloths. From the results of these measurements it can be decided which property of the wire cloths will probably have a large influence on the heat transfer and friction and therefore has to be investigated further.
There are several differences that might be the cause of the higher ratio of heat transfer and friction of the wire cloths, compared to that of flat plates. These possible causes are listed below with recommendations to find out what their influence on the heat transfer and friction is. In most cases this can be done by comparing the wire cloths with a plate that is the same in as many aspects as possible, but differs in the aspect that has to be investigated.

- The copper wires from the wire cloth that are placed in the direction of the flow guide the air straight along the cloth, so that less velocity fluctuations in the horizontal plane, perpendicular to the direction of flow exist.

To investigate the influence of the direction of the copper wires compared to the direction of flow, the wire cloths can be turned for example over 90 degrees, so that the air still flows along the cloths, but parallel to the capillaries and perpendicular to the woven copper wires. Then, the headers should be changed, because they would have too much influence on the flow if they are placed perpendicular to it.When the heat transfer and friction are measured in this way, it can be seen whether the direction of the cloths has much influence on the heat transfer and friction.

- The capillaries give the wire cloths a 'wavy' shape and prevent the boundary layer to grow. It would be expected that this effect causes a higher heat transfer and friction. The higher heat transfer of the wire cloths that was measured corresponded to this expectation, but the friction of the wire cloths appeared to be lower.

The influence of this wavy shape can be measured by comparing the results of the wire cloths and of the flat plates with that of a plate that consists of capillaries on which two wavy sheets of metal are soldered to each side, so that the sheets touch each other in the middle.

- The wire cloths are porous, so that part of the flow can travel through the wire cloths and the velocity close to the wall does not have to be equal to zero.

This influence of the porosity of the wire cloths is more difficult to investigate. A wire cloth that has the same shape as a normal wire cloth, but is not porous is difficult to make. It might be possible to use the plates that are described above, with capillaries on which wavy sheets of metal are soldered that touch each other in the middle, and copper wires are soldered unto these plates. However, it is very difficult and labour-intensive to solder all these copper wires next to each other on these plates. It is easier to etch lines into the metal sheats, so that their surface has about the same shape as the wire cloths, but is not porous.

The recommendations that are mentioned above are all meant to get more data on the functioning of the wire cloths and a better understanding of the flow along the wire cloths. For the specifications of the Fiwihex fan, it is also useful to measure the behaviour of a Fiwihex in a controlled environment. For example a very good insulated room that is heated by a Fiwihex, in which the temperature of the warm water in the Fiwihex, the temperature of the room and the power of the fan are measured. A project has already be launched in which a number of Fiwihex are placed in a greenhouse, in combination with heat storage in the ground, to investigate the effects and the amount of energy that can be saved.

Appendix A

Uncertainty analysis

Before drawing conclusions from the measured data, the uncertainties in this data should first be considered. When a quantity, like for example the friction factor, depends on many variables, there are a lot of sources of uncertainty and it is necessary to investigate how these uncertainties influence the uncertainty of the result. In this appendix the elaboration of the calculation of the uncertainties is given for the Reynolds number (section A.1), the heat transfer (section A.2), and the friction factor measured with a pressure difference meter (section A.3). The uncertainties for the measurements that were done with a mass balance, from chapter 3 are given in section A.4.
If a variable, z is a function of independent measured variables, x and y, the uncertainty propagates as [Practicum, 1997]:

$$u(z) = \sqrt{(\frac{\partial f}{\partial x}u(x))^2 + (\frac{\partial f}{\partial y}u(y))^2} \tag{A.1}$$

The propagation of uncertainty for some of the most occurring cases is:

$$\begin{array}{ccccc} z = ax + by & or & z = ax - by & & u^2(z) = a^2u^2(x) + b^2u^2(y) \\ z = cxy & or & z = \frac{cx}{y} & & (\frac{u(z)}{z})^2 = (\frac{u(x)}{x})^2 + (\frac{u(y)}{y})^2 \\ z = cx^\alpha y^\beta & & & & (\frac{u(z)}{z})^2 = (\alpha\frac{u(x)}{x})^2 + (\beta\frac{u(y)}{y})^2 \end{array} \tag{A.2}$$

These equations are used to calculate the uncertainty of the results.
Uncertainties can be divided into two types: systematic and non-systematic uncertainties. Systematic uncertainties have to do with the measuring device, or with the measurement method. If a quantity is measured a few times, its systematic uncertainty stays the same. A non-systematic uncertainty differs for each measurement. The total uncertainty is calculated by extracting the root of the sum of the squares of the systematic and non-systematic uncertainty.

A.1 Uncertainty in the Reynolds number and air velocity

The Reynolds number is calculated with the following equation:

$$Re_D = \frac{\rho v_a D_h}{\eta} \tag{A.3}$$

in which v_a is the velocity of the air, that can be calculated with:

$$v_a = \frac{P_c}{c_a \cdot \Delta T_{a,end}} \cdot \frac{1}{\rho_a A_f} \tag{A.4}$$

To calculate the uncertainty in the velocity, also equation A.5 is needed to calculate the free flow area:

$$A_f = b \cdot (H - n_{cloth} \cdot d_{cloth}) \tag{A.5}$$

The equation that can be used to calculate the hydraulic diameter, D_h:

$$D_h = \frac{4A_f}{n_{cloth}\pi b} \tag{A.6}$$

These equations can be combined into:

$$Re_D = \frac{4P_c}{\pi n_{cloth}\eta_a c_a T_{a,end} b} \tag{A.7}$$

In this equation is used:

P_c	power that is used to heat the air with the wire rack
η_a	dynamic viscosity of the air
c_a	specific heat of the air
$\Delta T_{a,end}$	temperature difference of the air before and after the wire rack
b	width of the cloth
ρ_a	density of the air
H	heigth of the tube
n_{cloth}	number of cloths
d_{cloth}	thickness of the cloth

The temperature is measured with temperature sensors that are calibrated by keeping them at the same temperature. Only temperature differences are measured, so that the systematic uncertainty could be neglected. However, the temperature sensors are used at different temperatures, which introduces a small systematic error.
The uncertainties that are used, to calculate the uncertainty in the Reynolds number and air velocity, can be seen in the following table:

	systematic uncertainty		non-systematic uncertainty		unity
	absolute	relative	absolute	relative	
P_c	2.0	0.02	-	-	W
η_a	5.10^{-8}	0.003	-	-	kg/ms
c_a	0.5	0.0005	-	-	J/kgK
$\Delta T_{a,end}$	0.1	0.02	0.1	0.02	K
b	0.001	0.005	-	-	m
ρ_a	0.0005	0.0004	-	-	kg/m^3
H	0.001	0.01	-	-	m
d_{cloth}	0.00017	0.1	-	-	m

With this data the relative systematic uncertainty in the Reynolds number becomes 0.03 and the relative non-systematic uncertainty about 0.02. The total relative uncertainty becomes 0.04. The uncertainty in the velocity of the air becomes about 0.04 for the relative systematic uncertainty and 0.02 for the relative non-systematic uncertainty, the total uncertainty is about 0.05.

A.2 Uncertainty in the heat transfer

For the calculation of the heat transfer coefficient of the water, the following equation is used:

$$h_w = \frac{\lambda_w n_{cap} Nu}{L_{cap}} = \frac{1.62\lambda_w n_{cap}}{L_{cap}} \left(\frac{a_w \mathrm{L}_{cap}}{d_{cap}^2 v_w}\right)^{-1/3} \tag{A.8}$$

In this equation:

λ_w	heat conductivity of water
n_{cap}	number of capillaries in a wire cloth
L_{cap}	length of a capillary
a_w	thermal diffusivity of the water
d_{cap}	diameter of the capillaries
v_w	velocity of the water

In the following table the uncertainties of the different quantities are printed. The uncertainties are split into a systematic and non-systematic part, and given as absolute and relative uncertainty.

	systematic uncertainty		non-systematic uncertainty		unity
	absolute	relative	absolute	relative	
λ_w	0.0008	0.001	-	-	W/mK
L_{cap}	0.001	0.01	-	-	m
a_w	$5 \cdot 10^{-10}$	0.00350	-	-	m^2/s
d_{cap}	0.00001	0.01	-	-	m
v_w	0.01	0.02	0.01	0.02	m/s

These uncertainties lead to an systematic relative uncertainty in the heat transfer coefficient of the water of 0.01 and a non-systematic relative uncertainty of 0.007. This is a total relative uncertainty of 0.02.

For the calculation of the overall heat transfer, $h_{overall}$ this equation is used:

$$h_{overall} = \frac{P_a}{\Delta T_{ln}} \tag{A.9}$$

in which:

P_a	power that is transferred to the air
ΔT_{ln}	logarithmic temperature difference

Equation (A.10) is used to calculate the logarithmic temperature difference:

$$\Delta T_{ln} = \frac{T_{w,in} - T_{a,in}}{T_{w,out} - T_{a,out}} \cdot \frac{1}{ln(\frac{T_{w,in} - T_{a,in}}{T_{w,out} - T_{a,out}})} \tag{A.10}$$

in which:

$T_{w,in}$	temperature of the water before the wire cloths
$T_{a,in}$	temperature of the air before the wire cloths
$T_{w,out}$	temperature of the water after the wire cloths
$T_{a,out}$	temperature of the air after the wire cloths

The uncertainties that can be derived in this way, are given in the following table:

	systematic uncertainty		non-systematic uncertainty		unity
	absolute	relative	absolute	relative	
P_a	2	0.02	-	-	W
ΔT_{ln}	0.07	0.02	0.07	0.02	K
$h_{overall}$	0.6	0.03	0.5	0.02	W/m^2K

The heat transfer from the wires to the air can be calculated by the following equations:

$$\frac{1}{h_{wire\to a}} = \eta_{fin}(\frac{1}{h_{overall}} - \frac{1}{h_w}) \tag{A.11}$$

$$\eta_{fin} = \frac{\tanh N}{N} \tag{A.12}$$

$$N = \sqrt{\frac{h_{wire\to a} \cdot L_{fin}^2}{\lambda_c d_{wire}}} \tag{A.13}$$

in which:

η_{fin}	efficiency of the wires
L_{fin}	length of the 'wire fins', half the distance between the capillaries in the cloth
λ_c	heat conductivity of copper
d_{wire}	diameter of the wires

Because of the iteration in the calculation of η_{fin}, it is difficult to calculate the systematic uncertainty in the efficiency of the wires. With the characteristic values of $h_{wire\to s}$ from the measurements, it appears that the uncertainty in the efficiency of the wires is very small, so that it is a careful estimation if the relative errors are taken to be 0.01. The relative systematic uncertainty for the heat transfer coefficient from the wires to the air becomes: $h_{wire\to a}$ 0.03 and the relative non-systematic uncertainty 0.02.
The heat transfer expressed as $StPr^{2/3}$ can be calculated with:

$$StPr^{2/3} = \frac{h_{wire\to a}}{\rho_a c_a v_a} \cdot Pr^{2/3} \tag{A.14}$$

In this equation:

Pr	Prandtl number
$h_{wire->a}$	heat transfer coefficient from the wires to the air
v_a	velocity of the air along the cloth

The relative systematic uncertainty becomes 0.05 and the relative non-systematic uncertainty 0.03. The total uncertainty therefore becomes 0.06.

A.3 Uncertainty in the friction factor

In this section the uncertainty is calculated for the friction factor when the pressure drop is used to determine the friction.
The shear stress, tau, can be calculated with:

$$\tau = \frac{\Delta p_{tot} \cdot b \cdot s}{2 \cdot b\frac{\pi}{2} L_{cloth}} = \frac{\Delta p_{tot} \cdot s}{\pi L_{cloth}} \tag{A.15}$$

in which L_{cloth} is the length of the cloth. The total pressure difference, Δp_{tot}, over the cloth, without entrance and exit effects, can be calculated with:

$$\Delta p_{tot} = \frac{\partial p}{\partial x} L_{cloth} \tag{A.16}$$

and the stitch, s, of the cloths with:

$$s = \frac{H}{n_{cloth}} \tag{A.17}$$

Then, the friction factor, f, can be calculated with:

$$f = \frac{\tau}{\frac{1}{2}\rho v_a^2} \tag{A.18}$$

After combination of equations, we find for the friction factor:

$$f = \frac{2}{\pi \cdot n_{cloth}} \cdot \frac{c^2 \rho b^2 H (H - n_{cloth} \cdot d_{cloth})^2 \Delta T_{a,end}^2}{P_c^2} \cdot \frac{\partial p}{\partial x} \tag{A.19}$$

The pressure measurements are in fact pressure difference measurements, so that the relative systematic error of the pressure difference is taken to be 0. The relative non-systematic error is taken to be 10%. With these uncertainties and rules of propagation of errors and uncertainties from [Chatfield, 1970] the uncertainty in the friction factor due to the systematic uncertainty can be calculated. This leads to a relative systematic uncertainty in the friction factor of almost 0.07 and a relative non-systematic uncertainty of 0.11. This is a total relative uncertainty of 0.13.

A.4 Uncertainty analysis measurements with the mass balance

In this chapter the calculation of the uncertainties in the drag coefficients is given. In table A.1 the uncertainties are given of the direct measured quantities.

	systematic uncertainty		unity
	absolute	relative	
$d_{cyl}(large)$	0.0005	0.02	m
$l_{cyl}(large)$	0.0005	0.004	m
$d_{cyl}(small)$	0.0005	0.03	m
$l_{cyl}(small)$	0.0005	0.006	m
d_{pp}	0.0005	0.001	m
w_{tube}	0.001	0.004	m
d_{tube}	0.001	0.02	m
ρ_a	0.0005	0.0004	kg/m^3
η_a	5.10^{-8}	0.003	kg/ms
ϕ_v	·	0.04	m^3/s

Table A.1: The uncertainties of the direct measured quantities

The equations that are used to calculate the propagation of uncertainty are given in appendix A. These equations are used to calculate the friction factor:

$$f = \frac{(m - m_0) g \xi}{\frac{1}{2}\rho v_a^2 \cdot A_{cyl}} \tag{A.20}$$

in which $(m - m_0)$ is the mass difference between a situation with and without airflow; ξ is the ratio of the two arms of the lever and is left out in the measurements without lever. The velocity of the air is calculated by:

$$v_a = \frac{\phi_v}{w_{tube} d_{tube}} \tag{A.21}$$

The Reynolds number finally is calculated with:

$$Re_D = \frac{\rho v_a d_{obj}}{\eta_a} \tag{A.22}$$

in which d_{obj} is the diameter of the cylinder or the pingpong-ball. The uncertainty of the mass is taken to be 0.01 g and the relative uncertainty of the volume flow 0.08. With this equations and given uncertainties it is possible to calculate the uncertainty for each separate measurement.

A.5 Conclusions for the uncertainty analysis

The non-systematic uncertainties that were estimated in previous sections, are for one measurement. If the same measurement is repeated a few times, this non-systematic uncertainty can be divided by $\sqrt{n}$, in which n is the number of equal measurements. The problem is that it is difficult to estimate this uncertainty, because it differs much in different measurements.
The results for the uncertainties (if only one measurement is done) are given in table A.2:

	relative systematic uncertainty	relative non-systematic uncertainty	total relative uncertainty
Re_D	0.03	0.02	0.04
v_a	0.04	0.02	0.05
$StPr^{2/3}$	0.05	0.03	0.06
f	0.07	0.11	0.13

Table A.2: Overview of the uncertainties for the different quantities.

The other way to determine the non systematic uncertainty is statistical. This means that the measurement has to be repeated several times and that the uncertainty is derived from the difference between the results of one measurement series. An advantage of this statistical determination of the uncertainty is that it is not possible to estimate wrong values for the uncertainty of even forget sources of uncertainty. A disadvantage of this method is that when the measurements happen to lie close to each other completely by chance, the statistical uncertainty can become very small.
The statistically derived non-systematic uncertainties seemed to be larger than the non-statistically derived uncertainties. Therefore, the total uncertainty of the results is calculated by extracting the root of the sum of the squares of the non-statistically derived, systematic uncertainty and the statistically derived non-systematic uncertainty.

Appendix B

Simulations on the pressure drop between flat plates

Simulations are done by H.P. Kritzinger to compare the measured pressure curve between the flat plates with the simulations. For these simulations the CFD flow simulation code Fluent is used.

B.1 3D and 2D

The more complicated a model is, the more time and computer power does it take to solve it. Therefore the idea was to simulate the pressure distribution with a two dimensional model instead of a three dimensional model. To validate that this is possible, a three dimensional simulation of the flow between just two plates was compared with the two dimensional simulation between two plates. The configurations of the three dimensional simulation is given in figure B.1. The small cylinder in figure B.1 is one of the ends of the pressure meter and is called the pressure sensor in this Appendix. The other arm is placed before the cloths and does not have as much influence on the flow.
In the two dimensional simulations this pressure sensor was modelled by a small cylinder over the whole width (or else it would not be 2D any more), which blocks the flow just as much as in the 3D case. The results of these simulations are plotted in figure B.2: In this figure the top two lines are those of the pressure without a pressure sensor in the flow, the lower two lines draw the pressure drop while a pressure sensor is placed in the middle of the plates. The length of the plate is 8.5 cm and it is placed from -0.0425 to 0.0425. At the place of the pressure meter a sharp negative peak can be seen, that is higher for the three dimensional simulation. Apart from this peak, the pressure curve is about the same between the plates, only the exit effect differs for the two and three dimensional case.
The differences between the 2D and 3D simulations are so small, that for the simulations with more plates a two dimensional model was used.

B.2 Configuration of the 2D simulation

The configuration of the two dimensional simulation is plotted in figure B.3: In this figure three

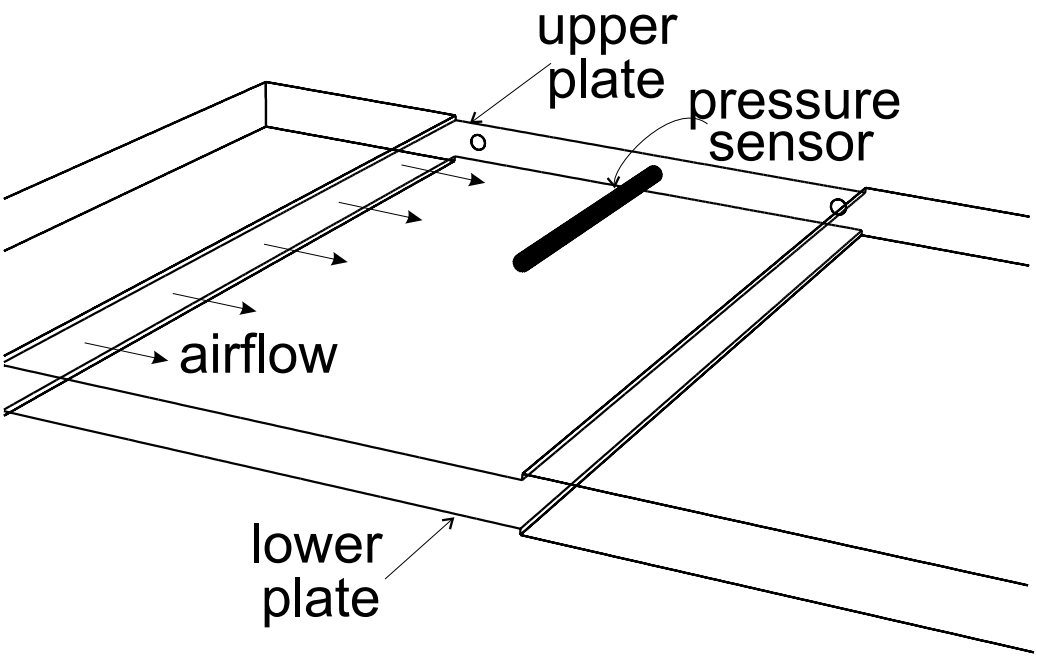

Figure B.1: Configuration of the three dimensional simulation

possible positions of the pressure sensor are drawn. The dimensions of the plates and the tube are the same as in reality, the velocity between the tubes is 3.0 m/s.

B.3 Results of the 2D simulation

The pressure drop in different channels in the tube, without a pressure sensor anywhere in the flow, was simulated to compare the channels with each other. The pressure is drawn in figure B.4: The pressure distribution in the middle channel and of the channel at 1/4 of the tube is about the same, but the pressure drop in the edge channel is lower. After the plates the pressure has to be equal again, so that the exit pressure gain of the edge channel is smaller.
The velocity of the channel at the edge is probably lower than that of the channel in the middle, because of the velocity profile before the channels. The distribution of the velocity gives an idea of the difference in velocity. In figure B.5 the distribution of the velocity in the flow direction is plotted for the simulation without a pressure sensor, but also for the simulations with the pressure sensor at different places between the middle plates.
In table B.1 the mean velocity is given for the channels from the middle (channel 1) to the edge (channel 5). The pressure drop in the middle channel with the pressure sensor at different positions is drawn in figure B.6. In this figure it can be seen that the gradient of the lines is almost the same between the plates, but a pressure drop occurs over the pressure sensor. In the real measurements only the pressure drop at the tip of the pressure sensor is measured: when the minima at these measurement points are connected, the gradient is about the same as the other gradients.

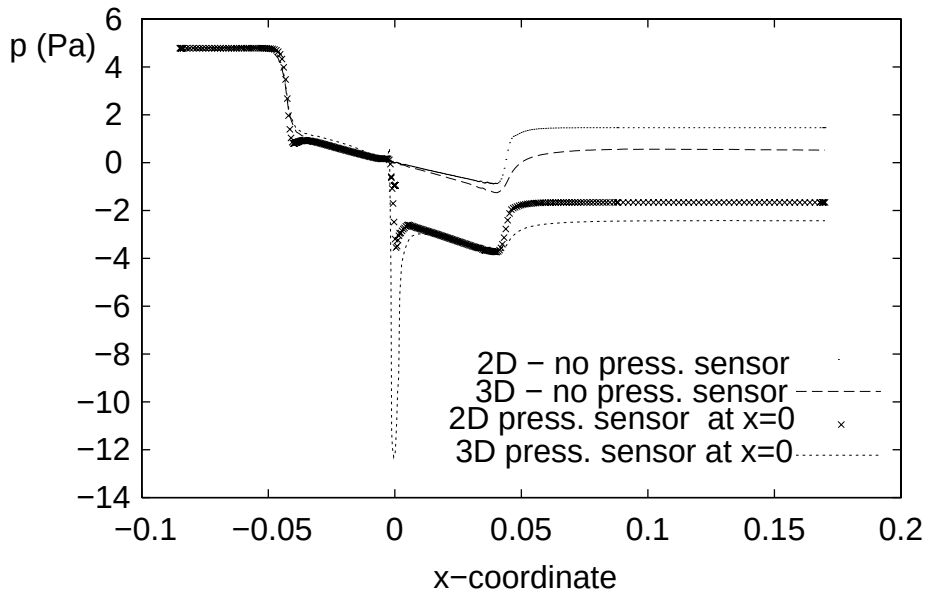

Figure B.2: Pressure distribution of the 2D and 3D simulation, with and without a pressure sensor at x=0, in the middle of the channel

	v $(none)$ (m/s)	v $(pos1)$ (m/s)	v $(pos2)$ (m/s)	v $(pos3)$ (m/s)	v_{rel} $(none)$	v_{rel} $(pos1)$	v_{rel} $(pos2)$	v_{rel} $(pos3)$
channel 1	3.13	2.78	2.77	2.77	1.03	0.92	0.91	0.91
channel 2	3.15	3.17	3.18	3.18	1.04	1.05	1.05	1.05
channel 3	3.10	3.15	3.15	3.15	1.03	1.04	1.04	1.04
channel 4	3.02	3.07	3.07	3.07	1.00	1.02	1.02	1.01
channel 5	2.77	2.83	2.83	2.83	0.92	0.94	0.94	0.94

Table B.1: The mean velocity distribution over the channels from the middle of the tube (channel 1) to the edge channel (channel 5), both absolute and relative with respect to the mean velocity of all channels. (none = no pressure tube, pos n = pressure sensor at position n, see figure B.3)

B.4 Comparison of simulations with the theory

The results from the simulations were also compared to the theory, according to section 2.7. The pressure curve for the simulations and the theory is plotted in figure B.7.
The theoretical results for the pressure drop at the entrance and the pressure gain at the exit are higher than the simulations show. The theoretical entrance- and exit pressure changes however are for a sudden contraction or expansion of one tube, see also figure B.8. According to the simulations these values are too high. The pressure gradient between the cloths is about the same for the theoretical and simulated curves.

B.5 Conclusions of the simulations

From the simulations we can draw conclusions that can be used to discuss the results for the measurements with the flat plates.

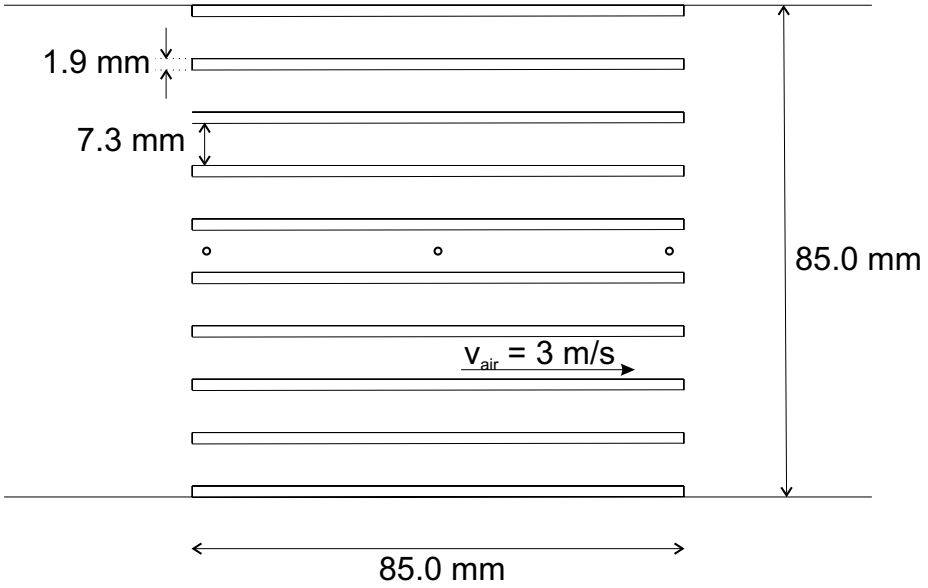

Figure B.3: Configuration of the two dimensional simulation

- The overall pressure drop over the channels is the same for the situation with and without pressure meter and is not dependent on the place of this pressure meter tube.
- The pressure meter tube has a large influence on the pressure between the plates. Due to the stagnation point before the tube and the low pressure after the tube, the pressure that is measured is lower than it would have been without the meter. The place of the tube has no influence on this deviation, so that the gradient of the measured pressure remains the same.
- The velocity profile of the air at the end of the channel has an almost parabolic profile. When the pressure meter was placed more closely to the wall, it has probably less influence on the pressure, so that the negative peak is less deep.
- The mean velocity in the channel where the pressure meter is placed is almost 10% lower than the mean velocity over the whole tube. For a more accurate determination of the friction factor and the heat transfer, this corrected velocity should be used.

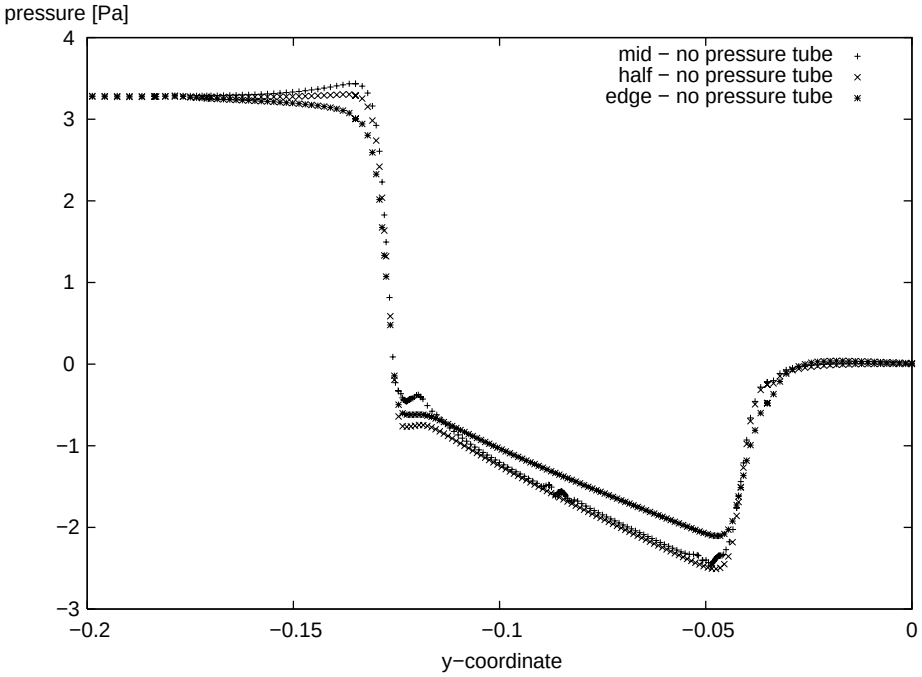

Figure B.4: Pressure distribution in channels at different places in the tube, 'mid' is in the middle of the tube, 'edge' in the channel closest to the wall and 'half' is between 'mid' and 'edge'.

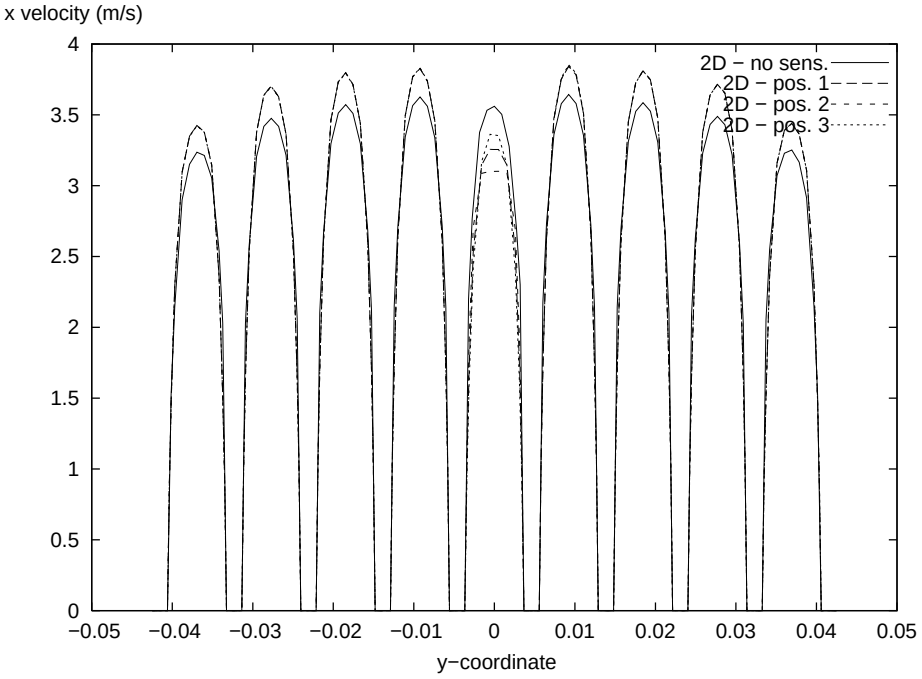

Figure B.5: The velocity distribution over the channels with and without the pressure sensor at different positions in the channel (none= no pressure sensor, pos.n = pressure sensor at position n, see figure B.3)

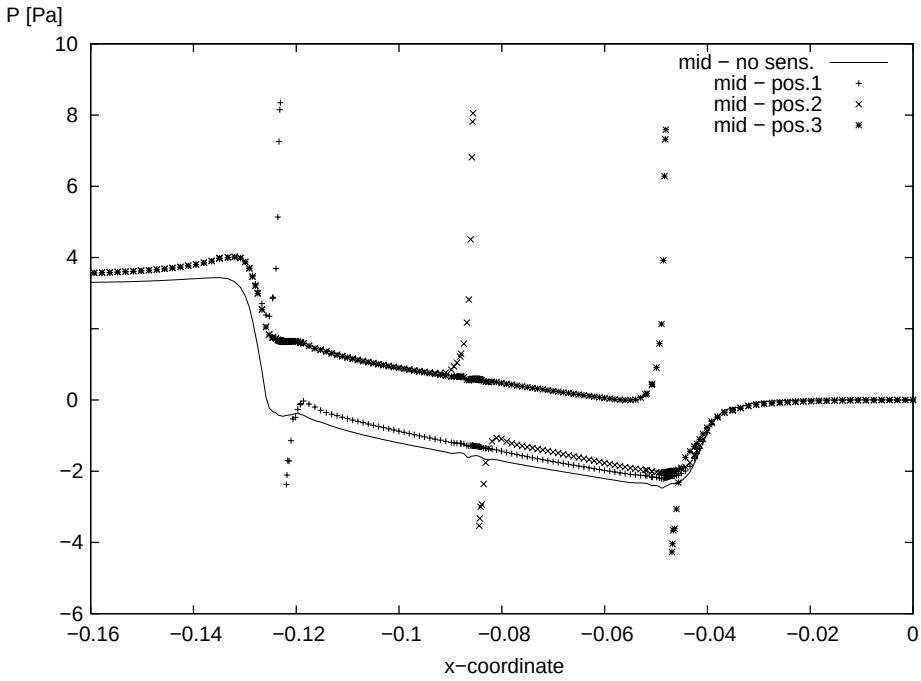

Figure B.6: Pressure distribution in the middle channel, for different positions of the pressure sensor, see also figure B.3

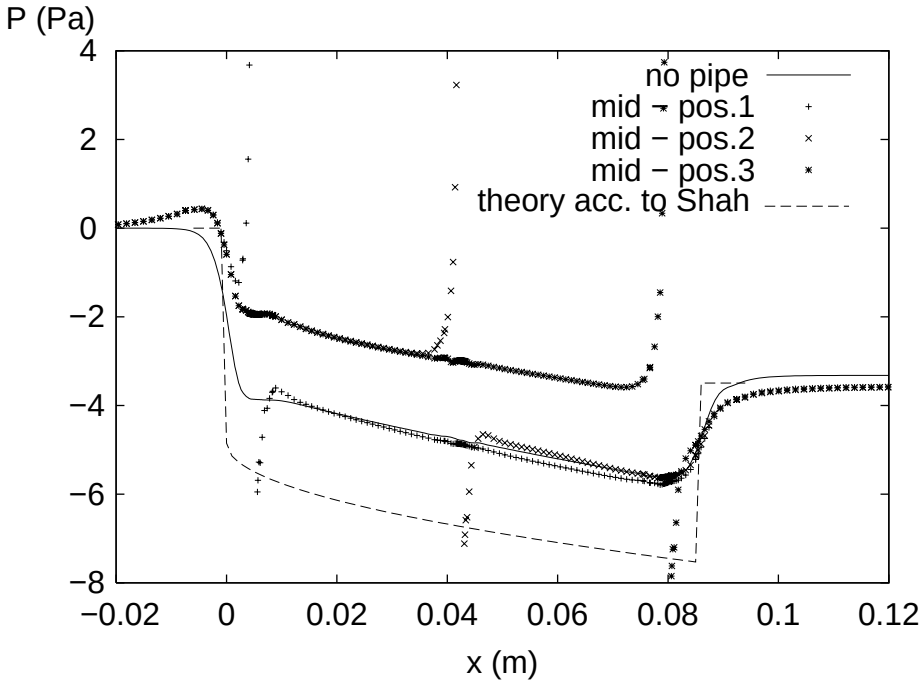

Figure B.7: Pressure distribution according to the simulations and to the theory

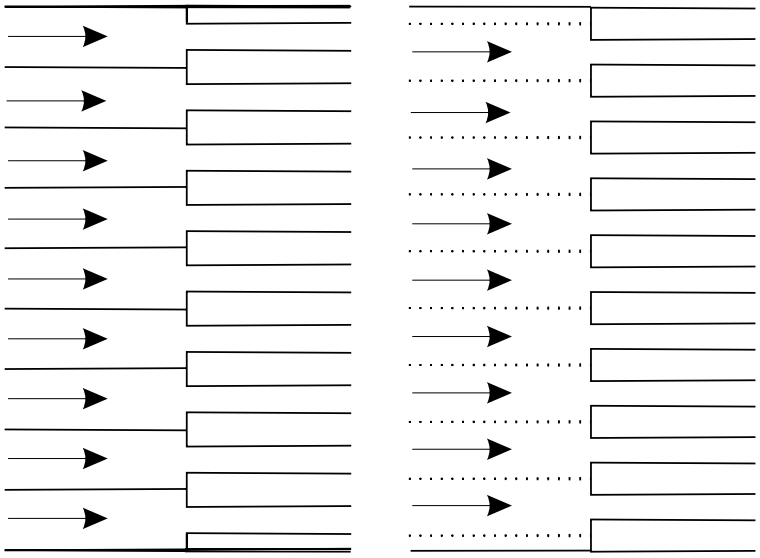

(a) Simplified set-up used for the calculation of the friction coefficient of the entrance

(b) Real set-up of the entrance

Figure B.8: Simplified and real set-up of the entrance of the plates

Appendix C

The meaning of $\frac{StPr^{2/3}}{f}$

Dimensionless numbers are useful to compare the results from different measurements, but sometimes it is difficult to see what it means when a dimensionless number has a certain value. Therefore the ratio between heat transfer and friction, expressed in $\frac{StPr^{2/3}}{f}$, is converted to the total heat transferred (in W/K) and the energy dissipation (in J/kg).

The power that is needed to overcome the friction is the energy dissipation, e_{fr}, times the mass flow. The energy dissipation can be expressed as:

$$e_{fr} = 4f \cdot \frac{L}{D_h} \cdot \frac{1}{2} v_a^2 \tag{C.1}$$

In this equation is f the friction factor, L the length of the cloths or plates, D_h the hydraulic diameter and v_a the velocity of the air. In this equation the friction coefficients of entrance and exit are left out of consideration.
The hydraulic diameter can be calculated with equation (2.2), in which the following expressions are used for the total heat transfer area, A_h:

$$A_{h,cl} = 2n_{cl} b L_{cl} \frac{\pi}{2} \tag{C.2}$$

$$A_{h,pl} = 2n_{pl} b L_{pl} \tag{C.3}$$

This leads to this ratio between the hydraulic diameter of a cloth and of a plate:

$$\frac{D_{h,cl}}{D_{h,pl}} = \frac{2}{\pi} \tag{C.4}$$

The thickness of the cloths, d_{cl} and of the plates, d_{pl}, is almost the same, so that the free flow area is also almost the same. The cloths and plates are compared at the same air velocity, v_a. Using equations (C.1), (2.2), (C.2) and (C.3) is derived that:

$$\frac{f_{pl}}{f_{cl}} = \frac{e_{fr,pl}}{e_{fr,cl}} \cdot \frac{A_{h,cl}}{A_{h,pl}} = \frac{e_{fr,pl}}{e_{fr,cl}} \cdot \frac{\pi}{2} \tag{C.5}$$

The heat transfer, expressed in $StPr^{2/3}$ can be converted to the absolute heat transfer in W/K.

$$St = \frac{h_{w \to a}}{\rho c_p v_a} \tag{C.6}$$

$$h_{w \to a} = \frac{1}{\eta_{fin}} \cdot \left(\frac{1}{\frac{1}{h_{overall}} - \frac{1}{h_w}}\right) \tag{C.7}$$

We assume that $\eta_{fin,cl} \approx \eta_{fin,pl}$. The ratio between the heat transfer coefficients from the water is:

$$\frac{h_{w,pl}}{h_{w,cl}} = \frac{\pi}{2} \tag{C.8}$$

From the measurements it seems that $h_w \approx 12 \cdot h_{overall}$, using this we derive:

$$\frac{St_{pl}}{St_{cl}} = \frac{\pi}{2}(\frac{11}{12\frac{Q_{cl}}{Q_{pl}} - 1}) \tag{C.9}$$

Equation (C.9) can be approached by:

$$\frac{Q_{cl}}{Q_{pl}} \approx 1.5 \cdot \frac{St_{cl}}{St_{pl}} \tag{C.10}$$

The equations for the friction and heat transfer can be combined to:

$$\frac{[\frac{StPr^{2/3}}{f}]_{cl}}{[\frac{StPr^{2/3}}{f}]_{pl}} = \frac{1}{1.5} \cdot \frac{Q_{cl}}{Q_{pl}} \cdot \frac{\pi}{2} \cdot \frac{e_{fr,pl}}{e_{fr,cl}} \approx \frac{Q_{cl}}{Q_{pl}} \cdot \frac{e_{fr,pl}}{e_{fr,cl}} = \frac{[\frac{Q}{e_{fr}}]_{cl}}{[\frac{Q}{e_{fr}}]_{pl}} \tag{C.11}$$

The ratio between heat transfer and friction, $StPr^{2/3}/f$ for flat plates and cloths is approximately the same as the ratio between the transferred heat and the energy dissipation for plates and cloths.

Dankwoord

Met dit verslag ben ik aan het eind gekomen van mijn studie technische natuurkunde. Ik ben dankbaar dat ik de mogelijkheden gekregen heb om deze studie te doen en ook voor alle mensen die mij daarbij geholpen hebben.
Dit onderzoek was niet mogelijk geweest zonder de hulp van ontzettend veel mensen.
Veel dank aan alledrie de Japen, Jan en Wouter voor het maken van mijn opstelling en het lekkers bij de koffie, en vooral aan Ab, voor al dat soldeerwerk dat je voor me gedaan hebt.
Chris: bedankt voor je begeleiding en je kritische commentaar.
Noor en Eur van Andel: ik vond het erg leuk en leerzaam om een aantal weken in jullie werkplaats door te brengen en naar jullie bijzondere ideeën en discussies te luisteren.
HP, dankjewel voor het simuleren van de vlakke plaatjes!
Veel dank ben ik ook verschuldigd aan het KLFT-opvangteam, vooral in de persoon van Linda, maar ook aan Remy, Frank, Roel, Joost, Hille, Anouk, Jeroen, Kim, en al die andere mensen die het vaak zo gezellig maakten om hier af te studeren.
Peter, dankjewel voor je hulp als ik weer eens niet begreep wat mijn computer aan het doen was.
En verder wil ik al die mensen buiten het Kramerslab bedanken die belangstelling toonden en steun als het allemaal niet zo meezat, speciaal mijn ouders, Louise, Margriet en Sijbrand.

Marian

Bibliography

Achenbach, E. (1974). The effects of surface roughness and tunnel blockage on the flow past spheres. *Journal of Fluid Mechanics*, **65, part 1**, 113–125.

Akker, H.E.A., v. d. (2000). *Collegedictaat: Fysische Technologie van Conversieprocessen en Produktbewerkingen*. Faculteit Technische Natuurwetenschappen, TU Delft, Delft.

Andel, E., v. (2002). *Concept voor een energieproducerende kas, Rapportnr. 02.2.015*. Innovatienetwerk Groene Ruimte en Agrocluster and Stichting Innovatie Glastuinbouw, Den Haag.

Arkel, W., v. et al. (2001). *Energieverslag Nederland 2000*. Energieonderzoek Centrum Nederland, Petten.

Beek, W. and Muttzall, K. (1975). *Transport Phenomena*. John Wiley & Sons Ltd., London.

Bird, R., Stewart, W., and Lightfoot, E. (2002). *Transport Phenomena*. John Wiley & Sons Ltd., New York.

Boeker, E. and Grondelle, R. (1995). *Environmental Physics*. John Wiley & Sons Ltd., Chichester.

Boonekamp, P. et al. (1998). *Nationale Energieverkenning 1995-2020*. ECN, ECN-C–97-081, Petten.

Brundtland, G. et al. (1987). *Our Common Future*. Oxford University Press, Oxford.

Carson, R. (1962). *The Silent Spring*. Penguin Books.

CBS (2003a). *Energieverbruik land- en tuinbouw 1994-1998*. CBS, Voorburg/Heerlen.

CBS (2003b). *Nederlands Energiehuishouding 1980-1998*. CBS, www.cbs.nl, Voorburg/Heerlen.

Chatfield, C. (1970). *Statistics for technology*. Chapman & Hall, London.

Clift, R., Grace, J., and Weber, M. (1978). *Bubbles, Drops and Particles*. Academic Press, New York.

Club of Rome (1972). *Limits to growth*. Pan Books, London.

Commoner, B. (1972). The environmental cost of economic growth. *Population, Resources and the environment, Washington US Government Printing Office*, pages 339–363.

Di Felice, R., Foscolo, P., and Gibilaro, L. (1995). On the hindered settling velocity of speres in the inertial flow regime. *Chemical Engineering Science*, **50**, 3005–3006.

Donoughs, P. and Livingood, J. (1954). Exact solutions of laminar-boundary-layer equations with constan property values for porous wall with variable temperature. *National Advisory Committee for Aeronautics*, **Report 1229**.

ECN (2003). *Energie in Nederland, www.energie.nl.*

Ecofys (2003). *www.zonnewijzer.nl.*

Feng, J., Hu, H., and Joseph, D. (1994). Direct simulation of initial value problems for the motion of solid bodies in a newtonian fluid. part 1: sedimentation. *Journal of Fluid Mechanics*, **261**, 95–134.

Fidleris, V. and Whitmore, R. (1961). Experimental determination of the wall effect for spheres falling axially in cylindrical vessels. *British Journal of Applied Physics*, **12**, 490–494.

Fleming, D. and Sparrow, E. (1969). Flow in the hydrodynamic entrance region of ducts of arbitrary cross section. *Journal of Heat Transfer*, **91**, 345–354.

Janssen, L. and Warmoeskerken, M. (1987). *Transport Phenomena Data Companion.* Delftse Universitaire Pers, Delft.

Kay, J. and Nedderman, R. (1985). *Fluid mechanics and transfer processes.* Cambridge University Press, Cambridge.

Kays, W. and Crawford, M. (1980). *Convective Heat and Mass Transfer.* McGraw-Hill Book Company, New York.

Kays, W. and London, A. (1984). *Compact Heat Exchangers.* McGraw-Hill Book Company, New York.

Mulder, K. (2000). *Environmental Challenges and Sustainable Development.* TU Delft, vakgroep Onderwijs in Duurzame Ontwikkeling, Delft.

Newton, I. (1687). *Principia.* Book II, Prop. XXXIX, Theor. XXXI.

Novem (2002). *www.epn.novem.nl.*

Pisters, R. (2003). *Exploitatie mijnwater technisch mogelijk.* afd. Communicatie, Gemeente Heerlen.

Practicum, N. (1997). *Algemene Instructie 3.* Technische Natuurkunde, TU Delft, Delft.

Remery, K. (1997). *Afstudeerverslag: Diffusie van een omgevingsgas in een laminaire impinging jet.* Kramers Laboratorium voor Fysische Technologie , TU Delft, Delft.

Schlichting, H. (1951). *Grenzschicht-Theorie.* G. Braun, Karlsruhe.

Shah, R. (1978). A correlation for laminar hydrodynamic entry length solutions for circular and non-circular ducts. *Journal of Fluids Engineering*, **100**, 177–179.

Sieder, E. and Tate, C. (1963). Heat transfer and pressure drop of liquids in tubes. *Ind. Eng. Chem*, **28**, 1429.

Tjallema, G. (2001). *Introduction to a new type of heat exchanger, Literature Paper.* Delft University of Technology, Department of Applied Physics, Delft.

White, F. (1988). *Heat and Mass Transfer.* Addison-Wesley Publishing Company, Reading.

Zovatto, L. and Pedrizetti, G. (2001). Flow about a circular cylinder between parallel walls. *Journal of Fluid Mechanics*, **440**, 1–25.